DEVELOPMENT AND EVALUATION OF VISIBLE LIGHT-RESPONSIVE PHOTOCATALYST SYSTEMS

March 2008

SOMEKAWA Shouichi

DEVELOPMENT AND EVALUATION OF VISIBLE LIGHT-RESPONSIVE PHOTOCATALYST SYSTEMS

(可視光で機能する光触媒システムの開発と評価)

This thesis is submitted as a partial fulfillment of the requirement for the award of a phD of Chemistry

March 2008

Shouichi Somekawa

(染川正一)

Graduate School of Science and Engineering
Kagoshima University

INDEX

CHAPTER 1

GENERAL INTRODUCTION

CHAPTER 2

FABLICATION OF N-DOPED TITANIUM OXIDE THIN FILMS BY LASER ABLATION METHOD: MECHANISM OF N-DOPING AND EVALUATION OF THE THIN FILMS

CHAPTER 3

EFFECT OF GRAPHITE SILICA ON TITANIUM OXIDE PHOTOCATALYSIS IN HYDROGEN PRODUCTION FROM WATER-METHANOL SOLUTION

CHAPTER 4

FABRICATION OF TWO-LAYER THIN FILM BY LASER ABLATION METHOD AND APPLICATION TO PHOTOCATALYTIC PHOTODECOMPOSITION AND HYDROGEN PRODUCTION

CHAPTER 5

EFFECT OF CARBON NANOMATERIALS ON TITANIUM OXIDE PHOTOCATALYSIS FOR HYDROGEN PRODUCTION FROM WATER-ALCOHOL MIXTURES

CHAPTER 6

VISIBLE-LIGHT INDUCED HYDROGEN PRODUCTION USING CHLOROPHYLL-A OR CO-TETRA PHENYL PORPHYRIN IN PT-LOADED POLY (L-GLUTAMATE)-DECYLAMMONIUM CHLORIDE COMPLEX AND THE CHARACTELIZATION

CHAPTER 7

A NOVEL TYPE SOLAR CELLS BASED ON HEMATITE THIN FILMS

CHAPTER 8

PREPARATION OF TaON OR Ta_3N_5 BY LASER ABLATION METHOD

CHAPTER 9

GENERALIZATION

CHAPTER 1

GENERAL INTRODUCTION

1.1. Background

The earth is facing difficult problems regarding the global environment and energy resources. Global warming due to the increase of carbon dioxide concentration in the atmosphere (greenhouse effect) as well as acid rain due to NO_x and SO_x are typical environmental problems caused by the combustion of fossil fuels. In this regard it is important to create renewable energy resources instead of using fossil fuels. Environmental pollution is also regarded as a serious global problem, for example the dioxin contamination.

The solar energy impinging on the earth's surface is about 3.0×10^{24} J /year. The amount of photosynthesis on the earth is about 3.0×10^{21} J /year. It is equivalent to 0.1% of total solar energy impinging on the earth for a year. The amount of total energy used by the human is about 3.0×10^{20} J /year. The solar energy impinging on the earth's surface is about approximately 10^4 times the worldwide yearly consumption of energy. Therefore it is suggested that we can get energy enough to serve the human's energy from the part of the solar energy. The most important advantage of solar energy is its ecological purity, offering the possibility of accomplishing energy cycles without pollution of the environment and additional heating of the earth. The search for the efficient conversion of solar energy into other useful forms has attractive considerable attention in view of the increasing anxiety over the exhaustion of energy resources from

fossil fuel and also due to the pollution caused by these fossil fuels.

1.2. Photocatalysis

Catalysis under light irradiation, called photocatalysis, is attracting a great deal of attention from view points of fundamental science and applications for practical use. A. Fujishima and K. Honda in 1972 achieved ultraviolet light-induced water cleavage using a titanium dioxide (TiO_2) photoanode in combination with platinum counter electrode soaked in an electrolyte aqueous solution and reported it just before the oil shock of 1973. This opened up the possibility of solar energy conversion by semiconductor or sensitizers. Recently, this type of reaction has been commercially applied to hydrogen production and environmental cleaning by utilizing photocatalytic oxidation of organic compounds and reduction of protons by photocatalysts, respectively [1]. These monographs are published for use by researchers interested in energy and environment since the photocatalysis involves important science and technology for creating new energy resources and cleaning the environment from sunshine.

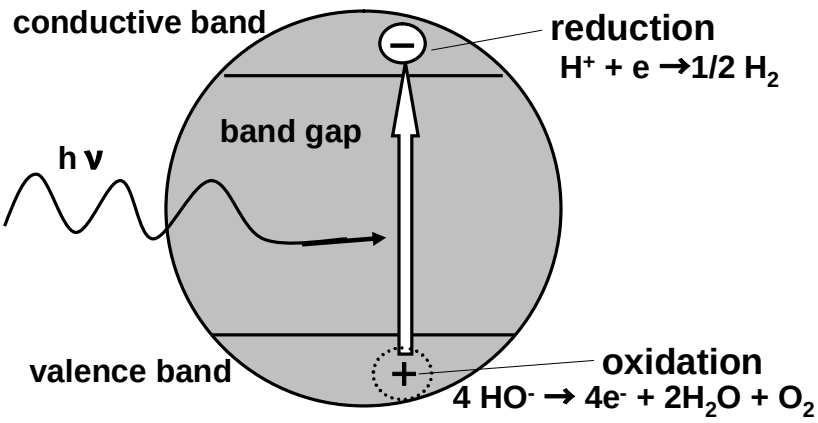

Fig. 1.1. A schematic figure of photocatalytic water splitting using TiO_2.

Much work was carried out on photochemical solar energy conversion by semiconductors or sensitizers to produce fuels by solar energy. The most typical system for such fuel production is water cleavage by light ($2H_2O + h\nu \rightarrow 2H_2 + O_2$) as shown in Fig. 1.1. Since the bandgap of TiO_2 is 3 eV and can utilize only UV light below 400 nm, many attempts have been made to sensitize large bandgap semiconductors or to utilize narrow bandgap semiconductors that can absorb visible light. However, as far as water photolysis is concerned, utilization of visible light for water cleavage has been unsuccessful due to its instability or inactivity. Many scientists are excreting to fabricate a high quality visible light-responsible photocatalyst [2], for example, RuO_2/GaN:ZnO has recently been reported to be active for overall water splitting. This material is a solid solution of GaN and ZnO. The band gap depends on the composition of the solid solution. The photocatalyst with the highest activity among the solid solutions can use visible light up to about 450 nm. The improvement of the efficiencies for these photocatalyst systems and the discovery of new systems are urged.

1.3. Laser ablation method

Laser ablation is the process of removing material from a solid (or occasionally liquid) surface by irradiating it with a laser beam [3]. At low laser flux, the material is heated by the absorbed laser energy and evaporates or sublimes. At high laser flux, the material is typically converted to plasma. Generally, laser ablation refers to removing material with a pulsed laser, but it is possible to ablate material with a continuous wave laser beam if the laser intensity is high enough. The depth which the laser energy is absorbed and the amount of material removed by a single laser pulse depend on the material's optical properties and the laser wavelength. Laser pulses can vary over a very

wide range of duration (milliseconds to femtoseconds) and fluxes, and can be precisely controlled. This makes a laser ablation very valuable for both research and industrial applications.

Here we explain the principle of lasers. The word laser is an acronym formed from light amplification by stimulated emission of radiation. In stimulated emission, an excited state is stimulated to emit a photon by radiation of same frequency; the more photons that are present, the greater the probability of the emission.

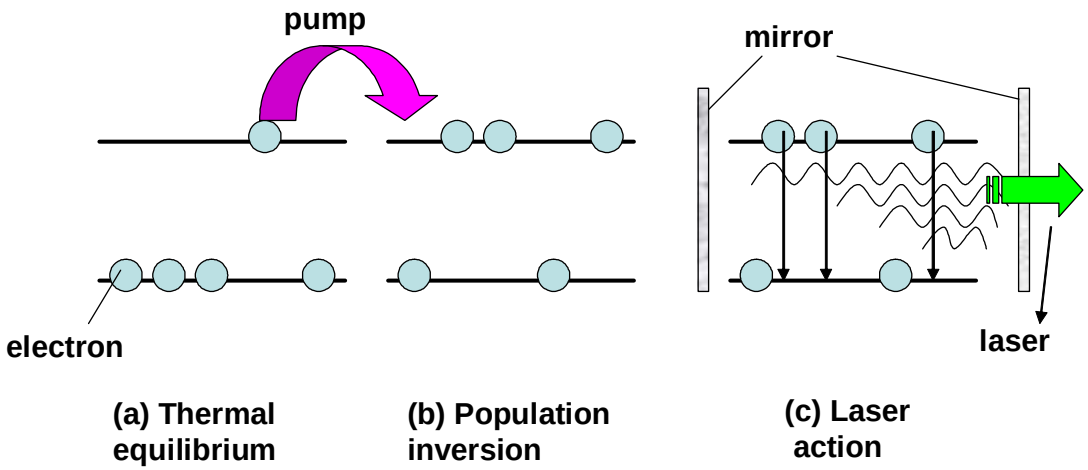

Fig. 1.2. A schematic illustration of the steps leading to laser action. (a) The Boltzmann population of states, with more atoms in the ground states. (b) When the initial state absorbs, the populations are inverted (the atoms are pumped to the exited state). (c) A cascade of radiation then occurs, as one emitted photon stimulates another atom to emit, and so on. The radiation is coherent.

Photons with correct wavelength for the resonant modes of the cavity and the correct frequency to stimulate the laser transition are highly amplified. One photon might be generated spontaneously, and travel through the medium. It stimulates the emission of another photon, which in turn stimulates more. Fig. 1.2 shows the processes. The cascade of energy builds up rapidly, and soon the cavity is an intense reservoir of radiation at all the resonant modes it can sustain. Some of this radiation can be

withdraw if one of the mirrors is partially transmitting.

Next we explain how to achieve the population inversion in which there are more molecules in the upper state than in the lower. Fig. 1.3 shows the schematic illustration of the system. The X → I transition is stimulated with an intense flash of light in the process celled pumping. The pumping is often achieve with an electric discharge

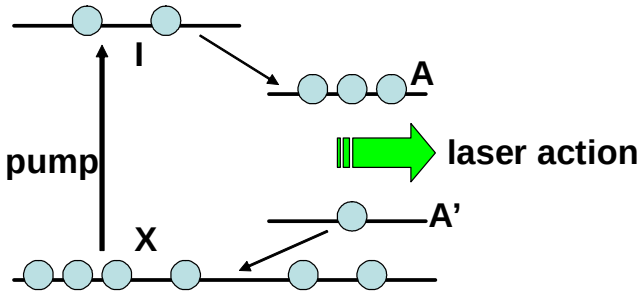

Fig. 1.3. The transition involved in a four-level laser. Because the laser transition terminates in an excited state (A'), the population inversion between A and A' is much essier to achieve.

through Xenon or with the light of another laser. The conversion of I to A should be rapid and the laser transition from A to X should be relatively slow. A' is unpopulated initially, any population in A corresponds to a population inversion, and we can expect laser action if A is sufficiently metastable. This population inversion can be maintained if the A' → X transitions are rapid.

Laser ablation is becoming a dominant technology for direct solid sampling in analytical chemistry. Laser ablation refers to the process in which an intense burst of energy delivered by a short laser pulse is used to sample (remove a portion of) a material. The advantages of laser ablation chemical analysis include direct characterization of solids, no chemical procedures for dissolution, reduced risk of contamination or sample loss, analysis of very small samples not separable for solution analysis, and determination of spatial distributions of elemental composition. Current

research related to contemporary experimental systems, calibration and optimization, and fractionation is discussed, with a summary of applications in several areas. Laser ablation in analytical chemistry has grown substantially over the past few years; several recent reviews each list approximately 200 references describing fundamental or applied studies related to analytical chemistry. Conceptually, laser ablation is a simple and straightforward process. A short-pulsed high-power laser beam is focused onto a sample surface. The laser beam converts a finite volume of the solid sample instantaneously into its vapor phase constituents. For laser ablation, any type of solid sample can be

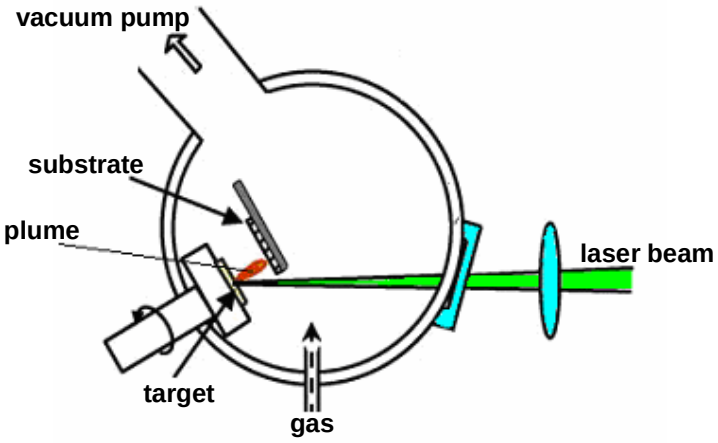

Fig. 1.4. Schematic figure of the laser ablation system

ablated for analysis; there are no sample-size requirements and no sample preparation procedures. In addition, a focused laser beam permits spatial characterization of heterogeneity in solid samples, with typically micron resolution both in terms of lateral and depth conditions. Interest in analytical optical and mass spectrometry associated with laser ablation for sample introduction has increased markedly during the past few years. Laser ablation optical and mass spectrometry with inductively coupled plasma (LA-ICP-AES/MS) appears to be the only analytical approach for nearly

non-destructive determination of a large number of elements with very low detection limits. Applications of LAICP- AES/MS now span a great range of academic and industrial fields that include environmental, geological, archaeological, forensic, and semiconductor manufacturing sectors.

Laser ablation can be used to transfer momentum to a surface, since the ablated material applies a pulse of high pressure to the surface underneath it as it expands. The effect is similar to hitting the surface with a hammer. Preparation of thin film can be possible by using the process as shown in Fig. 1.4. Irradiation of the target with a laser beam melted the target to form a plume. The plume was accumulated on the substrate to form a thin film. The process is also used in industry to work-harden metal surfaces, and is one damage mechanism for a laser weapon. It is also the basis of pulsed laser propulsion for spacecraft.

1.4. Aim and objectives

It is important to develop the high quality photocatalysis system. This thesis mainly comprises the experimental results and discussion on studies of visible light-responsive photocatalysis systems. N-doped TiO_2 films were prepared by the laser ablation and evaluated. The doping process was clarified on the basis of the data. The basic research for the enhancement of the hydrogen production, the decomposition of organic compounds using the photocatalyst films, the artificial photosynthetic system and a novel type solar cell using Fe_2O_3 were carried out under visible light irradiation.

1.5. References

[1] M. Ni, M.K.H. Leung, D.Y.C. Leung, K. Sumathy, Renew. Sust. Energ. Rev. 11 (2007) 401.

[2] A. Kudo, International Journal of Hydrogen Energy 32 (2007) 2673.

[3] R.E. Russo, X Mao, H. Liu, J. Gonzalez, S.S. Mao, Talanta 57 (2002) 425.

CHAPTER 2

FABLICATION OF N-DOPED TITANIUM OXIDE THIN FILMS BY LASER ABLATION METHOD: MECHANISM OF N-DOPING AND EVALUATION OF THE THIN FILMS

2.1. Introduction

The earth is facing difficult problems such as the global environment and energy resources. It is important to create renewable energy resources such as hydrogen instead of using fossil fuels. Environmental pollution is also regarded as a serious global problem, for example dioxin contamination. Titanium (IV) oxide (TiO_2) is well known as an efficient photocatalyst which can decompose pollutants and produce hydrogen [1,2]. However, it is only activated under UV light because of its wide band gap. Therefore, visible light-responsive photocatalysts have received considerable attention because visible light occupies the main part of solar light. The development of the future generation of photocatalytic materials is important for the efficient use of solar light. Many works described the enhanced photocatalytic properties of TiO_2 under visible light by doping of nitrogen [3-5], sulfur [6] and carbon [7].

A laser ablation method has several characteristic: e.g., highly purified thin films can be prepared because of its simple system, any materials from pure elements to multicomponent compounds can be used as a target, deposition time is

short and there are many experimental parameters [8-12].

Recently, Suda et al. reported the preparation of N-doped TiO_2 films from TiN and TiO_2 by the laser ablation method under mixed gas of N_2 and O_2 [13,14].

For development of the study at a different point of view, we mainly studied the dependence of the N-doping on N_2 gas pressures. Here we propose the mechanism of N-doping by the laser ablation method on the basis of the results obtained. The decomposition of methylene blue and the hydrogen production using the N-doped TiO_2 films under visible light irradiation were also performed.

2.2. Experimental

A quartz substrate of 25 × 5 × 1 mm^3 was used as a substrate. TiO_2 targets were prepared by mixing 5.5 g of TiO_2 (Degussa P25) with 0.55 g of paraffin (10%) to prevent cracking. The mixed powder was pressed at 20 MPa for 1 h and calcined at 400 °C for 6 h to form a TiO_2 pellet. A schematic configuration of the laser ablation system is shown in Fig. 1.4.

The second harmonics of a Nd:YAG pulse laser (Spectra-Physics Co., GCR-130-10) was used with the pulse width of 7 ns and the repetition rate of 10 Hz. The laser beam of cross section 0.8 cm2 was focused into an area of about 0.03 cm2 using a quartz lens with focal distance of 30 cm. To avoid the damage of the target by a continuous irradiation of the laser beam, the target was rotated at 14 rpm during the deposition.

The pellet was introduced into the chamber and the experimental conditions were adjusted. Irradiation of the target with a laser beam melted the target to form a plume ablated TiO_2 particles. The plume was accumulated on the quartz

substrate to form the TiO_2 thin film. The fluence of 2.8 J / pulse cm^2 and the laser irradiation time of 12 min were used throughout the experiment. The wavelength of the laser was 532 nm. The distance between the substrate and the target was

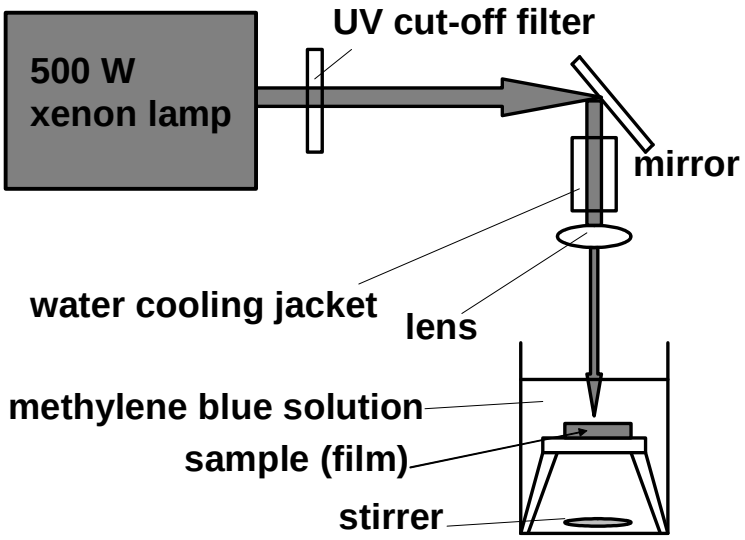

Fig. 2.1. A schematic figure of the methylene blue decomposition system.

measuring the rate of decomposition of methylene blue (Fig. 2.1) and the hydrogen production (Fig. 2.2) in 50 vol% aqueous methanol under visible light irradiation. For the decomposition of methylene blue, the thin film was fixed on a stand and dipped into a 50 cm^3 beaker containing 1×10^{-5} mol / dm^3 methylene

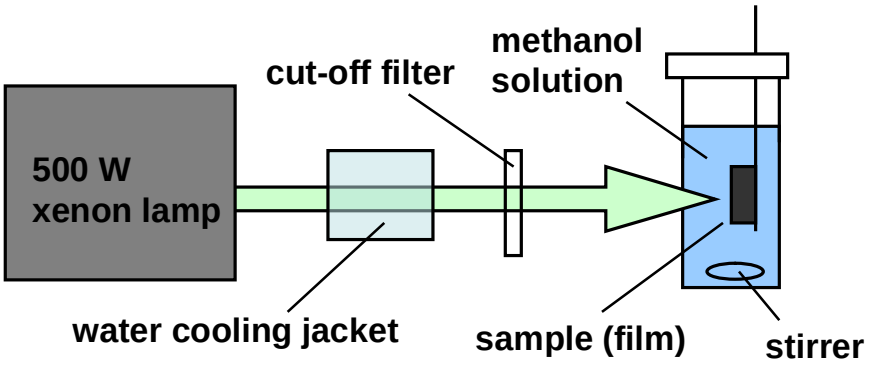

Fig. 2.2. A schematic figure of the hydrogen production system.

blue solution. This solution was irradiated under visible light from the top of the beaker. A xenon lamp (Ushio, 500 W) was also used as a visible light source with a L42 cut-off filter. The rate of decomposition of methylene blue was determined by measuring the change in the absorbance of methylene blue during irradiation.

To enhance the photocatalytic activity for the hydrogen production, Pt-loading was carried out as follows (Fig. 2.3). The prepared thin film was stirred in an aqueous methanol solution (H_2O:MeOH=1:1 by volume) containing a required amount of H_2PtCl_6 and irradiated by a super high pressure mercury lamp (Ushio, 500 W). Photoreduction of H_2PtCl_6 to Pt particles took place, and Pt was deposited on the TiO_2 surface.

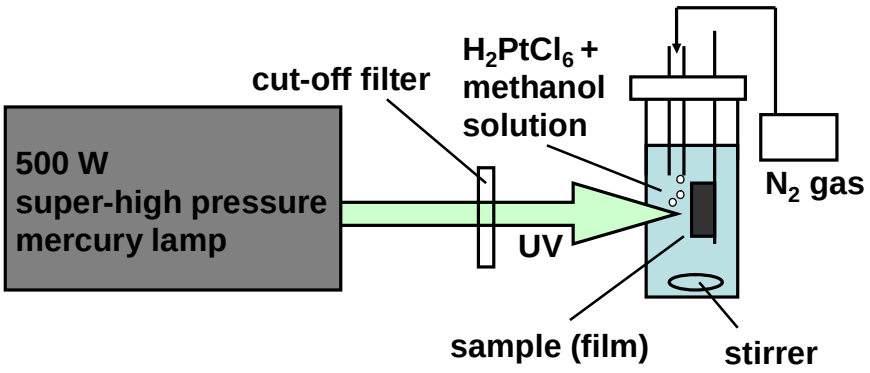

Fig. 2.3. A schematic figure of the photo deposition system.

For hydrogen production, the thin film was dipped into 10 cm^3 aqueous methanol (50 vol%) contained in a 40 cm^3 cylindrical flask. The top of the flask was sealed with a silicone rubber septum. To remove oxygen gas, the suspended solution was bubbled with Ar gas (about 5 ml / min) for 1 h with stirring. Then photoirradiation was carried out under an Ar atmosphere of about 1 atm with stirring. The evolved gas was sampled through the silicone rubber septum by using a locking-type syringe at a constant time interval and the sampled gas was

quantitatively analyzed by a gas chromatograph (detector; thermal conductivity detector (TCD), column packing; molecular sieve 5 Å, carrier gas; Ar). A super-high-pressure mercury lamp (Ushio 500 W) was used as a UV light source with a UV-D33S filter. A xenon lamp (Ushio, 500 W) was used as a visible light source with an L42 cut-off filter.

2.3. Results and Discussion

Fig. 2.4 shows the absorption spectra of (a) the non-doped TiO_2 thin film prepared at 600 °C under O_2 gas of 133 Pa and (b) the N-doped TiO_2 thin film prepared at 600 °C under N_2 gas of 133 Pa. The nitrogen substitutional doping of TiO_2 is thought to be a method for narrowing the band gap by changing the valence band structure without any change in the position of conduction band 15.

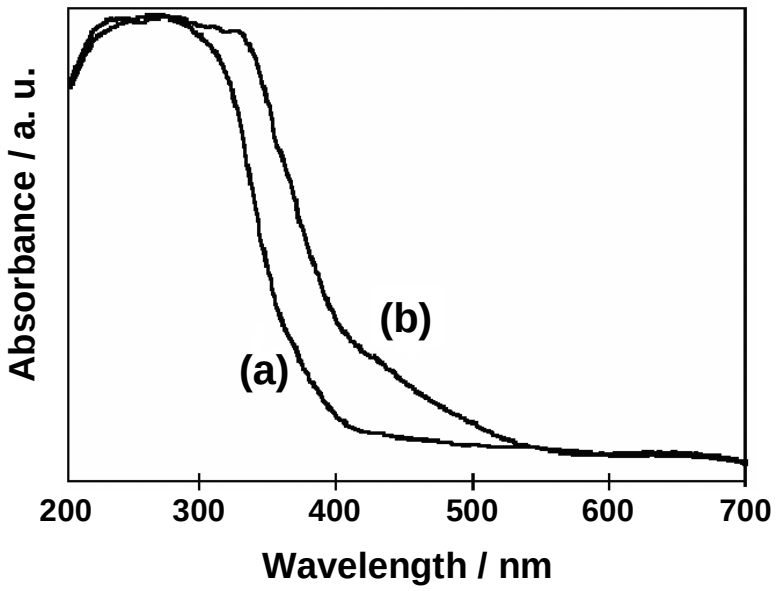

Fig. 2.4. Absorption spectra of (a) non-doped and (b) N-doped titanium oxide thin films in the atmosphere of (a) O_2 133 Pa and (b) N_2 133 Pa, respectively. The substrate temperature was 600 °C, the distance between substrate and target was 3 cm, the deposition time was 12 min, the fluence was 2.8 J / cm^2 pulse.

XRD spectra of the N-doped thin films indicate an increase in the anatase phase with increasing N_2 gas pressure under 200 Pa, and the anatase peaks decreased at 267 Pa as shown in Fig. 2.5. The intensity in the rutile phase in turn increases with decreasing N_2 gas pressure.

The relative amount of N doped in the N-doped TiO_2 thin films was estimated on the basis of the XPS data using h / hmax ratios.

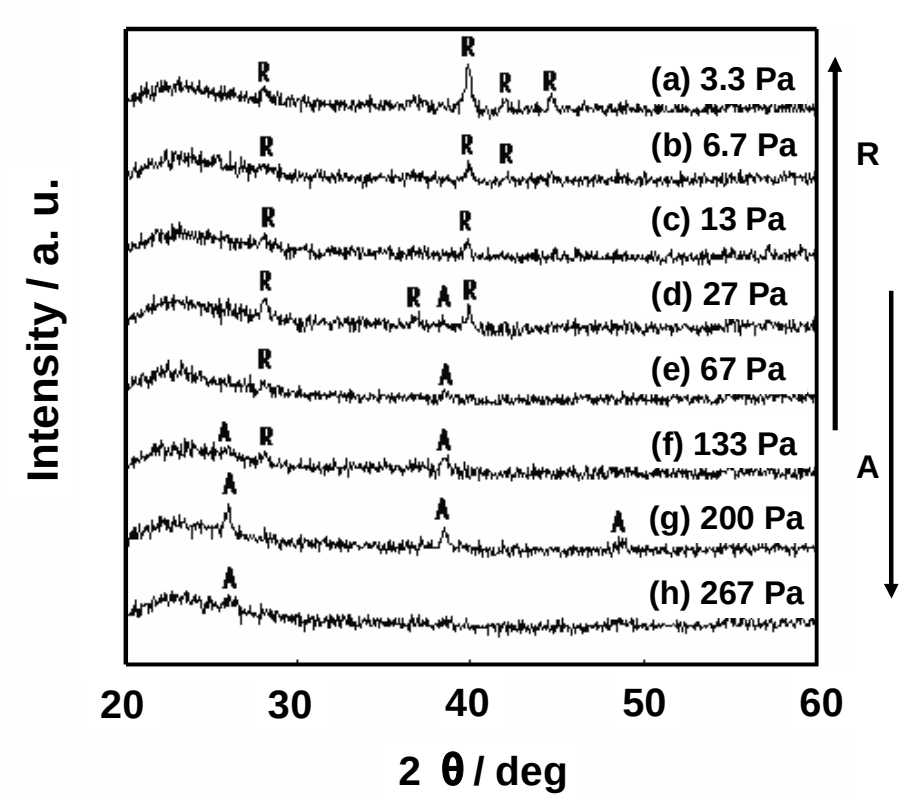

Fig. 2.5. The XRD patterns of the thin films prepared under various nitrogen pressures. A and R denote anatase and rutile, respectively.

To explain how to estimate the relative amount of N doped, we show parts of the raw XPS data in Fig. 2.6. h is the height of the XPS peak of nitrogen in titanium dioxide lattice (the binding energy is ca. 397 eV, it is shown as B in Fig. 2.6) [13] and h_{max} is the maximum peak height of nitrogen under an N_2 pressure of 27 Pa. The heights of the XPS peaks of nitrogen in air, which are adsorbed on the

titanium dioxide surface (the binding energy is ca. 406 eV, it is shown as A in Fig. 2.6) [13] were almost constant. Fig. 2.7 shows the dependence of the amount of N doped on N_2 gas pressures. The amount of N doped sharply increased with increasing N_2 gas pressure up to the N_2 pressure of around 40 Pa and decreased through the maximum.

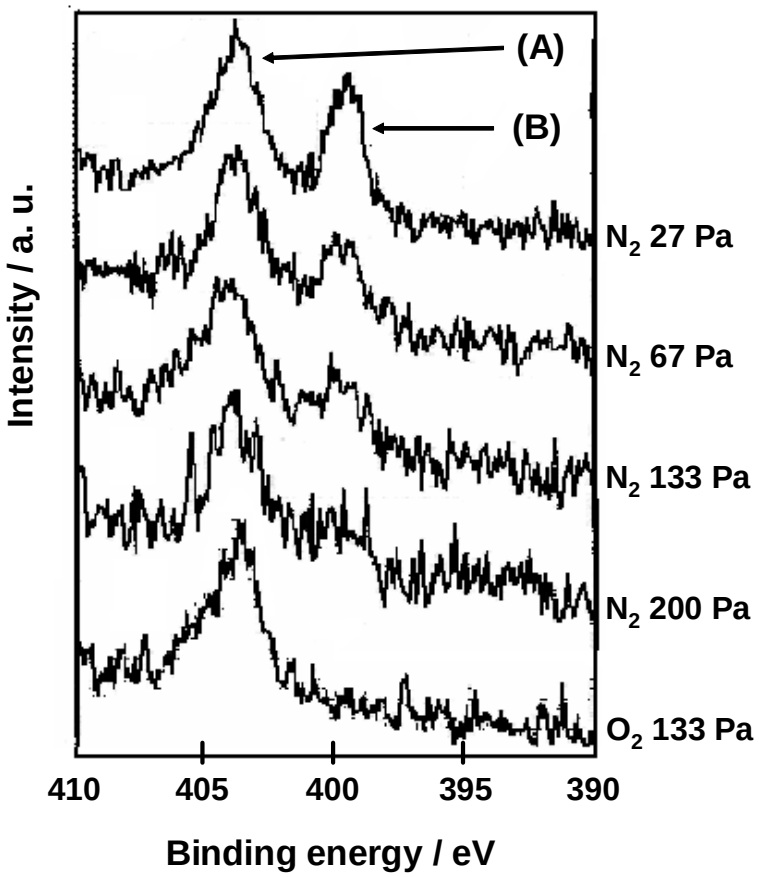

Fig. 2.6. XPS spectra of the thin films prepared under various nitrogen pressures. (A) and (B) denote N species adsorbed on the films from air and N species in titanium oxide lattice, respectively.

On the basis of the XRD (Fig. 2.5) and the XPS (Fig. 2.7) data, we considered a plausible mechanism of the N-doping by the laser ablation. It is important that the crystal point of the crystal transition to anatase from rutile can be found at the nitrogen pressure of around 40 Pa as shown in Fig. 2.5, and the pressure coincides

the maximum point of the amount of N doped (Fig. 2.7). The N-doping was easy to occur near the critical point of the crystal transition because of its instability of

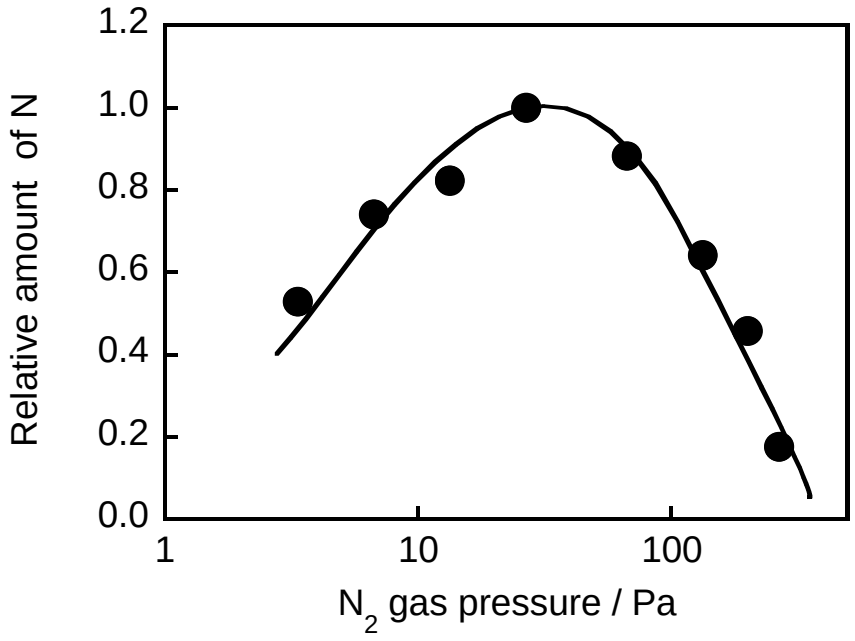

Fig. 2.7. N_2 gas pressure-dependence of the relative amount of the doped nitrogen estimated from XPS data.

the crystal forms.

To consider the effect of the nitrogen species adsorbing on the substrate, we used the BET isotherm 16 as shown in equation (1).

$$\mathbf{V/V_{mon} = cz / (1-z)(1-(1-c)z)} \qquad \mathbf{(1)}$$

In this expression, z is P/P*, P is the nitrogen pressure, P* is the vapor pressure of nitrogen, Vmon is the volume corresponding to monolayer coverage of nitrogen, V is the volume of total nitrogen and c is a constant. The constant c depends on temperature T、a standard enthalpy of the nitrogen desorption Δ desHø and a standard enthalpy of the nitrogen evaporation ΔvapHø as shown in

equation (2).

$$c = \exp((\Delta \mathrm{desH}ø - \Delta \mathrm{vapH}ø) / RT) \qquad (2)$$

R is the gas constant. We assumed that here T is the substrate temperature. We can estimate c = 1 because the temperature (873 K) of the substrate is very high and ΔdesHø is very small due to the physical adsorption. If we substitute c = 1 for equation (1) and plot V/Vmon for z, V/Vmon is almost zero when z is small. In this case, z is very small because the substrate temperature is 873 K, N_2 pressure is low (3.3 - 267 Pa) and P* is high (75800 Pa at 75 K). We concluded that nitrogen almost did not adsorb on the substrate in the conditions. Moreover, the film turned yellow when the substrate temperature was higher than 500 °C. Therefore, it is suggested that the thermal energy originating from the heater of the substrate is also needed for the N-doping. In addition, very recently it has been reported that molecular nitrogen (N_2) is easy to become monoatomic (N) under low pressures [17]. This report can explain the reason why the N-doping is easy to occur in the conditions in spite of the presence of triple bonds in the N2 molecule. From the results, we concluded that N-doping did not occur in the gas phase between the target and the substrate, but mainly on the quartz substrate when N species and ablated TiO_2 particles collided on the substrate.

Fig. 2.8 shows the dependence of the decomposition rate of methylene blue under visible light irradiation on the N_2 gas pressures. Generally, methylene blue is decomposed by a OH radical (OH•) which is produced by an oxidation of a hydroxide ion (OH^-). OH^- is oxidized with a hole (+) produced by the charge separation of the semiconductor. The decomposition rate of methylene blue is in proportion to the concentrations of methylene blue and OH•. Here, we can suppose the concentration of OH• is so high that the decomposition rate is in

proportion to only the concentration of methylene blue as shown in equation (3)

$$-d[MB]/dt = k\,[MB] \qquad (3)$$

and after integration of equation (3):

$$\ln ([MB] / [MB]_0) = -kt \qquad (4)$$

where $[MB]_0$ is the initial concentration of methylene blue, [MB] is the concentration of methylene blue after time t of photocatalytic decomposition and k is a rate constant related to the reaction properties of the solute. The rate constants k for the pseudo first order reaction were obtained from the initial linear portion using equation (4).

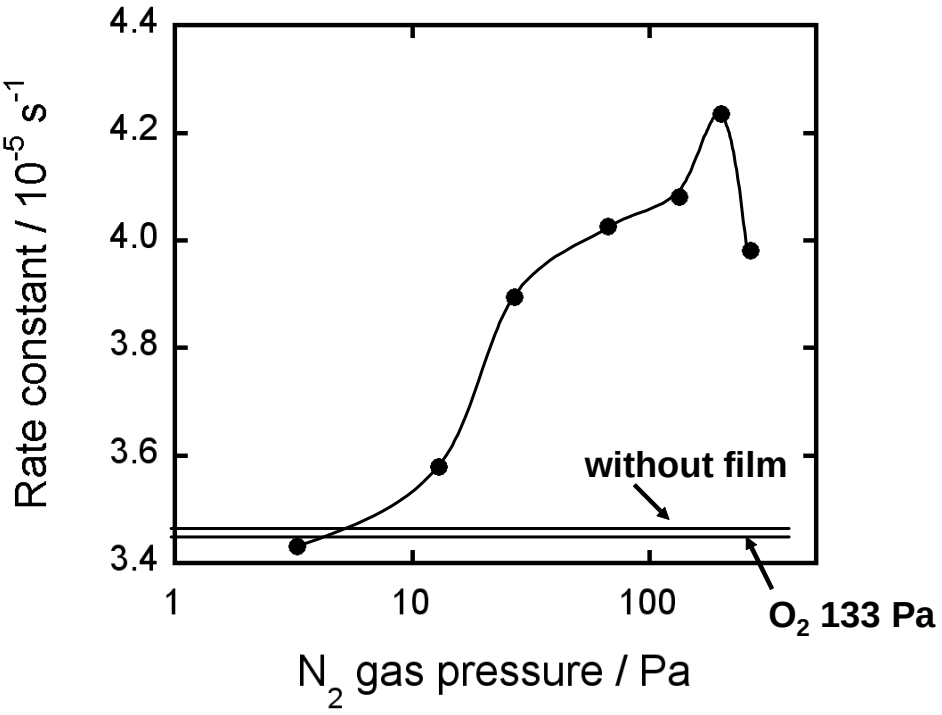

Fig. 2.8. N_2 gas pressure-dependence of the rate constant of methylene blue decomposition under visible light. The rate constant of methylene blue for without film and non-doped titanium oxide film are also shown in the figure.

An increase in the rate of methylene blue decomposition can be noticed from

3.3 Pa to 200 Pa and the rate decreased at 267 Pa as shown in Fig. 2.8 and Table 1 (Their values are shown in the table). This increase (3.3 Pa – 200 Pa) is explained by the change in the crystal structure from rutile to anatase. The photocatalytic activity decreased at 267 Pa because of a decrease of the amount of N doped and

N_2 pressure (Pa)	Relative amount of N doped	Rate constant of the methylene blue decomposition (10^{-5} s^{-1})
3.3	0.53	3.43
13	0.82	3.58
27	1.00	3.89
67	0.88	4.03
133	0.64	4.08
200	0.46	4.23
267	0.18	3.98
O_2 133 Pa	0.00	3.46
without film		3.44

Table 2.1. The amounts of N doped and the rate constants of the methylene blue decomposition by various N_2 gas pressure.

anatase contained in the film.

Next, the distance between the target and the substrate was changed to 2 cm from 3 cm under the fixing condition (600 °C, N_2 200 Pa) where photocatalytic activity is maximum under the condition of 3 cm, resulting in we can get a deeper yellow thin film than that of 3 cm. Fig. 2.9 shows the XRD spectra of the thin films prepared under the distances are 2 cm and 3 cm. Fig. 2.10 shows the amount of N doped under the conditions of the distance between 2 cm and 3 cm. It is clear that the crystallinity and N-doping of 2 cm is better than 3 cm.

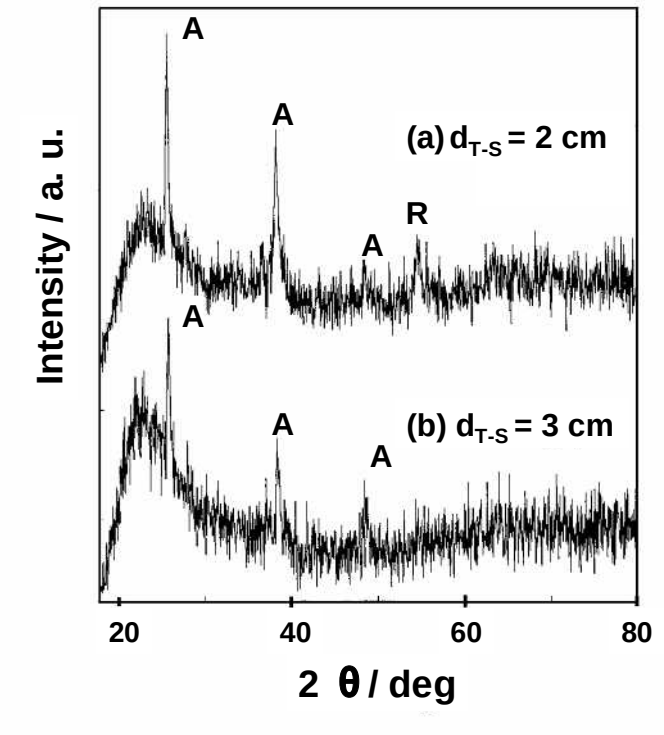

Fig. 2.9. The XRD patterns of the N-doped titanium oxide films under conditions of distance between substrate and target (a) d_{S-T} = 2 cm and (b) 3 cm. The substrate temperature was 600 °C, the deposition time was 12 min, the fluence was 2.8 J / cm^2 pulse. A and R denote anatase and rutile, respectively.

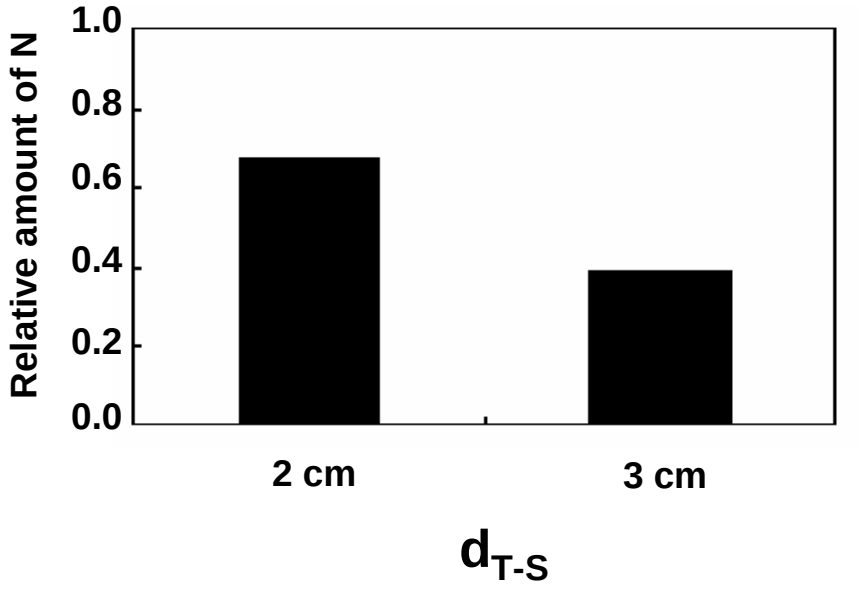

Fig. 2.10. The relative amount of nitrogen in the N-doped titanium oxide thin films. For the experimental conditions, see the figure caption to Fig. 2.9.

Fig. 2.11 shows the rate constants of the methylene blue decomposition under the conditions of the distances of 2 cm and 3 cm. It is found in this figure that the photocatalytic activity of 2 cm for the methylene blue decomposition was better than that of 3cm. We suggest three reasons for the enhancement of the photocatalytic activity. First is the improvement of the crystallinity. Second is an

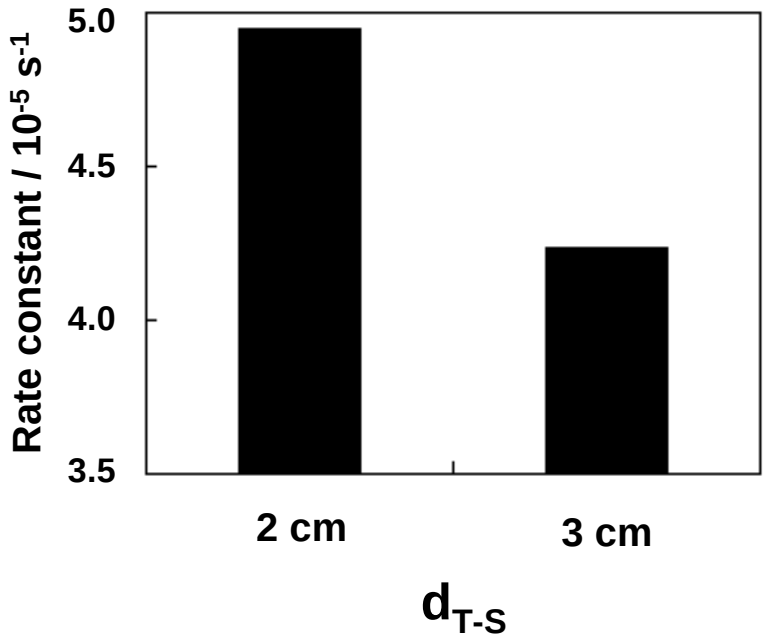

Fig. 2.11. The rate constant of methylene blue decomposition using the N-doped titanium oxide thin films under visible light. For the experimental conditions, see the figure caption to Fig. 2.9.

increase of the surface area. Third is an increase of the amount of N doped in the TiO_2 thin films. Under low pressure of N_2, the speed at which the ablated particles travel did not decrease sharply because the mean free path increased, resulting in occurring the collision against the substrate with the much collision and migration energy. It is worthy of note that the growth of anatase was found as well as rutile in spite of a increase of the thermal energy. Rutile is easy to growth with much thermal energy because of the thermodynamic stability property. Therefore, it is

also obvious from the previous results (see Fig. 2.5) that the amount of rutile increased as decreasing the nitrogen pressures due to increasing the thermal energy. In the distance of 2 cm, it is suggested as the reason of the growth of anatase as well as rutile that the active species in the plume colliding on the substrate increased because the plume was near the substrate.

Fig. 2.12 shows the SEM image of the typical N-doped TiO_2 thin film

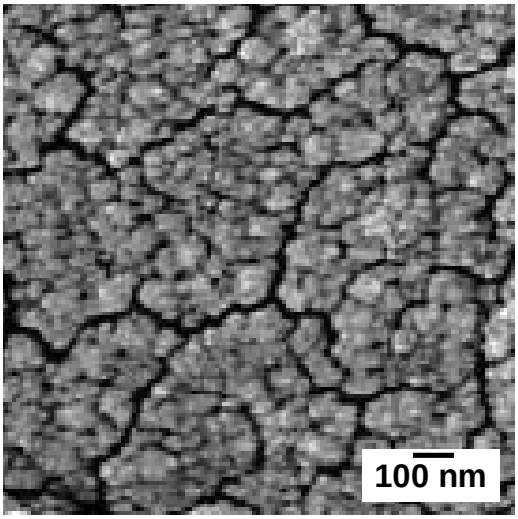

Fig. 2.12. The SEM image of the typical N-doped TiO_2 thin film (N_2: 133 Pa, substrate temperature: 600 °C, distance between substrate and target: 3cm, deposition time: 12min, laser power: 2.8 J/ cm^2 pulse).

prepared by the laser ablation method (N_2 133 Pa, 600°C). From this image, we can see that the surface is rough and there are a large number of pores.

To enhance the hydrogen production activity, Pt is deposited on the TiO_2 thin film by the photo-deposited method. Fig. 2.13 shows the hydrogen production-dependence on the UV irradiation time (the Pt deposition time). The amount of Pt deposited on TiO_2 thin film was in proportional the UV irradiation time. It is found that the optical value of the irradiation time exists around 30 s. The amount of hydrogen gas evolved under visible light irradiation was only

one-500th (ca. 0.05 μmol/h^{-1}, it is shown as a closed circle in Fig. 2.13) of the amount of hydrogen gas evolved under UV light irradiation (it is shown as a open circle in Fig. 2.13) in spite of the usage of Pt-deposited (30 s) N-doped TiO_2 thin films. The bare N-doped TiO_2 thin film generated no hydrogen gas under visible light irradiation. It can be concluded that the photocatalytic activity of the N-doped TiO_2 thin films prepared by the laser ablation method is very small for the hydrogen production. This may be due to that the N-doped TiO_2 thin films

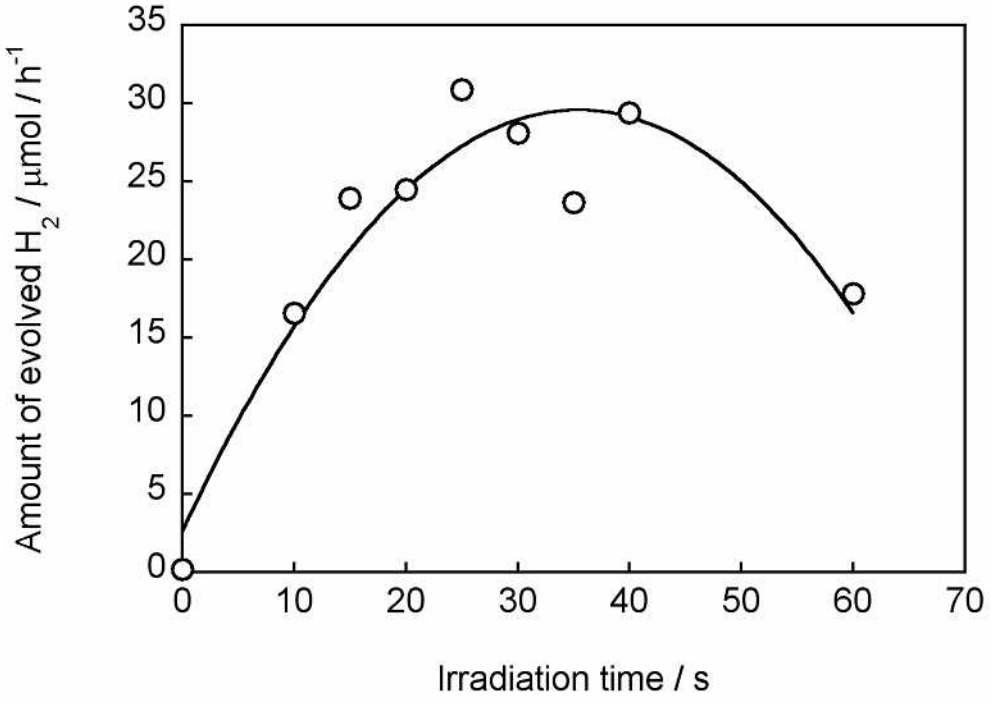

Fig. 2.13. The amount of hydrogen evolved from 50 vol% aqueous methanol using the N-doped TiO_2 film under visible or UV light. Open circles in this figure show the dependence of the amount of hydrogen evolved under UV on the amount of Pt deposited. A closed circle shows the amount of hydrogen evolved using the Pt-deposited N-doped TiO_2 thin film (Pt-deposition time: 30 s) under visible light.

have some defects such as the oxygen defects which trap electrons necessary to reduce H^+, resulting in low hydrogen production efficiency.

2.4. Conclusion

N-doped TiO_2 thin films were prepared by the laser ablation method under an N_2 gas atmosphere. Properties of the films such as color, the doped amount of N and the crystal structure were examined by changing the atmospheric pressure of N_2. The N_2 pressure of both of the critical point of crystal transition and the maximum of the amount of N doped was around 40 Pa. Their thin films were evaluated by the methylene blue decomposition and the hydrogen production under visible light-irradiation. The rate of the methylene blue decomposition depended on the N_2 gas pressures. N_2 gas pressure of the maximum rate for the methylene blue decomposition under visible light was ca. 200 Pa. The hydrogen production using the N doped TiO_2 thin film under visible light was very poor. We proposed the N-doping mechanism as follows: N-doping by the laser ablation occurs by the collision of ablated particles with the substrate and the migration processes. Amount of N doped increases as an increase due to the instability of the crystal structure near the critical point of the crystal transition. The elucidation of the mechanism will contribute to the development of preparation of more useful visible light-responsive photocatalyst thin films.

2.5. References

[1] A. Fujishima, K. Honda, Nature 37 (1972) 238.

[2] A. Heller, Acc. Chem. Res. 28 (1995) 141.

[3] R. Asahi, T. Ohwaki, K. Aoki, Y. Taga, Science 293 (2001) 269.

[4] Y. Sakatani, K. Okusako, H. Koike, H. Ando, Photocatalysis 4 (2001) 51. (in Japanese)

[5] T. Ihara, M. Ando, S. Sugihara, Photocatalysis 5 (2001) 19. (in Japanese)

[6] H. Irie, Y. Watanabe, K. Hashimoto, Chem. Lett. 32 (2003) 772.

[7] T. Umebayashi, T. Yamaki, H. Ito, K. Asai, Appl. Phys. Lett. 81 (2002) 454.

[8] X. Zou, N. Maesako, T. Nomiyama, Y. Horie, T. Miyazaki, Sol. Energy Mater. Sol. Cells 62 (2000) 133.

[9] H. Usui, O. Miyamoto, T. Nomiyama, Y. Horie, T. Miyazaki, Sol. Energy Mater. Sol. Cells 86 (2005) 123.

[10] S. Somekawa, Y. Kusumoto, M. Ikeda, B. Ahmmad, Y. Horie, Catal. Commun. 9 (2008) 437.

[11] N. Inoue, H. Yuasa, M. Okoshi, Appl. Surf. Sci. 197 (2002) 393.

[12] S. Kitazawa, Y. Choi, S. Yamamoto, Vacuum 74 (2004) 637.

[13] Y. Suda, H. Kawasaki, T. Ueda, T. Ohshima, Thin Solid Films 453 (2004) 162.

[14] Y. Suda, H. Kawasaki, T. Ueda, T. Ohshima, Thin Solid Films 475 (2005) 337.

[15] Y. Wang, D.J. Doren, Solid State Commun. 136 (2005) 186.

[16] S. Brunauer, P.H. Emmett, E.J. Teller, Am. Chem. Soc. 60 (1938) 309.

[17] S. Maret, E.A. Bergin, C.J. Lada, Nature 442 (2006) 425.

CHAPTER 3

EFFECT OF GRAPHITE SILICA ON TITANIUM OXIDE PHOTOCATALYSIS IN HYDROGEN PRODUCTION FROM WATER-METHANOL SOLUTION

3.1. Introduction

Co-catalysts are indispensable for the hydrogen production using photocatalytic semiconductors. At present, expensive noble metals such as platinum (Pt) and ruthenium (Ru) are used as the co-catalysts. The Pt metal shows especially outstanding performance for photocatalytic hydrogen production, but it is a fairly rare metal. To realize a hydrogen-based society, the cocatalysts derived from abundant natural minerals seem to be interesting and important as a co-catalyst in low cost. We are strongly concerned with graphite silica (GS, also called “black silica” and “silica black”), one of natural minerals, as a low cost co-catalyst. Here, it should be emphasized that the GS is much cheaper and more abundantly available than metals such as Pt. The GS is siliceous ore containing several percent of carbon in a black mudstone of pre-tertiary. It is mainly composed of quartz, clay and carbon. The GS is usually used as an addition to concrete blocks and an adulterant for soil improvement or snow melting. In industrial application, it has been studied as a source for the preparation of -SiC or -Si_3N_4 whiskers [1,2]. Generally, co-catalysts are roughly classified into two types. One is a support-type in which co-catalysts are deposited on photocatalysts. The other is a mixing-type in which co-catalysts are mixed with

photocatalysts in suspension. The support-type has high efficiency, but the supporting process is complicated. The mixing-type has lower efficiency than the support-type, but the mixing process is very easy and convenient for practical use. For the support-type, many metals such as Pt, Ni and Ru are used [3–8]. On the other hand, Cu, Ni, Ag, Co, etc. are known as mixing-type co-catalysts [9,10]. For both types, roles of the co-catalysts are summarized as follows: (1) the co-catalysts efficiently accept electrons or holes from TiO_2 to avoid recombination of the electron and hole; (2) the co-catalysts adsorb reactants on the surface which is the reaction field of electrons (or holes) and the reactants. In case of the mixing-type, the frequency of collisions and the degree of aggregates are important factors. Moreover, it is needed that the co-catalysts hold the reactants sufficiently. In this paper, the co-catalytic ability of GS itself and its components was studied. We obtained the following significant results. The clay component in GS showed good co-catalytic performance close to that of as-powdered GS. The pH values of water increased by adding GS, irrespective of whether the TiO_2 powder was present. Both TiO_2 and GS particles were aggregated in suspension. On the basis of these experimental results, we here report the role of GS as a co-catalyst for the hydrogen production from water–methanol suspension containing powdered GS and TiO_2 and propose a plausible mechanism of the synergy effect between GS and TiO_2.

3.2. Experimental.

The photocatalyst was TiO_2 (Degussa, P 25) with a mainly anatase structure (ca. 80%) under the shape of non-porous polyhedral particles of ca. 20 nm mean size with a surface area of 49.9 m^2/g.

The GS powder was obtained from Nishinihon Environmental Engineering Inc. The

Table 3.1. A typical example of composition of GS.

Name	Chemical formula	Content (wt.%)
Quartz	SiO_2	67.9
Sericite	$K_2Al_6Si_6O_{22}$	18.9
Carbon[a]	C	5.80
Dolomite	$(Ca, Mg)CO_3$	3.50
Kaolinite	Al_2SiO_2	1.77
Hematite	Fe_2O_3	0.87
Rutile	TiO_2	0.77
Pyrite	FeS_2	0.48

[a] Contain graphite.

GS powder has a surface area of 11 m^2/g. The typical composition of GS is shown in Table 3.1. It was estimated by using the norm method based on X-ray diffraction and X-ray fluorescence analysis [11,12]. Main components are quartz, carbon, and several kinds of clay such as sericite and kaolinite. Fig. 3.1 shows a typical example of thermogravimetry– differential thermal analysis (TG–DTA) curves of GS.

A weight loss of about 4% was observed at around 923K on the TG curve. One exothermic peak was observed on the DTA curve, which was accompanied by the weight loss. The loss mainly corresponds to the total mass of carbon in GS as seen in Table 3.1. These results suggest that most of carbon was removed by heat treatment at around 923 K. As shown in Fig. 3.2, the GS color changed from black to pale-pink after the measurement of TG–DTA. The calcined GS was obtained by heat treatment for 5 h at 923K in air. The pale-pink colored GS contains negligible carbon, as mentioned above. The clay fraction in the calcined GS was separated by the following method [13]. The calcined GS powder was dispersed in water by ultrasonication for 30 min. After the

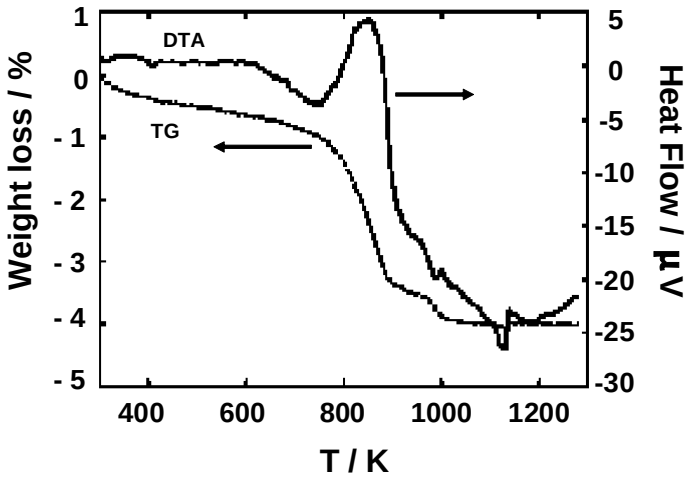

Fig. 3.1. Typical DTA-TG curve of GS.

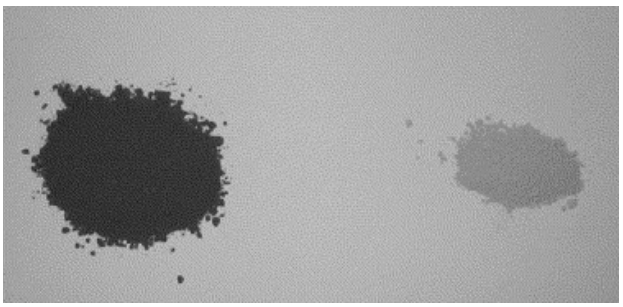

Fig. 3.2. The color change of GS by heat treatment. Left and right: before and after heating at around 923 K, respectively.

suspension was allowed to stand in a dark place for 6 h, its suspension was separated into two layers of the supernatant and the sediment. The supernatant was centrifuged at 3500 rpm for 15 min. After the precipitate was dried on standing, the pale-pink colored clay was obtained. After supernatant was removed, the sediment was washed to remove the clay fraction remaining on the GS surface. The sediment was then treated ultrasonically for 20 min in water of 160 cm^3. The obtained suspension was centrifuged at 3500 rpm for 15 min, and the supernatant was removed. This process was repeated 19 times. The ash-like colored powder was obtained after drying. The powder containing mostly quartz was thus obtained from the calcined GS.

Graphite (99%, Nacalai Tesque), activated carbon (for chromatography, Wako), quartz (99%, Wako), and platinum (99.98%, Nilaco) were used without further purification. Methanol (Wako) was of the highest grade available and was used as received. Laboratory deionized water was distilled twice.

The amount of hydrogen gas evolved photocatalytically from water–methanol mixtures was measured by following procedures. (1) A mixture of powdered TiO_2 and an additive such as GS, several kinds of GS components, or Pt powders was added to aqueous methanol (20 cm^3) in a batch photoreactor of a cylindrical flask (154 cm^3) whose top was sealed with a silicone rubber septum. (2) To remove oxygen gas, the suspended solution was bubbled with Ar gas (about 1 ml/min) for 1 h with stirring after ultrasonication for 1 min. (3) Photoirradiation was carried out under an Ar atmosphere of about 1 atm with stirring. (4) The evolved gas was sampled through the silicone rubber septum by using a locking-type syringe at a constant time interval. (5) The sampled gas was quantitatively analyzed by a gas chromatograph (detector; thermal conductivity detector (TCD), column packing; molecular sieve 5 °A or Porapak N, carrier gas; Ar). The photoirradiation was provided by a super-high-pressure mercury lamp (Ushio, 500-W USH-500SC) with an optical band pass filter (300–400 nm, Asahi Techno Glass, UV-D33S).

The co-catalytic properties of recycled GS were examined in the following manner. After the hydrogen production experiment was finished, the suspension used was centrifuged at 1000 rpm for 7 min, and then the supernatant was removed. A fresh water–methanol mixture was added to the remaining sediment. Again, the hydrogen production experiment was performed. These recycling processes were repeated consecutively five times.

The variations of pH and the eluting metals from GS in water were measured by following procedures. Proper amounts of GS were added to 50 cm^3 of water with or without TiO_2. The suspension was stirred for 20 min. The pH of the suspension was measured using a pH meter (Horiba, D-51). Then the suspension was filtered and the filtrate was analyzed by inductively coupled plasma emission spectroscopy (Thermo Elemental, IRIS).

To investigate the aggregation of TiO_2 and GS particles in water, the size distribution of particles was measured by a laser diffraction particle size analyzer (Shimadzu, SALD-3100). The measurement was carried out with and without ultrasonication. The images of aggregates of TiO_2 and/or GS were taken with a scanning electron microscope (Hitachi S-4100).

3.3. Results and discussion

Fig. 3.3 shows the GS content dependence of the evolution rate of hydrogen gas from 40 vol.% aqueous methanol suspension. The GS content of the GS–TiO_2 mixture was varied in the range of 0–100 wt.%, keeping the total amount of the mixture at 30 mg. The maximum production rate of hydrogen gas, 22.3 μmol h^{-1}, was observed at a GS content of 50 wt.%. On the other hand, TiO_2 or GS only resulted in 0.23 and 0.03 μmol h^{-1}, respectively. By adding GS to TiO_2 suspension, the amount of hydrogen gas was increased by a factor of ca. 100 (a ratio of 22.3 and 0.23 μmol h^{-1}). These results show that the photocatalytic hydrogen production was enhanced by the synergy effect of GS and TiO_2. Fig. 3.4 shows the hydrogen production by recycled TiO_2 and GS. The amount of hydrogen gas under 1 h irradiation in the 2^{nd} cycle was larger approximately two times than that in the initial cycle. Furthermore, the amount of H_2 gas was larger

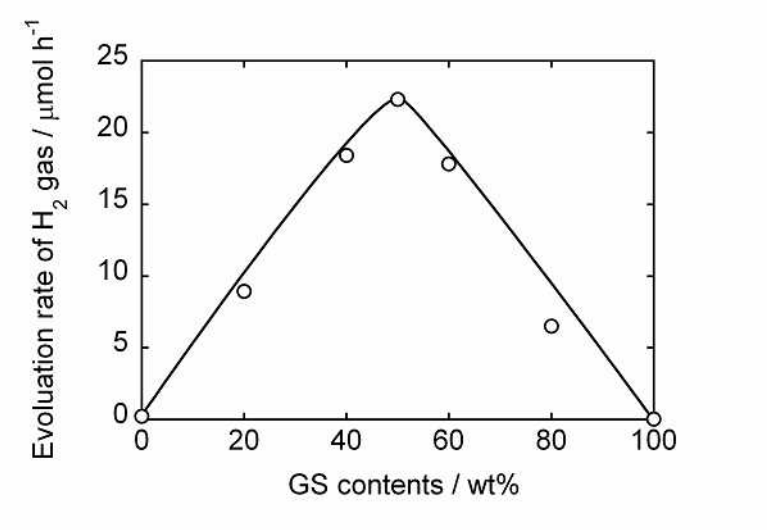

Fig. 3.3. The GS content dependence of the evolution rate of H_2 gas from water-methanol mixtures containing 40 vol% methanol under UV ittadiation(35 mW cm^{-2}).

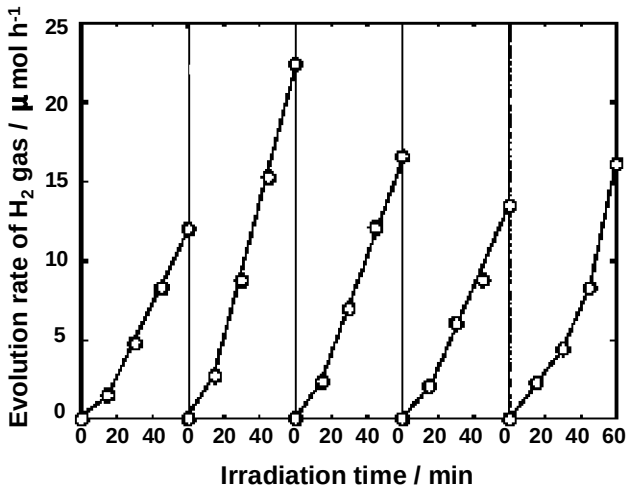

Fig. 3.4. Hydrogen production by recycled TiO_2 and GS. Methanol: 40 vol.%, UV strength: 15mWcm^{-2}.

than that of the initial cycle in all runs. The cleaning effect of the GS and TiO_2 surfaces in the recycling process may be responsible for the increment of hydrogen production. Fig. 3.5 shows the irradiation-time course of hydrogen production from suspension of TiO_2 with GS or Pt powder. The hydrogen evolution from platinized TiO_2 (0.3 wt.% Pt/TiO_2) was also studied for comparison [14]. The amount of H_2 gas evolved with the

powdered GS–TiO_2 mixture was about one-eighth of that evolved with 0.3 wt.% Pt/TiO_2. Since GS could not be deposited to TiO_2, the mixture of powdered Pt and TiO_2 was also examined. The synergy effect by the powdered GS was comparable to that by the powdered Pt. Therefore, the GS powder is considered to bear comparison with the co-catalytic Pt in the photocatalytic activity. Fig. 3.6 shows the amount of hydrogen gas evolved from various suspended mixtures of TiO_2 with untreated GS, SiO_2, graphite,

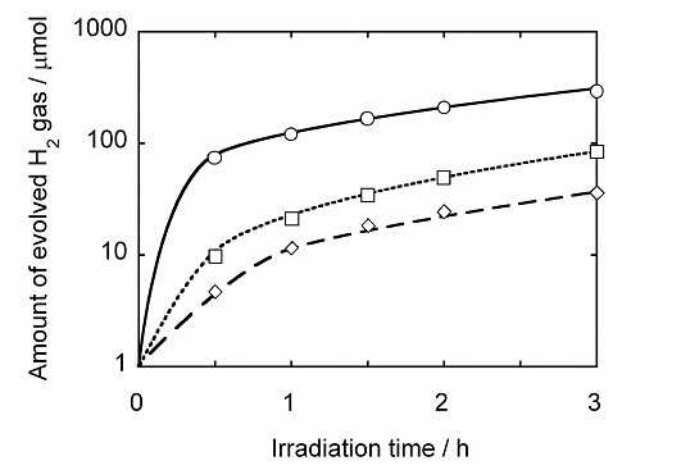

Fig. 3.5. Comparison of hydrogen production from various kinds of suspensions: (○) Pt/TiO_2, (□) Pt and TiO_2, (◇) GS and TiO_2. Methanol: 40 vol.%, UV strength: 15 mW cm^{-2}: 15 mWcm^{-2}. Note the logarithmic ordinate.

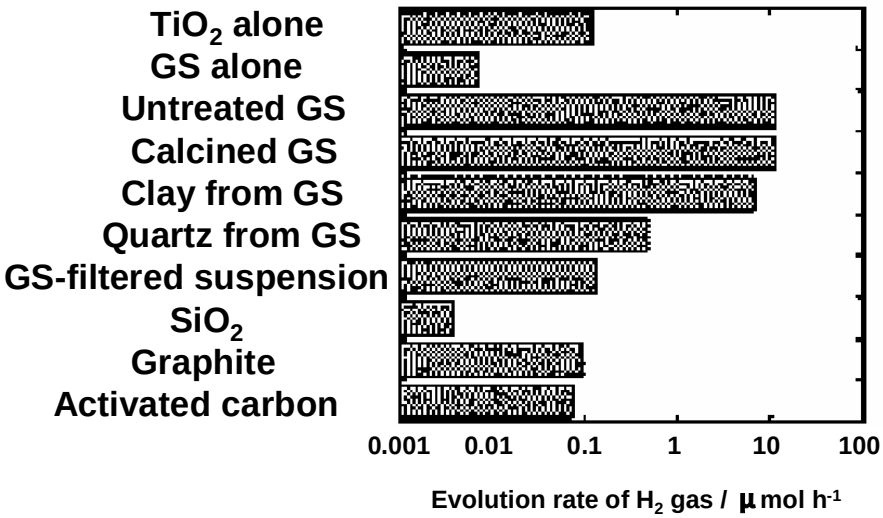

Fig. 3.6. Comparison of hydrogen production. Each powdered additive (15 mg) was added to powdered TiO_2 (15 mg). For TiO_2 alone and GS alone systems, the total amount of 30 mg was used. Methanol: 40 vol.%, UV strength: 15 mW cm^{-2}. Note the logarithmic abscissa.

activated carbon, calcined GS, clay from GS, or quartz from GS. An addition of powdered SiO_2 to TiO_2 suspension did not enhance the photocatalytic hydrogen production, but it was rather detrimental. The quartz from GS was also insufficient to enhance the hydrogen evolution. These indicate that the SiO_2 fraction is not effective for

Table 3.2. Metal species eluted from GS (30 mg) in water (50 cm^3).

Eluting species[a]	Amount (μmol)
Na	2.44
K	1.46
Ca	1.20
Ga	0.68
Si	0.61
Al	0.28
Mg	0.16
Nb	0.08
Mn	0.07
Hf	0.05

[a] Main species are listed.

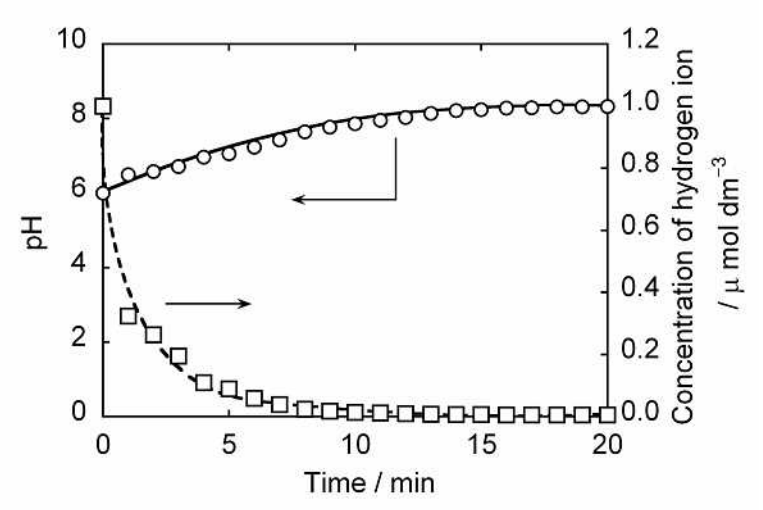

Fig. 3.7. Time course of pH variation of 40-cm^3 water containing 30 mg of the GS power.

the photocatalytic reaction. The suspended mixture of TiO_2 with graphite or activated carbon (Fig. 3.6) showed no enhancement effect for hydrogen production. However, the

calcined GS with negligible carbon maintained ability to enhance the hydrogen gas evolution. The ability was almost equal to that of the untreated powder of GS. These results strongly suggest that the carbon in GS dose not play an important role in the synergy effect between GS and TiO_2. The clay fraction separated from GS showed the synergy effect comparable to both powders of untreated and calcined GS as shown in Fig. 3.6. This fact indicates that the clay in GS is mainly responsible for the synergy effect of GS and TiO_2 for the hydrogen production. Table 3.2 shows the metal species eluted from GS. We can see that various metal species are eluted from GS. As shown in Fig. 3.6 (see "GS-filtered suspension"), the presence of these metal species alone in the absence of the GS particles was not effective in the photocatalytic hydrogen production by TiO_2. This means that the interaction between GS and TiO_2 particles is important for the synergy effect. Fig. 3.7 shows the time variation of pH after adding 30 mg of GS to 40 cm^3 of water containing no TiO_2. The pH values increased with time and reached equilibrium pH of about 8 after ca.10 min from starting pH of 6, resulting in pH

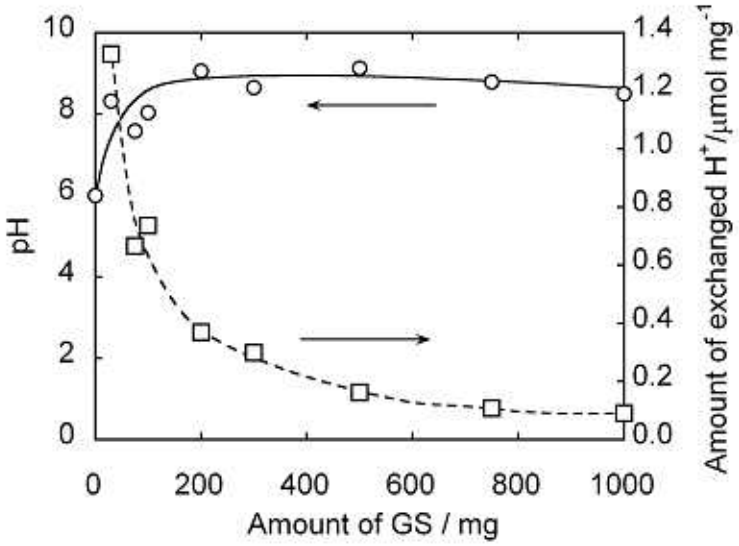

Fig. 3.8. The dependence of both the equilibrium pH and the exchanged hydrogen ions per 1-mg GS on the amount of GS. Various amounts of GS were added to 50 cm^3 of water.

increments of about 2. The very similar pH increment by the presence of GS was also observed in water containing TiO_2. The pH increment and the elution of metal ions strongly suggest that GS particles exchange their metal ions for hydrogen ions in water. This suggests that most metal ions at active ion-exchange sites are replaced by the hydrogen ions in the suspension used for hydrogen production. Sayama and Arakawa

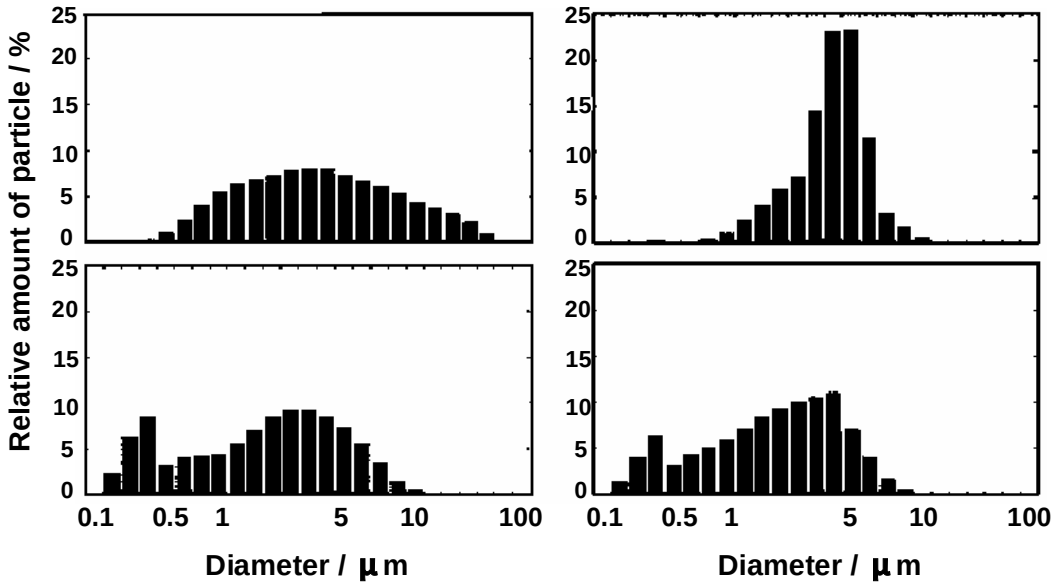

Fig. 3.9. Particle size distribution of several kinds of powders in water. (a) GS alone, (b) TiO_2 alone, (c) GS-TiO_2 mixture and (d) after ultrasonication of GS-TiO_2 mixture. Note the logarithmic abscissa.

reported that an addition of carbonate salts to Pt-loaded TiO_2 suspensions leads to highly efficient stoichiometric photocatalytic decomposition of liquid water into H_2 and O_2 [15]. They found that neither the pH nor cation directly contributes to the water splitting, but the presence of a high concentration of carbonate ions is essential for the catalytic photodecomposition of water. This also strongly suggests that a simple shift of pH to higher values and the presence of cations are not effective, but the coexistence of GS and TiO_2 powders is essential for the photocatalytic hydrogen production in the

present system. Fig. 3.9 shows the particle size distribution of various suspensions. Fig. 3.9(a) and (b) are size distributions of GS and TiO_2 particles, respectively, which were added to water and allowed to stand for 1 day. It is considered that some particles of GS or TiO_2 are self-agglutinated. The size distribution of the GS–TiO_2 mixture is shown in

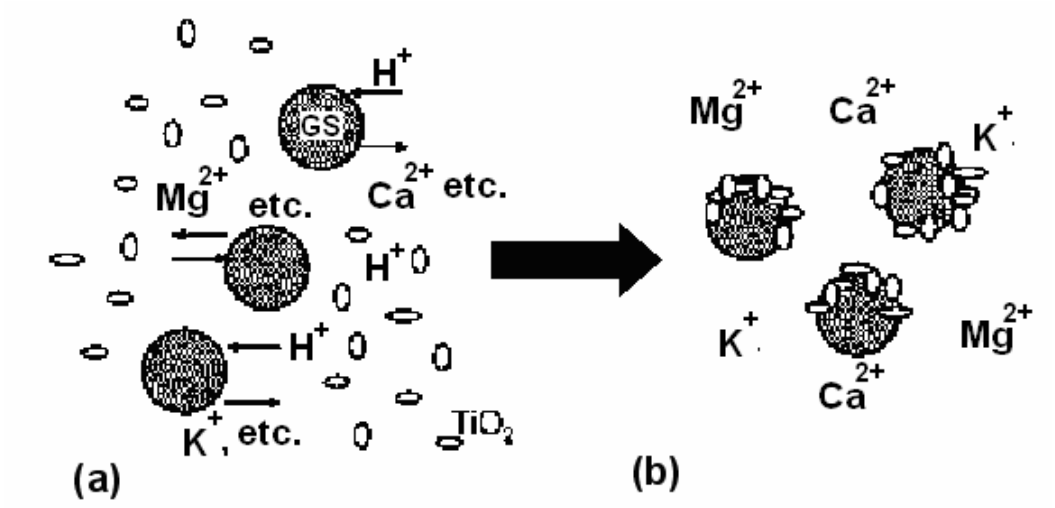

Scheme 3.1. (a) Ion exchange between metal ions and hydrogen ions by the clay in GS. (b) Aggregation of both particles of GS and TiO_2.

Fig. 3.9(c). The pattern of distribution differs from a simple composite of those shown in Fig. 3.9(a) and (b). This result shows that the self-aggregates of GS or TiO_2 were reconstructed to co-aggregates of GS and TiO_2 by mixing them together. Fig. 3.9(d) shows the size distribution of the GS–TiO_2 mixture after ultrasonication. Some of co-aggregates were separated into small particles below around 1 μm in diameter by ultrasonication. Fig. 3.10 shows SEM images of samples after drying suspensions. Fig. 3.10(A) and (B) are photographs of GS and TiO_2 samples, respectively. The SEM images of the GS–TiO_2 mixture are shown in Fig. 3.10(C) and (D). We can see that TiO_2 particles agglutinate with certain parts of GS surface, especially as seen in Fig. 3.10(C).

All the obtained data reveal that there is the strong interaction between GS and TiO_2.

Scheme 3.1 shows a plausible aggregation process between GS and TiO_2 in a stirring step before irradiation. The GS particles elute several kinds of metal ions and exchange them for hydrogen ions in suspension. The ion–exchange makes the surface of

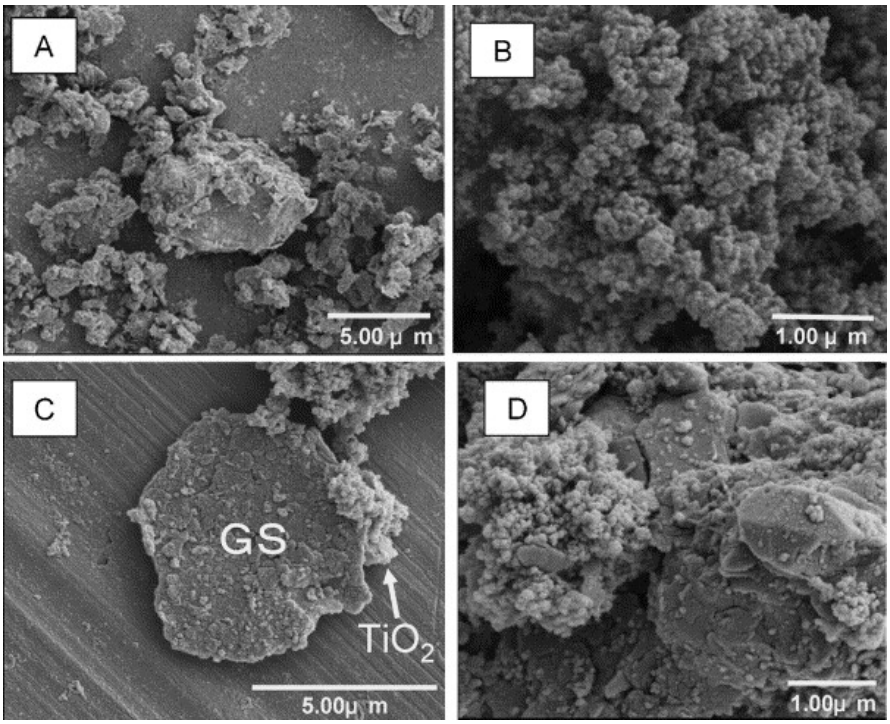

Fig. 3.10. SEM image of samples after drying suspensions.
(A) GS, (B) TiO_2,(C)and(D) GS-TiO_2 mixture.

GS to a more hydrophilic and hydrogen-ion-rich one. The surface of a TiO_2 powder (Degussa, P 25) is hydroxylated (–TiOH) at around pH 6.6 [16,17]. However, the –TiO− groups coexist and become dominant at pH values higher than 6.6. Hence, GS clumps together with negatively charged TiO_2 to give the particles centered at a particle size of about 4 μm. Taking these results into consideration, the reaction model is illustrated as shown in Scheme 3.2. It is considered that the hydrogen ions held in the clay are the main source of hydrogen gas evolved. Though 15 mg of GS contains the clay

components of about 3 mg, the co-catalytic property of GS itself was comparable to that of 15 mg of the clay. This suggests that the synergy effect of GS and TiO_2 is not fully induced by the clay alone. In this connection, we also studied the addition effect of commercially and naturally available clay to TiO_2. The addition of the clay such as Kunipia F (99% sodium montmorillonite), Kunigel-V1 (natural Na-type bentonite) and

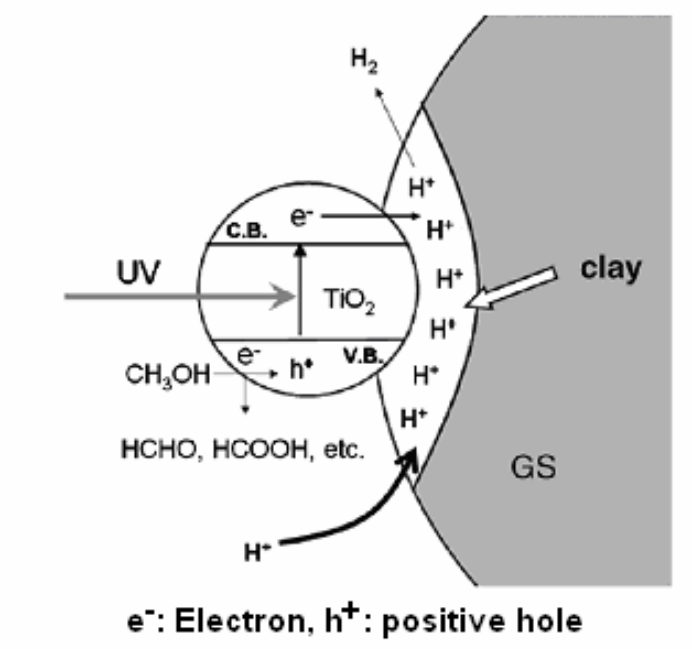

Scheme 3.2. Increment of hydrogen production by the photocatalytic reduction of hydrogen ions held in the clay in GS.

Sumecton SA (synthesized smectite) of Kunimine Industries Co. Ltd., Bengel A (purified montmorillonite, Hojun Co. Ltd.) and kaolin (natural clay, mostly kaolinite) instead of GS to TiO_2 did not enhance the hydrogen production at all. This suggests that clay itself may not have the active sites for the hydrogen production and also that the clay may play the lead in the hydrogen production when it is in GS. Further studies are needed to clarify all aspects of the mechanism of the synergy effect and the detailed surface structure of GS.

Moreover, we report the enhancement of photocatalytic hydrogen production from methanol aqueous solution containing mixture of TiO_2 and GS by the laser ablation in liquid. It was found that the amount of hydrogen gas with the GS-TiO_2 mixture lased

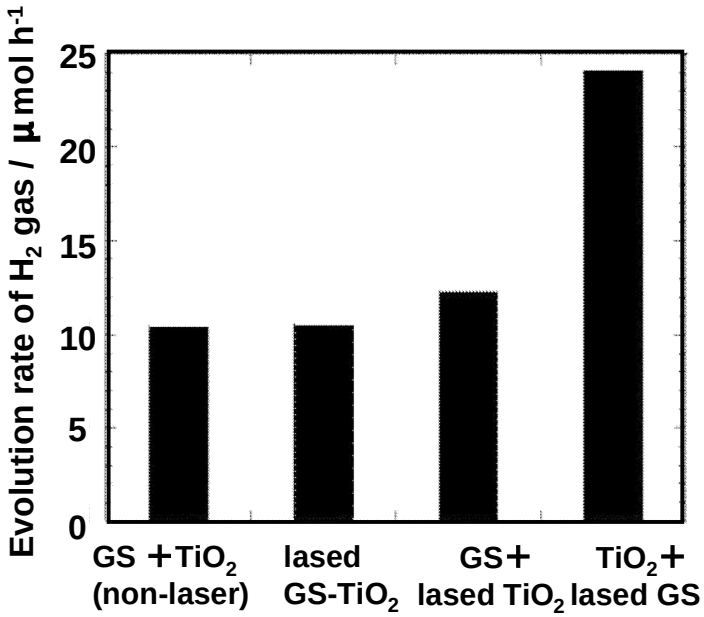

Fig. 3.11. The effect of laser ablation on the rates of hydrogen production from the aqueous methanol solution containing TiO_2 and GS.

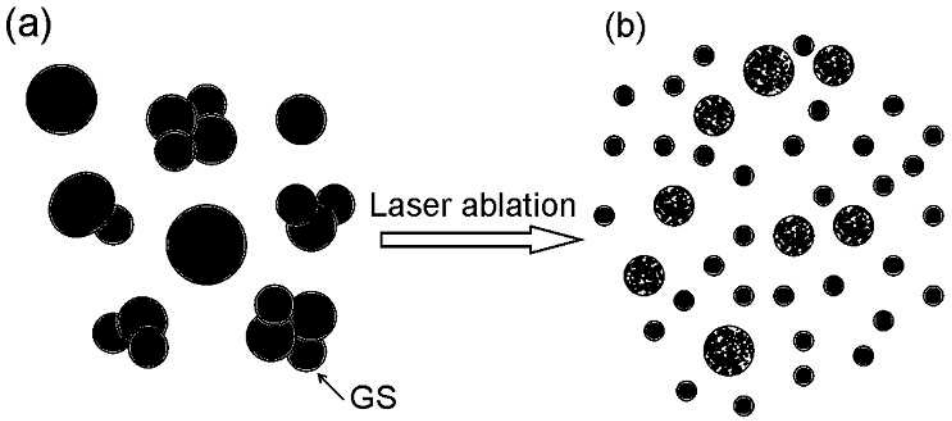

Fig. 3.12. A plausible model for the change of GS particulate aggregation. (a):

was two times as large as that of the raw GS-TiO_2 mixture as shown in Fig. 3.11. This enhancement effect may be attributed to increase in the reaction surface area by the fine-subdivided GS particles as shown in Fig. 3.12.

3.4. References

[1] S. Shimada, N. Akazawa, J. Ceram. Soc. Jpn. 106 (1998) 935.

[2] S. Shimada, N. Akazawa, K. Kudo, J. Ceram. Soc. Jpn. 104 (1996) 992.

[3] G.R. Bamwenda, S. Tsubota, T. Nakamura, M. Haruta, J. Photochem. Photobiol. A: Chem. 89 (1995) 177.

[4] M. Kawai, T. Kawai, S. Naito, K. Tamaru, Chem. Phys. Lett. 110 (1984) 58.

[5] T. Sreethawong, Y. Suzuki, S. Yoshikawa, Int. J. Hydrogen Energy 30 (2005) 1053.

[6] K.E. Karakitsou, X.E. Verykios, J. Catal. 134 (1992) 629.

[7] M. Haruta, Catal. Today 36 (1997) 153.

[8] T. Kawai, T. Sakata, Chem. Phys. Lett. 72 (1980) 87.

[9] K. Hirano, K. Inoue, T.Yatsu, J. Photochem. Photobiol. A: Chem. 64 (1992) 255.

[10] K. Hirano, H. Asayama, A. Hoshino, H. Wakatsuki, J. Photochem. Photobiol. A: Chem. 110 (1997) 307.

[11] K.L. Currie, Comput. Geosci. 17 (1991) 77.

[12] J. Sato, J. Kohno, S. Ono, Chikyuu-no-megumi (1990) 255.

[13] C.R. Schmitt, S.T. Benton, Powder Technol. 6 (1972) 109.

[14] S. Sato, J.M. White, Chem. Phys. Lett. 72 (1980) 83.

[15] K. Sayama, H. Arakawa, J. Chem. Soc., Faraday Trans. 93 (1997) 1647.

[16] H.P. Boehm, Angew. Chem. 78 (1966) 617.

[17] H.P. Boehm, Discuss. Faraday Soc. 52 (1971) 264.

CHAPTER 4

FABRICATION OF TWO-LAYER THIN FILM BY LASER ABLATION METHOD AND APPLICATION TO PHOTOCATALYTIC PHOTODECOMPOSITION AND HYDROGEN PRODUCTION

4.1. Introduction

Photocatalysts have attracted much interest due to their numerous applications in the decomposition of pollutants and in the photoinduced hydrogen production. Since Fujishima and Honda discovered the photocatalytic splitting of water on TiO_2 electrodes [1], TiO_2 has drawn considerable attention. TiO_2 is a nontoxic, cheap and very stable compound, which has numerous applications such as production of white pigments and cosmetics. Photocatalytic hydrogen production is a valuable sustainable-energy technology. This is because solar energy is converted to chemical energy in the form of hydrogen. Hydrogen is considered as an ideal fuel for the future because it can be produced from clean and renewable energy sources such as solar energy and water. There have been many reports on the production of hydrogen from water using TiO_2 [2-7]. When TiO_2 is exposed to light, it absorbs the UV portion of light. This leads to the generation of electrons (e^-) and holes (h^+) at the conduction band and valence band, respectively. The electrons found in the conduction band of TiO_2 can reduce protons from water to produce hydrogen gas. This process is usually catalyzed by platinum catalyst. The addition of a sacrificial electron donor such as alcohols can enhance

hydrogen production by preventing the reverse reaction which is the recombination of electrons and holes.

TiO_2 has also been extensively used for the decomposition of organic wastes [8-10]. The surface properties of TiO_2 such as pH, surface defects and crystalline phase are important parameters in determining the photocatalytic activities because the photocatalytic reaction occurs on the surface of TiO_2. The modification of the surface charge of TiO_2 by nafion has been reported [11] and led to enhance the photocatalytic activities for the decomposition of charged organic compounds. It was found in our laboratory that graphite silica (GS) has the ability to enhance the hydrogen production as a co-catalyst due to its property to enrich the hydrogen ions [12, 13]. In these previous papers, we proposed the mechanism of the synergy effect between GS and TiO_2 as follows. (1) The clay components in GS particles have the ability to elute several kinds of metal ions and exchange them for hydrogen ions in the suspension. The resultant GS surface becomes more hydrophilic and hydrogen-ion-rich. (2) The pH values of the suspension increase to ca. 8 from starting pH of 6 by adding GS. At pH values higher than 6.6, the $-TiO^-$ groups dominate on the TiO_2 surface [14]. The negatively charged TiO_2 clamps together with GS. (3) The hydrogen production is therefore increased by the photocatalytic reduction of hydrogen ions held in the clay in GS.

In this paper, we report the fabrication and characterization of bilayer thin films composed of GS and TiO_2 (GS / TiO_2) prepared by the laser ablation method. A laser ablation method has several advantages [15-18]: high purified thin films can be prepared because of its simple system, we can control many experimental parameters and any materials from pure elements to multicomponent compounds can be used as a

target. In this study, we found the enhancement effect in the photocatalytic activity of TiO_2 thin films by using GS as a co-catalyst film.

4.2. Experimental

The experimental setup for the laser ablation is illustrated in Fig.1.4. Two types of target were used, one containing only TiO_2 and another containing only GS. The targets were prepared by mixing either 5.5 g of TiO_2 (Degussa P25) with 0.55 g of paraffin (10%) or a similar amount of GS (Nishi-nihon Environmental Engineering Inc. [11,12]) with paraffin to prevent cracking. The mixed powder was pressed at 20 MPa for 1 h and calcined at 400 °C for 6 h to form TiO_2 and GS pellets.

The pellet was introduced into the chamber and the experimental conditions were adjusted. A laser power of 2.8 J / (pulse cm^2) was used throughout the experiment. The wavelength of laser is 532 nm (Nd-YAG Laser). The distance between the substrate and the target was 3 cm when TiO_2 was used as the target, whereas it was 7 cm when GS was used as the target. O_2 gas was flowed into the chamber through a mass flow meter to control the pressure at 133 Pa when TiO_2 pellet was used as the target. The substrate temperature and the laser irradiation time were 600 °C and 12 min, respectively, when TiO_2 was used as the target, whereas the laser irradiation time was changed for adjusting the GS thickness when GS was used as the target.

Irradiation of the target with a laser beam melted the target to form a plume. The plume was accumulated on the quartz substrate to form the TiO_2 thin film. The process was repeated using the TiO_2 film as the substrate and GS as the target. Upon irradiation of the GS target with laser light, GS was melted and accumulated on the TiO_2-film surface to form the GS / TiO_2 thin film.

The thin films prepared were characterized by X-ray diffraction (XRD) using an X-ray diffractometer (Rigaku) with Cu Kα radiation. Scanning electron microscopy (SEM) images of the thin films were also taken using a Hitachi S-4100 microscope.

The photocatalytic activity of the prepared thin films was evaluated by measuring the rate of decomposition of methylene blue and also the production of hydrogen in water-methanol mixture. The thin film was fixed on a stand and placed in a 50 cm^3 beaker containing 1×10^{-5} mol / dm^3 methylene blue. This solution was irradiated from the top of the beaker under UV light by using a super-high-pressure mercury lamp (Ushio 500 W). A UV-D33S filter was used to cut-off visible light. The rate of decomposition of methylene blue was determined by measuring the change in absorbance of methylene blue during irradiation, using a Shimadzu MPS-2000.

For hydrogen production, the thin film was immersed in a 10 cm^3 water-methanol mixture contained in a 40 cm^3 cylindrical flask. The top of the flask was sealed with a silicone rubber septum. To remove oxygen gas, the suspended solution was bubbled with Ar gas (about 5 ml / min) for 1 h with stirring. Then photoirradiation was carried out under an Ar atmosphere of about 1 atm with stirring. The evolved gas was sampled through the silicone rubber septum by using a locking-type syringe at a constant time interval and the sampled gas was quantitatively analyzed by a gas chromatograph (detector; thermal conductivity detector (TCD), column packing; molecular sieve 5 Å, carrier gas; Ar). A super-high-pressure mercury arc lamp (Ushio 500 W) was also used as a UV light source with a UV-D33S filter.

4.3. Results and discussion

Initially the properties of TiO_2 thin films prepared by the laser ablation method were

studied. The epitaxial growth occurred at 600 °C and resulted in the rutile and anatase forms of TiO_2. The peaks of TiO_2 (rutile and anatase) decreased with decreasing substrate temperature. At room temperature (about 25 °C), the XRD spectrum of the TiO_2 thin film did not show any peak. It strongly suggests that the film is amorphous. The absence of XRD peak at room temperature and its presence at higher temperatures can probably be attributed to that there is no sufficient energy to crystallize TiO_2 at room temperature, whereas at higher temperatures the energy is sufficient to crystallize TiO_2 (rutile and anatase) in the thin film. It was found that the amorphous TiO_2 thin film had no photocatalytic activity for the hydrogen production, and that under the conditions of O_2 atmosphere and high temperature of the substrate, the anatase was easily formed (data not shown). Therefore, 600 °C (the maximum temperature of our apparatus) under 133 Pa O_2 pressure were used as substrate temperature for the preparation of the TiO_2 thin film. The XRD pattern of the TiO_2 thin film is shown in Fig. 4.1(c).

Next the GS thin film on the quartz substrate was prepared by the laser ablation method. GS is mainly composed of quartz and clay components [12, 13]. The XRD peaks of GS powder are almost composed of crystal-originating peaks as shown in Fig. 4.1(a), whereas the thin films of GS (Fig. 4.1(b)) did not show any peak corresponding to the quartz contained in GS. No growth of the crystal was observed even if substrate temperature was high. We show the XRD patterns of the GS thin film (laser power: 2.8 J / (pulse cm^2), distance between substrate and target: 7 cm, irradiation time: 30 min, atmosphere: O_2 133 Pa, substrate temperature: 600 ºC) in Fig. 4.1(b) as the representative of these GS films. This observation suggests that the laser ablation is responsible for the generation of amorphous silica from quartz in GS. It was found in

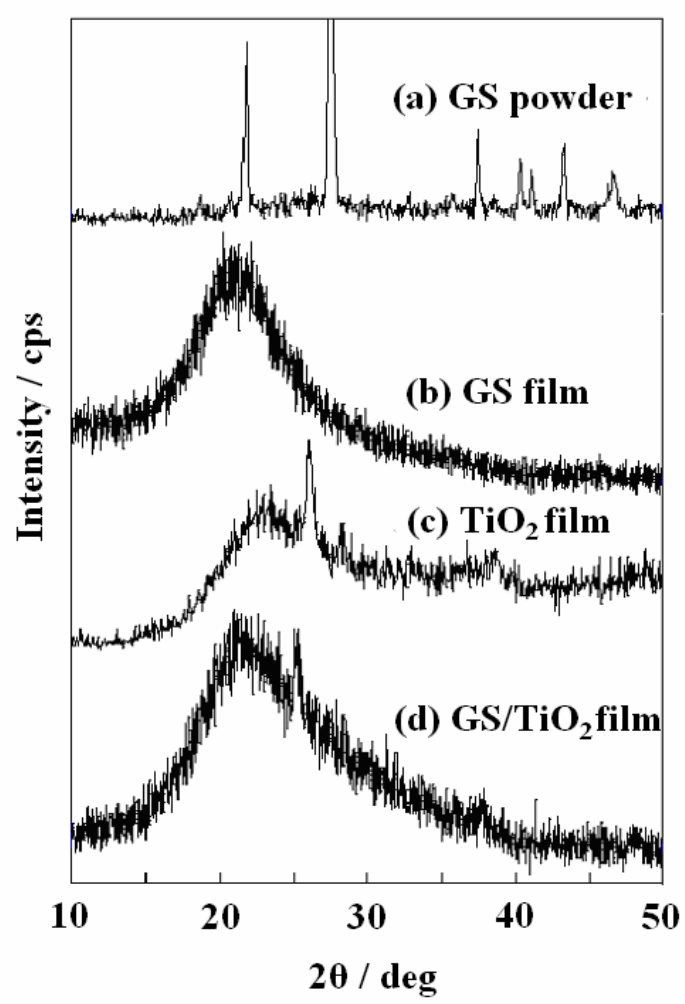

Fig. 4.1. XRD patterns of the (a) GS powder, (b) GS film (laser power: 2.8 J / pulse cm^2, distance between substrate and target: 7 cm, irradiation time: 30 min, atmosphere: O_2 133 Pa, substrate temperature: 600 ºC), (c) TiO_2 film (laser power: 2.8 J / pulse cm^2, distance between substrate and target: 3 cm, irradiation time: 12 min, atmosphere: O_2 133 Pa, substrate temperature: 600 ºC) and (d) GS/TiO_2 (the TiO_2 film was prepared under same conditions as (c), GS film on the TiO_2 film was prepared under the conditions: laser power is 2.8 J / pulse cm^2, distance between substrate and target is 7 cm, irradiation time is 5 min, atmosphere is O_2 133 Pa, substrate temperature is 600 ºC).

the previous papers [12, 13] that the clay portion in GS mainly contribute to the activity of hydrogen production as a co-catalyst. Therefore it is suggested that the GS film which had no quartz peaks of XRD may be also effective as a co-catalyst.

The preparation of bilayer film (GS / TiO_2 film) was tried on the basis of these results. The XRD pattern of the GS / TiO_2 film is shown in Fig. 4.1(d). We can find only

TiO_2 crystal peaks although the TiO_2 peaks shown in Fig. 4.1(b) are significantly affected in Fig. 4.1(d) by the strong GS amorphous intensity. Fig. 4.2 shows the SEM images of (a) TiO_2 and (b) GS / TiO_2 thin films (laser irradiation time of GS target is 2 min). In Fig. 4.2(a), larger particles were composed of smaller ones, the average particle size of which was around 50 nm. In Fig. 4.2(b), the smaller sized particles around 50 nm are mainly attributed to TiO_2, while the particles ranging from about 500 nm to about 1 μm are attributed to GS which was deposited on the surface of the TiO_2 thin film.

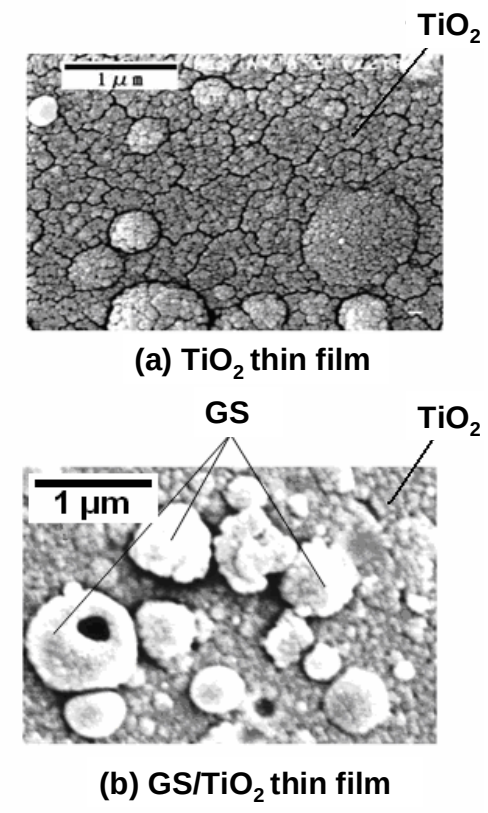

Fig. 4.2. SEM views of (a) the TiO_2 thin film and (b) the GS / TiO_2 thin film.

We also attempted to deposit TiO_2 on GS film (TiO_2/GS film). However, the GS film was easy to peel with an increase in the thickness of the GS film. It is suggested

that the clay in GS prevents the connection of Si-O bonds in quartz when the thickness is large. Therefore we used the GS/TiO_2 film (GS was deposited on the TiO_2 film) for the hydrogen production and the decomposition of the organic compound.

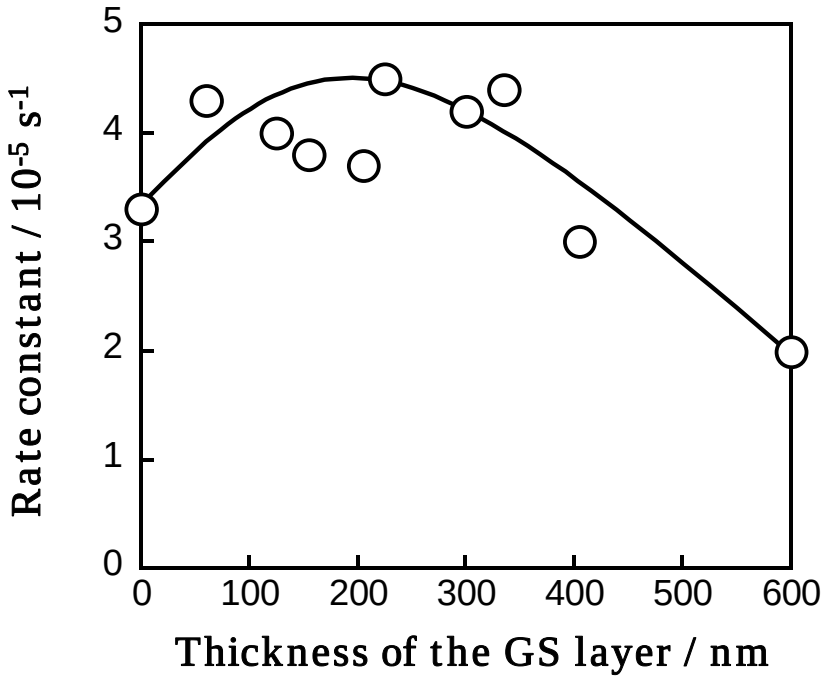

Fig. 4.3. Effect of GS loading on degradation rate of methylene blue.

Fig. 4.3 shows the effect of GS loading on the rate of degradation of methylene blue. This kind of reaction can be represented as follows.

$$-d[MB]/dt = k\,[MB] \qquad (1)$$

Integration of equation (1) gives

$$\ln ([MB] / [MB]_0) = -kt \qquad (2)$$

where $[MB]_0$ is the initial concentration of methylene blue, [MB] is the concentration of methylene blue after time t of photocatalytic decomposition and k is a rate constant related to the reaction properties of the solute. The rate constants (k) for the pseudo first

order reaction were obtained from the initial linear portion using equation (2). The rate of degradation of methylene blue increases up to a GS thickness of around 200 nm and decreases through the maximum. GS deposited on the TiO_2 thin film is probably responsible for the increase in the rate of degradation of methylene blue. This is because the clay portion of GS has an ion-exchange property which creates an excess of OH^- ions in the solution [13] as shown in Fig. 4.5 (a). These OH^- ions may be adsorbed on the TiO_2 surface giving the GS/TiO_2 thin film an overall negative charge. Since methylene blue is positively charged, it can be easily adsorbed to the surface of the TiO_2 thin film. A similar mechanism has been proposed for the surface modification of TiO_2 by an anionic Nafion-polymer [7]. The hydroxide ion (OH^-) can be changed to hydroxide radical (·OH) by giving its electron to a hole in TiO_2 under UV light. The ·OH radical can attack organic compounds. This is also one of the reasons for the enhancement in the photocatalytic activity for the decomposition of methylene blue.

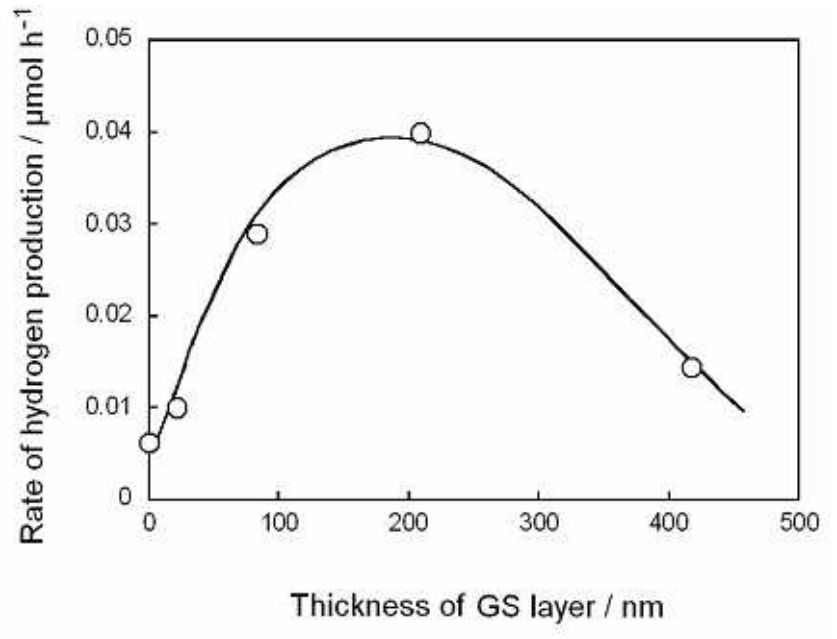

Fig. 4.4. Effect of GS loading on H_2 production rate.

Fig. 4.4 shows a similar trend on the rate of hydrogen evolution which also increases up to a GS thickness of around 200 nm and decreases through the maximum. The increase in the rate of hydrogen production is also related to the presence of GS in the film. It was found that the clay potion in GS enhances the activity of the hydrogen production [12, 13]. The clay elutes several kinds of metal ions and exchanges them for hydrogen ions in suspension. The proton stored in the clay in GS reacts with the electron in the conduction band of TiO_2 in the thin film as shown in Fig. 4.5 (b), resulting in the enhancement of the hydrogen production. The fact that there was optimal GS loading for the degradation of methylene blue and the H_2 production indicates that excessive GS loading on the TiO_2 thin film inhibits the overall photocatalytic activity. It seems that higher GS coverage on TiO_2 blocks the active sites for the photocatalytic activity.

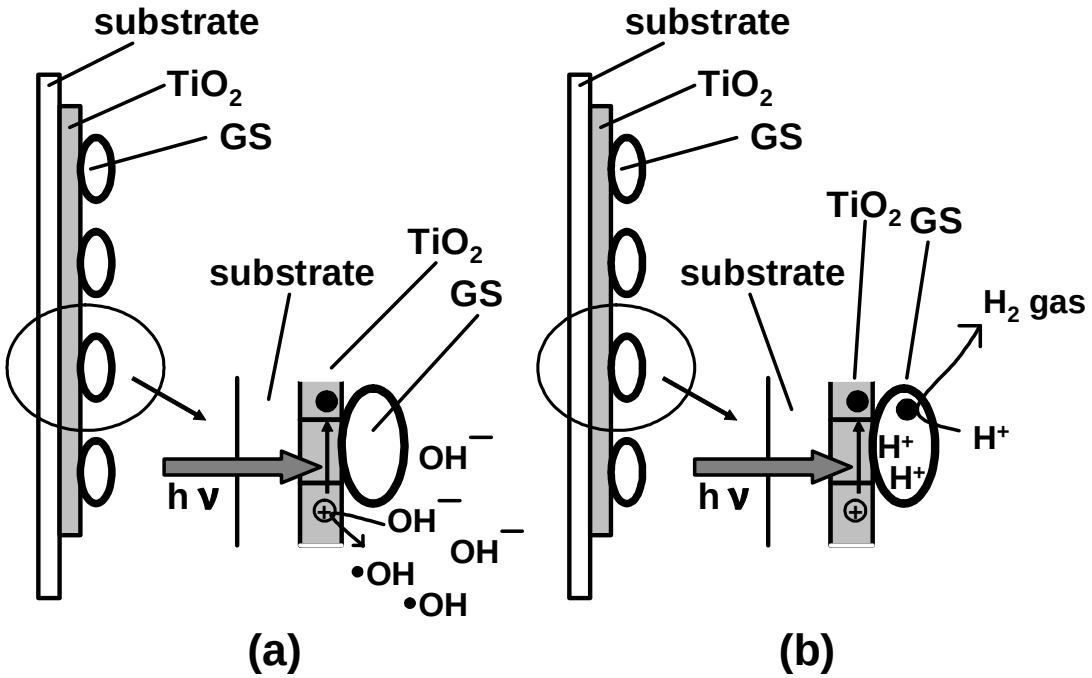

Fig. 4.5. Mechanism of enhancement of photocatalytic activities for (a) decomposition of methlene blue and (b) H_2 production rate by GS loading.

4.4. Conclusion

The photocatalytic activity of TiO_2 thin film for the hydrogen production and the decomposition of organic compound is enhanced by the deposition of GS which has a property of clay. The experimental results showed that the clay in GS was a key component. It was concluded that the enhancement is attributed to the enrichment of hydrogen ions in the clay components of GS. The present study may be expected to contribute to the novel development of the practical co-catalyst in the usage of thin films.

4.5. References

[1] A. Fujishima, K. Honda, *Nature* 38 (1972) 37.

[2] L. Loy, E.E. Wolf, Sol. Energy 34 (1985) 455.

[3] S.A. Nanan, N.H. Al-Mishhandani, L.M. Al-Shamma, Int. J. Hydrogen Energy 20 (1995) 303.

[4] E.A. Malinka, G.L. Kamalov, J. Photochem. Photobiol., A 81 (1994) 193.

[5] A. Selvaggia, C. Tosib, U. Barberinia, E. Franchib, F. Rodriguezb, P. Pedronib, J. Photochem. Photobiol., A 125 (1999) 107.

[6] M. Ni, M.K.H. Leung, D.Y.C. Leung, K. Sumathy, Renew. Sust. Energ. Rev. 11 (2007) 401.

[7] J. Zhang, P. Du, J. Schneider, P. Jarosz, R. Eisenberg, J. Am. Chem. Soc. 129 (2007) 7726.

[8] E. Obuchi, T. Sakamoto, K. Nakano, Chem. Eng. Sci. 54 (1999) 1525.

[9] K. Tanaka, K. Padermpole, T. Hisanaga, Wat. Res. 34 (2000) 327.

[10] K. Tanaka, W. Luesaiwong, T. Hisanaga, J. Mol. Catal. A: Chem. 122 (1997) 67.

[11] H. Park, W. Choi, J. Phys. Chem. A 109 (2005) 11667.

[12] M. Ikeda, Y. Kusumoto, Y. Yakushijin, S. Somekawa, P. Ngweniform, B. Ahmmad, Catal. Commun, 8 (2007) 1943.

[13] M. Ikeda, Y. Kusumoto, S. Somekawa, P. Ngweniform, B. Ahmmad, J. Photochem. Photobiol., A 184 (2006) 306.

[14] H.P. Boehm, Discuss. Faraday Soc. 52 (1971) 294.

[15] N. Inoue, H. Yuasa, M. Okoshi, Appl. Surf. Sci. 197 (2002) 393.

[16] S. Kitazawa, Y. Choi, S. Yamamoto, Vacuum 74 (2004) 637.

[17] H. Usui, O. Miyamoto, T. Nomiyama, Y. Horie, T. Miyazaki, Sol. Energy Mater. Sol. Cells 86 (2005) 123.

[18] S. Somekawa, Y. Kusumoto, M. Ikeda, B. Ahmmad, Y. Horie, Catal. Commun, 9 (2007) 437.

CHAPTER 5

EFFECT OF CARBON NANOMATERIALS ON TiO_2 PHOTOCATALYSIS FOR HYDROGEN PRODUCTION FROM WATER-ALCOHOL MIXTURES

5.1. Introduction

Scientists all over the world are very interested in hydrogen gas as the most promising energy resources to overcome the future energy crisis. The photocatalytic decomposition of water into hydrogen and oxygen has been regarded as one of the most potential approaches ever since Fujishima and Honda reported the photoelectrochemical water splitting using a TiO_2 electrode [1]. In the last two decades vast researches have been conducted which can be perceived by several review papers and books related to hydrogen generation [2-4].

Due to their unique chemical and physical properties, carbon nanotubes have attracted the interest of numerous researchers for their application in diverse fields. Catalysis, in particular heterogeneous catalysis, has also been envisaged as a potential field [5]. For example, Savva et al. [6] recently reported hydrogen production by ethylene decomposition over Ni supported on carbon nanotubes (CNTs) and nanofibers. They presented the development of a novel Ni catalyst supported on multi walled carbon nanotubes (MWNTs) and nanofiber for direct decomposition of ethylene at 400 °C to produce CO-free H_2.

To date CNTs have not been used as co-catalysts for H_2 production from

water-alcohol mixtures. To our best knowledge, we report here for the first time the photocatalytic H_2 gas production from aqueous alcohol solution using simple mixture of TiO_2 and CNTs.

5.2. Experimental

The photoreaction was carried out under Ar atmosphere in a pyrex tube of ca. 154 cm^3, maintaining the reaction mixture in suspension by a magnetic stirrer. A super high-pressure mercury lamp (Ushio 500W USH-500SC) was used as the light source. Single walled carbon nanotubes (SWNTs) with purity of 20-40% were obtained from Materials Technologies Research Ltd (USA) and were used without further purification. Preferred amounts of TiO_2 (Degussa P25) and SWNTs were put into the flask and then water/alcohol mixtures were added. Prior to irradiation, the suspension of the catalyst was dispersed in an ultrasonic bath for 5 min and Ar gas was bubbled through the reaction mixture for 1 h to remove oxygen gas. As for the decomposition reaction of methanol, O_2 gas was bubbled through the mixture for 30 min. Gas sampling was made through the silicon rubber septum using a locking-type syringe at a constant time interval, usually 15 min. The quantitative analysis of gas samples was performed by gas chromatography (column packing: MS5Å or porapak N, carrier gas: Ar, detector: TCD). After photoirradiation, the filtrate solution was analyzed by an ion chromatographic analyzer (IC 7000, Yokogawa) equipped with a recorder (SIS chromatocoder 12). The particle size was measured by a laser scattering particle size distribution analyzer (Horiba LA-920).

5.3. Results and discussion

Fig. 5.1 shows the dependence of the rate of H_2 gas evolution on the SWNTs content to TiO_2 after 1 h irradiation from 50 vol% methanol-, ethanol- and 1-propanol-water mixtures. We can see a drastic increase in the amount of evolved H_2 gas when small amounts of SWNTs are added to TiO_2. This is due to the synergy effect of TiO_2 and SWNTs, which emerges from the high electric conductivity of the latter [7].

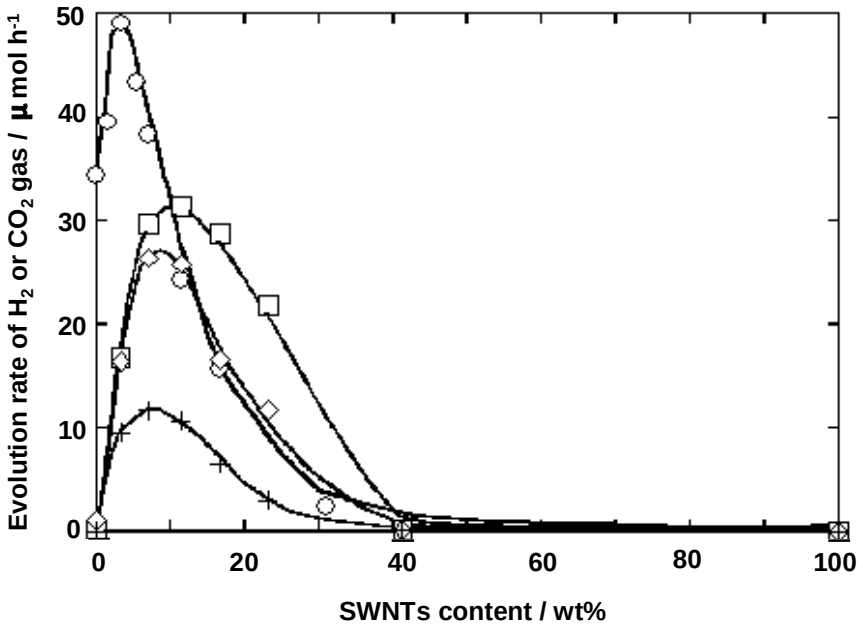

Fig. 5.1. Plots of the evolution rate of H_2 or CO_2 gas vs. the SWNTs content to TiO_2 (Total amount of catalyst: 30 mg, alcohol content: 50 vol%). ○ CO_2 from methanol aqueous solution, H_2 from □ methanol, ◇ ethanol, + 1-propanol aqueous solution.

With an increase in the amount of SWNTs, the surface area for reduction of H^+ ion increases. A maximum of H_2 gas generation is found around 7-11 wt% of SWNTs content. However, larger amounts of SWNTs will impair the absorption of UV light by TiO_2. This results in a decrease in the evolution rate of H_2 above ca. 11 wt% of the SWNTs. A similar trend for the decomposition of methanol is observed as shown in Fig.

1. The amount of CO_2 evolved increases up to ca. 3 wt% of SWNTs and then decreases through the maximum. It is easy to understand that the larger the amount of SWNTs in the mixed catalysts, the larger the possibility of contact and interaction between TiO_2 and SWNTs becomes, although excess amounts of SWNTs will make the UV absorption by TiO_2 impair as described above. Thus, more electrons migrating to SWNTs via collision reduce more H^+ ions as described in the mechanism shown later.

As seen from Fig. 5.1, the order of increasing H_2 gas production from various alcohols is: methanol > ethanol > 1-propanol. However, at present, we cannot explain the order of H_2 production from different alcohol solutions containing TiO_2/SWNTs. In order to clarify all aspects of the mechanism of the alcoholic effect for the H_2 production in the present system, further studies are need in terms of the morphological change of TiO_2 brought by the addition of SWNTs.

Multi walled carbon nanotubes (MWNTs) are also known to be good conductors [7] and have a larger surface area ranging from 200 to 400 m^2g^{-1} [5]. But it showed a lower effect on the photocatalytic activity of TiO_2: the maximum rate of H_2 evolution was found to be about 2 μmol h^{-1} in the TiO_2/MWNTs system. It is know that the rolling direction of simple graphite sheet has a large effect on the electrostatic characteristics of tubes and the presence of defects on the tube also affects its electric conductivity considerably [7]. The structure of MWNTs is complex. It is commonly known that there are some defects on the surfaces of the tubes and the direction of the rolled graphite sheets is not controlled [5]. These complexities may affect the photocatalytic effect of MWNTs on TiO_2.

The comparison of the photocatalytic activity for the production of H_2 gas between Pt/TiO_2 and SWNTs/TiO_2 mixed powders was made by using an equal quantity of Pt

and SWNTs (9.1 wt% each) together with TiO_2, keeping the methanol content constant at 50 vol% in the solution. The amount of H_2 gas evolved with irradiation time is shown in Fig. 5.2. The amount of H_2 gas evolved from the both systems are nearly same until 1

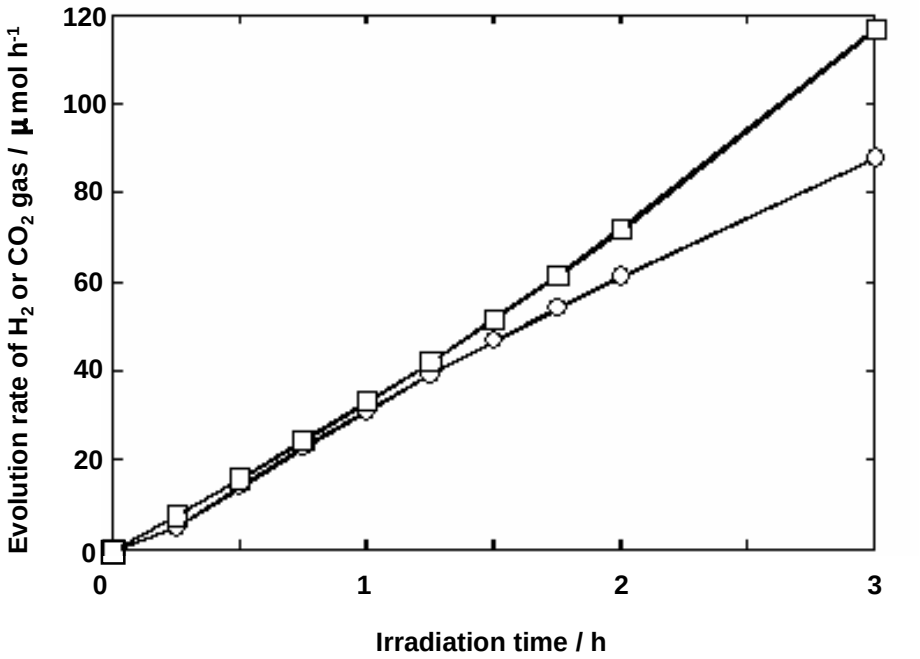

Fig. 5.2. Plots of amount of H_2 vs. irradiation time with SWNTs / TiO_2 and Pt/TiO_2 system(Total amount of catalyst: 30 mg, amount of SWNT and Pt are 9.1wt%). ○ SWNTs/TiO_2, □ Pt/TiO_2.

h irradiation, although after 1 h the amount of H_2 gas in the Pt/TiO_2 system increases a little over the SWNTs /TiO_2 system. It is known that Pt itself at the same time acts as light reflector and thus can remarkably improve the photocatalytic efficiency [8]. The lower H_2 production by the SWNTs/TiO_2 system may be partly attributable to H_2 adsorption, due to pressure increase in the gas phase, to carbon nanotubes and amorphous carbon present in SWNTs used [9]. This amorphous carbon contains graphitic carbon and soot that are unavoidable byproducts of the synthesis processes. These impurities also could decrease the amount of hydrogen generation by hindering

light absorption of TiO_2 photocatalyst. Moreover, “as-prepared SWNT” contains around 30 wt% Ni particles. Therefore, controlled experiments were performed to examine the effect of amorphous carbon and Ni particles present in SWNTs. After 1 h irradiation, the amount of H_2 gas evolved from the mixtures of TiO_2/active carbon/graphite and also TiO_2/Ni were 0.45 μmol h^{-1} and 7.6 μmol h^{-1}, respectively. The amount of H_2 evolution from the TiO_2/SWNTs system is 5 times higher than that from the TiO_2/Ni system.

Mechanically blended SWNTs/TiO_2 composites were also used for H_2 generation. For the preparation of the composite, SWNTs and TiO_2 were weighed in different amounts and blended adequately by smashing with an agate mortar. After 1 h irradiation, the hydrogen evolution rate for smashed powder was considerably higher than that of normal powder as shown in Fig. 5.3. For 9.1 wt% of normal powder a hydrogen evolution rate of about 32 μmol h^{-1} was observed, whereas the same rate was observed for ca. 5.0 wt% of SWNTs to TiO_2 in the case of smashed mixture. For 9.1 wt% of smashed SWNTs/TiO_2 mixture, the highest evolution rate was found to be about 39 μmol h^{-1}. The particle size becomes smaller due to smashing of the catalyst mixture resulting in increase in the surface area of the catalyst. Moreover, a part of TiO_2 particles can be physically deposited over the SWNTs surfaces resulting in easier transfer of electron between them. This fact could be confirmed from the particle size distribution of the mixture of TiO_2 and SWNTs, measured after photoirradiation of the mixtures (data not shown).

In the case of noble metal such as Pt, an electron from photoexcited TiO_2 is transferred to Pt and then it reduces H^+ ion to produce H_2 gas [6]. Carbon nanotubes can be metallic or semiconductive in nature [10]. It was reported by Yu et al. [11] that the

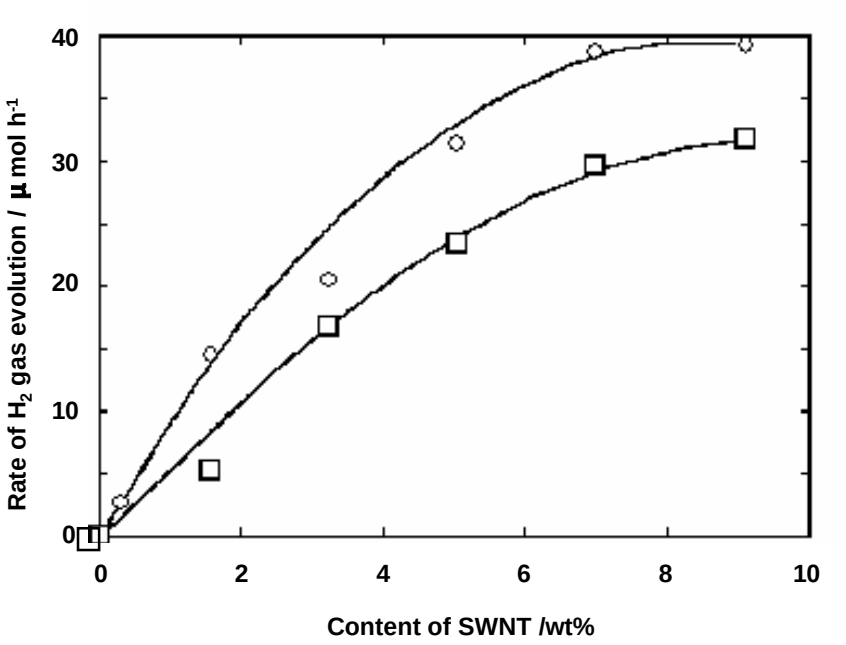

Fig. 5.3. Comparison curve for H_2 production from smashed and non-smashed mixtures of TiO_2 and SWNTs. ○ Smashed, □ Nomal powder.

higher surface area can not be the only factor for the enhancement of the TiO_2 photocatalytic degradation of acetone by SWNTs. They have also shown by photoluminescence spectra that electrons formed by the UV irradiation on the surface of TiO_2 migrate to the surface of SWNTs and thus the high rate of e^-/h^+ pair recombination, which reduces the quantum yield of the TiO_2 photocatalyst, can be decreased. As a result higher H_2 evolution is observed by the addition of SWNTs to TiO_2. Thus, based on the above results, it is possible to propose a mechanism as follows. Photoexcited electrons in TiO_2 are transferred to SWNTs through collision which are then reduce the proton available in the system as shown in Fig. 5.4.

It was reported by Kawai et al. [12] that CH_3OH is oxidized to HCHO, then HCHO to HCO_2H, and finally HCO_2H to CO_2 on a single crystal TiO_2 or ZnO photoanode by a current-doubling process. Since the TiO_2 powder can be regarded as a

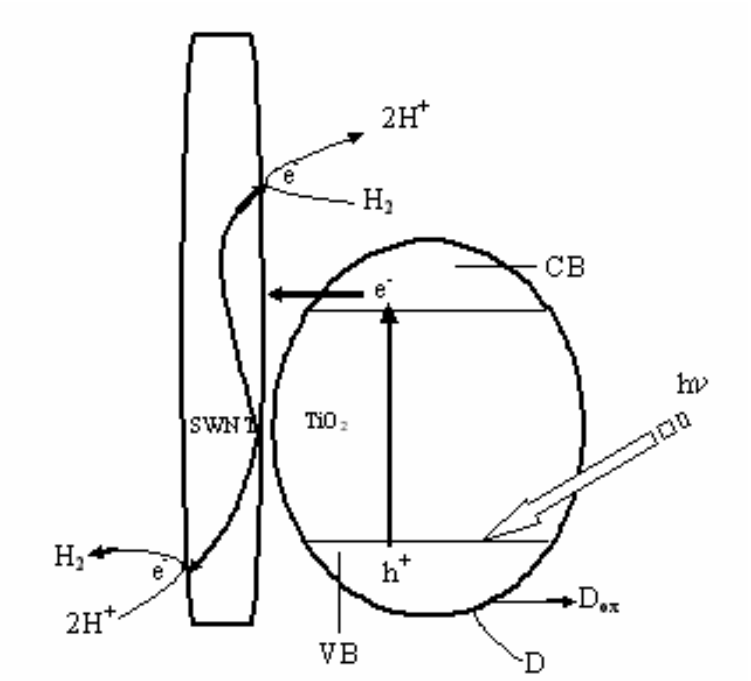

Fig. 5.4. Schematic diagram of proposed mechanism for photocatalytic H_2 production with the SWNTs/TiO_2 mixture system. D: alcohols, D_{ox}: oxidized alcohols.

photoelectochemical microcell, holes generated by the light would oxidize CH_3OH, HCHO and HCO_2H eventually to produce CO_2.

In order to confirm the reaction mechanism, the filtrates after the reactions were finished were analyzed. Formic acid and acetic acid (data not shown) were detected in the reaction mixtures of water and various alcohols by ion chromatography. Also a small amount of CO_2 was observed after 2 h irradiation. Observed results corresponded to the proposed mechanism.

5.4. References

[1] A. Fujishima, K. Honda, Nature 238 (1972) 37.

[2] M. Grätzel, Energy resources through photochemistry and catalysis (Eds.) Academic Press 1983, NewYork.

[3] M. Ni, M. K. H. Leung, D. Y. C. Leung, K. Sumathy, Rnew. Sust. Energ. Rev. 11 (2007) 401.

[4] M. Matsuoka, M. Kitano, M. Takeuchi, K. Tsujimaru, M. Anpo, J. M. Thomas, Catal. Today 122 (2007) 51.

[5] P. Serp, M. Corrias, P. Kalck, Appl. Catal. A: Gen. 253 (2003) 337.

[6] P. G. Savva, G. G. Olympiou, C. N. Costa, V. A. Ryzhkov, A. M. Efstathiou, Catal. Today 102-103 (2005) 78.

[7] R. H. Baughman, A. A. Zakhidov, W. A. de Heer, Science 297 (2002) 787.

[8] M. K. Nazeeruddin, A. Kay, I. Rodicio, R. Humpbry-Baker, E. Müller, P. Liska, N. Vlachopoulos, M. Grätzel, J. Am. Chem. Soc. 115 (1993) 6382.

[9] F. L. Darkrima, P. Malbrunota, G.P. Tartagliab, Int. J. Hydrogen Energ. 27 (2002) 193.

[10] P. M. Ajayan, Chem. Rev. 99 (1999) 1787.

[11] Y. Yu, J. C. Yu, J. G. Yu, Y. C. Kwok, Y. K. Che, J. C. Zhao, L. Ding, W. K. Ge, P. K. Wong, Appl. Cata. A: Gen. 289 (2005) 186.

[12] T. Kawai, T. Sakata, J. Chem. Soc.: Chem. Commun. (1980) 694.

CHAPTER 6

VISIBLE-LIGHT INDUCED HYDROGEN PRODUCTION USING CHLOROPHYLL-A OR CO-TETRA PHENYL PORPHYRIN IN PT-LOADED POLY (L-GLUTAMATE)-DECYLAMMONIUM CHLORIDE COMPLEX AND THE CHARACTELIZATIO

6.1. Introduction

Chlorophyll a (Chl) is a natural green pigment involved in lightharvesting and photochemistry in the photosynthetic energy conversion processes of green plants and related organisms [1,2]. It is the principal photoreceptor in the chloroplasts of green plants. It is also known that Chls are bound to protein in the thylakoid membranes to form Chl–protein complexes. These complexes play a crucial role in the overall conversion of sunlight to chemical energy [2,3]. Chl is a suitable photosensitizer for the conversion of solar energy to chemical energy, because it has very strong absorption bands around the visible region of the spectrum, where the solar output reaching the earth is also maximal. Also the peak extinction coefficient of Chl is higher than 10^5 cm^{-1} M^{-1}, among the highest observed for organic compounds [4]. Although Chl is a very suitable photosensitizer for photoinduced hydrogen production, it aggregates in aqueous solution [2,5,6]. A number of methods such as the use of water–methanol solutions, liposomes and micelle systems have been used to reduce the formation of Chl aggregates, and to enable electron transfer reactions between Chl and some electron

acceptor molecules [1,5–7]. Many reports exist in which hydrogen gas was produced using Chl in microemulsions and in micelle systems in a mixture made up of methylviologen, proton reduction catalyst (hydrogenase, Pt colloid, PtO_2) and a sacrificial electron donor such as ethylenediaminetetraacetic acid ($EDTA^{2-}$), cysteine, and nicotinamide adenine dinucleotide (NADH) [8–13]. In these systems, the electron donor is sacrificial and the reaction stops immediately after all the electron donor has been consumed. By combining oligosaccharide (sucrose or maltose) degradation with invertase and glucose dehydrogenase, NADH is regenerated continuously and hence the electron donor is no more sacrificial. In such a system, an improvement in the yield of hydrogen gas using Chl in a micelle system has been reported in the presence of methylviologen (MV^{2+}) and Pt colloid [13]. In order to get a clue to the role of proteins on the hydrogen evolution in artificial photosynthetic model systems, we have prepared a system in which Chl is solubilized in a Pt-loaded poly(L-glutamate) (Poly(Glu))–decylammonium chloride (DeAC) complex. In the previous works in which the Chl was solubilized in micelles and microemulsions, the solution had to be buffered for hydrogen evolution to occur. In our system there is no need of buffering as the pH is constant at ca. 6.5 and this system is closer to the natural photosynthetic system as it involves of a polypeptide. Visible-light induced hydrogen production was carried out using the above system in the presence of MV^{2+} as an electron acceptor and ethylenediaminetetraacetic acid sodium salt ($EDTA^{2-}$) as a sacrificial electron donor. Spectroscopic methods such as circular dichroism (CD), absorption and fluorescence spectra were used to characterize the reaction medium composed basically of Chl solubilized in the Pt-loaded Poly(Glu)–DeAC complex in the presence of methylviologen. The effect of some of the constituents on the rate of hydrogen evolution was determined. An increase in the rate of hydrogen evolution occurred at the

concentration of DeAC at which a distinct conformational change in Poly(Glu) was indicated from CD spectra.

6.2. Experimental

Chl from Chlorella (Wako, 99%), methylviologen (MV^{2+}) (Sigma, 99%), hydrogen hexachloroplatinate(IV) hexahydrate ($H_2PtCl_6 \cdot 6H_2O$) (Wako, 98.5%) and sodium borohydride ($NaBH_4$) (Wako, 99%) were used as received. Poly(L-glutamate) (Poly(Glu)) (Peptide Institute, molecularweight: 8000) was dissolved in 0.06M (1 M = 1 mol dm^{-3}) NaOH and dialyzed against redistilled water. The concentration of Poly(Glu) was determined by colloid titration with standard potassium poly(vinyl sulfate) solution [14]. Decylammonium chloride (DeAC) was prepared by titration of decylamine (Nacalai Tesque, 99%) with hydrochloric acid [15,16]. The resultant salt formed was recrystallized twice from ethanol and washed with ethyl ether. The other chemicals were analytical grade or the highest grade available. Laboratory deionized water was distilled twice and used throughout the experiment. Circular dichroism (CD) spectra were recorded (190–650 nm range) with a JASCO J-720 spectropolarimeter and digitized data were transferred to a microcomputer and processed. Absorption and steady state fluorescence spectra (excitation wavelength: 435 nm) were recorded on a Shimadzu MPS-2000 spectrophotometer and Shimadzu RF-5000 spectrofluorophotometer, respectively. The platinum colloid was prepared by reduction of hexachloroplatinate (IV) ions with $NaBH_4$ in aqueous Poly(Glu) solution in a mole ratio of 1 : 6 : 40. The presence of reduced platinum particles was confirmed by the disappearance of the 250 nm band attributed to platinum (IV) ions in the absorption spectrum [17]. For hydrogen evolution, a 10 cm^3 sample solution consisting of Chl (1×10^{-5} M), $EDTA^{2-}$ and MV^{2+}

was placed in a Schlenk tube (30 cm^3). The concentration of Pt colloid and that of the polypeptide were kept constant at 2.5×10^{-6} M and 1×10^{-4} M, respectively, throughout the experiment. The pH was not controlled, but was found to be about 6.5. It is well known that the pheophytinization and allomerization of Chl occur in acidic and basic solutions, respectively [18]. Here it should be noted that Chl was stable and did not undergo the pheophytinization nor allomerization. The Schlenk tube was sealed with a silicone rubber septum. Ar gas was bubbled into the solution for 3 h after 2 min sonication to remove oxygen in the solution. The photoirradiation was carried out for 3 h under Ar atmosphere and magnetic stirring. The light source was provided by a 500 W xenon lamp and filtered through a water cell and an L-42 filter (k>ca. 400 nm) and reaction was also carried out in the absence of the filter. Gas sampling was performed at a constant time interval, usually 1 h, through a silicone septum using a 1 cm^3 gas syringe. The gas produced by photoirradiation was quantitatively analyzed by using a Shimadzu GC-8A gas chromatograph (detector: TCD, column packing: MS 5 A˚, carrier gas: Ar). All measurements were carried out at room temperature (about 25 ◦C).

6.3. Results and discussion

To investigate the effect of Poly(Glu) on the overall rate of hydrogen production, the CD spectra of Pt-loaded Poly(Glu) (Pt–Poly(Glu)) in the presence of increasing concentrations of DeAC and then later in the presence of Chl were measured in the 190–250 nm region. We also measured the CD spectra of solutions of Poly(Glu) in the presence of increasing concentrations of MV^{2+}. The CD spectra of Chl were also measured for the same sample but in the Soret and Q-band region (400–700 nm).

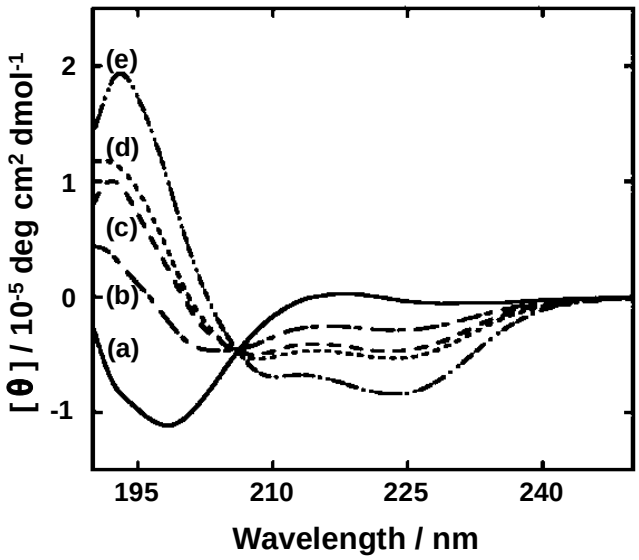

Fig. 6.1. [DeAC] dependence of CD spectra of Pt-Poly(Glu) system in aqueous DeAC solutions. (a) 0, (b) 0.2, (c) 0.4, (d) 0.5, (c) 0.6 mM.

Fig. 6.1 shows the CD spectra of Pt–Poly(Glu) in aqueous DeAC. The spectra vary from a spectrum characteristic of a random coil (with a small positive band at 217 nm and a strong negative shoulder band around 196 nm, Fig. 6.1(a)) to a typical a-helix spectrum which has a double minimum at 209 nm and 222 nm (Fig. 6.1(e)). In Fig. 1, an isobestic point can also be observed around 208 nm, which indicates the one-step transition from the random coil to the α-helix. The addition of Chl to the above system did not lead to any significant change in the CD spectral pattern in the UV region. The CD spectra of the above system in the presence of Chl, in the region of 400–700 nm, also did not show any significant induced circular dichroism. On the other hand, an induced CD with no clear conformation change was observed upon the addition of MV^{2+} to a solution of Poly(Glu) only. The absorption spectrum of Chl in aqueous Poly(Glu) solution shows two bands corresponding to the Soret band at 435 nm and the Q-band at 670 nm [6] with a shoulder around 710 nm. The presence of a shoulder band at lower concentrations of DeAC indicates the formation of Chl aggregates in solution [1,5,6]. Upon the addition of DeAC solution into this mixture, an increase in the absorbance of

the Q-band occurs as shown in Fig. 6.2(a), accompanied by a decrease in the absorbance of the shoulder around 710 nm. To investigate the electron transfer reaction from Chl to

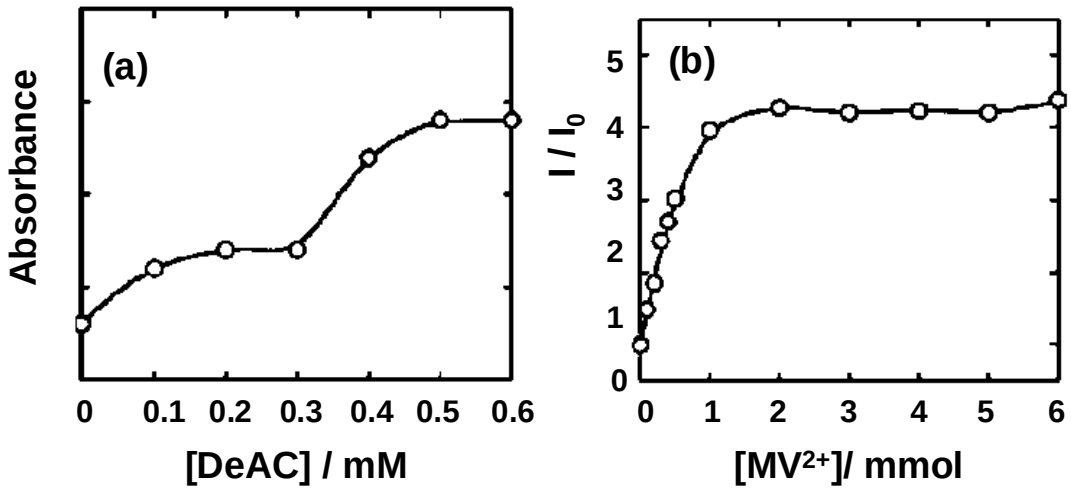

Fig. 6.2. (a) [DeAC] effect on the absorbance of the 670 nm band of Chl in poly(Glu)-DeAC complex and (b) Stern-Volmer type plot for the quenching of fluorescence intensity of Chl by MV^{2+} in the Poly(Glu)-DeAC(0.6 mM) system. The absorbance of Chl was measured at 670 nm and wavelength of excitation for fluorescence measurement was 435 nm.

MV^{2+} in the Poly(Glu)–DeAC complexes, we carried out fluorescence quenching experiments in the absence and presence of MV^{2+} for a reaction mixture containing Chl in the Poly(Glu)–DeAC complex. Fluorescence quenching did not occur in the absence of DeAC. As the concentration of DeAC increases, the degree of the fluorescence quenching also increased. Fig. 6.2(b) shows the Stern–Volmer plot for the quenching of the fluorescence intensity of Chl by MV^{2+} in the Poly(Glu)–DeAC (0.6×10^{-4} M) complex. The Stern–Volmer equation is given by

$$\mathbf{I_0/I = 1 + K_{SV}[MV^{2+}]} \quad (1)$$

Here, I_0 and I denote the fluorescence intensities of Chl in the absence and presence of MV^{2+}, respectively. KSV is the Stern–Volmer constant and $[MV^{2+}]$ is the quencher (MV^{2+}) concentration. The fluorescence intensity of Chl was quenched by MV^{2+} in the

present system as shown in Fig. 6.2(b). Also the quenching curve shows a downward curvature at higher concentrations of MV^{2+}. The downward curves in Fig. 6.2(b) may be ascribed to protected quenching in which one portion of chlorophyll is accessible to the quenching while the other is not [19–22]. The detailed mechanism is under study.

The photoinduced hydrogen evolution was performed using a reaction mixture consisting of Chl, Pt-loaded–Poly(Glu), MV^{2+} and $EDTA^{2-}$. As shown in Fig. 6.3, the

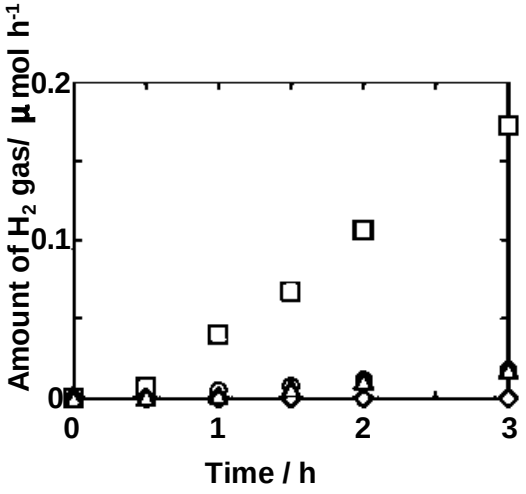

Fig. 6.3. The time course for hydrogen evolution in the presence of all components(□), and in the absence of Pt colloid alone(○), MV^{2+} alone(□) or any one of Poly(Glu) (◊) Chl, $EDTA^{2-}$, Poly(Glu) and DeAC.

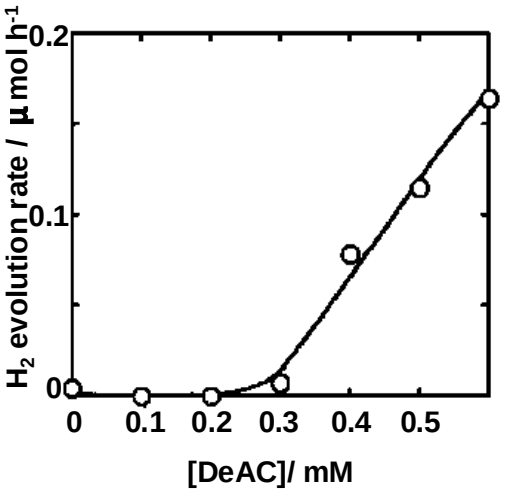

Fig. 6.4. The [DeAC] dependence of the rate of hydrogen evolution under visible light irradiation Chl(1×10^{-5} M), Pt(2.5×10^{-6} M, $EDTA^{2-}$(4 mM), Poly(Glu) (◊) Chl, $EDTA^{2-}$, Poly(Glu) and DeAC.

amount of hydrogen gas produced increases with irradiation time. No hydrogen gas was produced in the absence of any one of Chl, $EDTA^{2-}$, Poly(Glu) or DeAC. On the other hand, a little amount of hydrogen gas was produced when the experiment was carried out in the absence of Pt colloid alone or MV^{2+} alone.

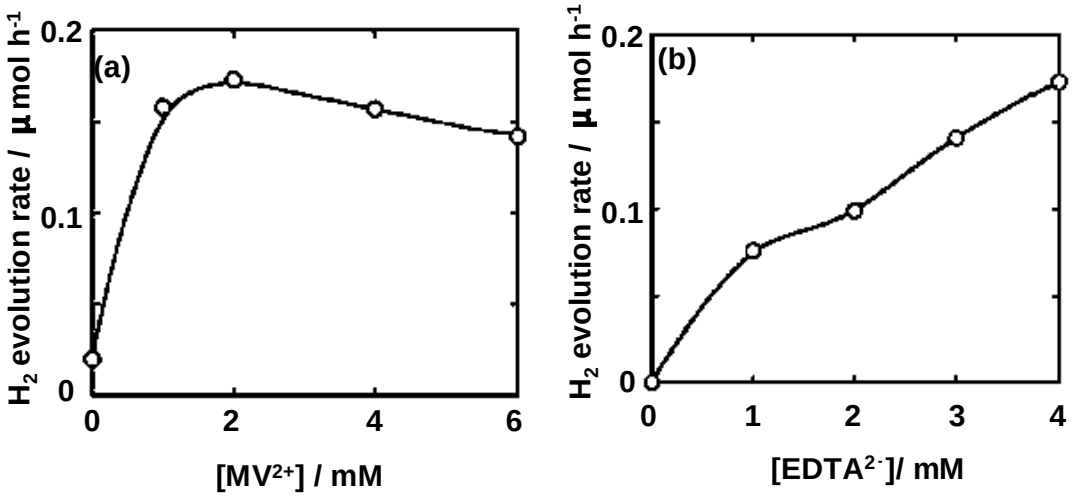

Fig. 6.5. Effect on (a) $[MV^{2+}]$ and (b) $[EDTA^{2-}]$ on the rate of hydrogen production under visible irradiation. Chl (1×10^{-5} M), Pt (2.5×10^{-6} M), DeAC (0.6 mM) and Poly(Glu) (0.1 mM), (a) $[EDTA^{2-}]$ = 4 mM and (b) $[MV^{2+}]$ = 2 mM.

This observation suggests that the Poly(Glu)–DeAC complex alone participate in the overall reaction of hydrogen production in this system. The effect of [DeAC] on the rate of hydrogen evolution is shown in Fig. 6.4. Hydrogen gas was not evolved below 0.3 mM DeAC and there was an increase in the rate of hydrogen evolution above this concentration. We also investigated the $[MV^{2+}]$ and $[EDTA^{2-}]$ dependence on the rate of hydrogen evolution under visible light irradiation, as shown in Fig. 6.5. In Fig. 6.5(a), the rate of hydrogen increases until 2 mM and then it decreases slightly through the maximum value, whereas in Fig. 6.5(b) the rate of hydrogen evolution increases almost linearly with increasing concentration of $EDTA^{2-}$ used in the experiment. No hydrogen gas was evolved in the absence of $EDTA^{2-}$, whereas the hydrogen evolution occurred only in excess of $EDTA^{2-}$ compared with the Chl concentration (Fig. 6.5(b)).

CD spectra are very sensitive to the microenvironment around a probe. The ellipticities between 190 and 250 nm are a good indicator of the conformation of a-helix, β-sheet and random coil of polypeptides and protein molecules [23]. The spectral

patterns in Fig. 6.1 clearly show a conformation change from the random coil to the α-helix of Pt–Poly(Glu). This behavior of the CD spectra suggests that the microenvironment produced by the presence of DeAC affects the rotatory strength of n–p* and p–p* transitions of Poly(Glu) [23]. Upon addition of DeAC into the Pt–Poly(Glu) solution (Fig. 6.1(d) and 6.1(e)), a strong electrostatic attraction occurs between anionic Pt–Poly(Glu) and cationic DeAC to form the Pt-loaded Poly(Glu)–DeAC complex [15]. This interaction is said to be a cooperative binding because it occurs at a [DeAC] much lower than its critical micelle concentration (cmc = 67 mM) [24]. The isobestic point at 208 nm suggests the 1 : 1 equilibrium state of the α-helix and the random coil of Poly(Glu) and also indicates that platinum colloid is more stabilized in the Poly(Glu)–DeAC complex system. The analogous behavior of CD spectra has been observed for Poly(Glu) in aqueous DeAC solutions as well as poly(L-glutamate, L-tyrosine) in aqueous cetylammonium chloride solutions [15,25,26]. The cooperative binding of surfactant ions to polypeptide ions of opposite charges arises from both the electrostatic attraction between the anionic polypeptide and the cationic surfactant and also additional hydrophobic interactions among the bound surfactant ions which induce the formation of a micelle-like surfactant cluster [27]. The hydrophobic interaction created around the Poly(Glu) is anticipated to solubilized Chl molecules. The increase in the absorbance of the Q-band (Fig. 6.2(a)) and the decrease in absorbance of the shoulder band at 710 nm occur around the concentration of DeAC at which a conformation change is indicated from the CD spectra. This observation suggests that aggregates of Chl are gradually destroyed as they are incorporated into the hydrophobic micelle-like clusters induced around the polypeptide. Kurawaki et al.[28,29] have reported a similar incorporation of Chl into copolypeptide (poly(L-ornithine, Ltyrosine))-sodium dodecyl sulfate complexes in which the electron and energy transfer

occurred from the tyrosine moiety to Chl in the Chl–copolypeptide–surfactant complexes. The incorporation of Chl into the hydrophobic clusters of DeAC leads to the electron transfer since fluorescence quenching occurred at 0.6 mM DeAC (Fig. 6.2(b)). The electron transfer can only occur if Chl is closer to the electron acceptor, MV^{2+}. A possible electrostatic attraction betweenMV^{2+} and the –CO O− group of Poly(Glu) may lead to the partial incorporation of MV^{2+} in the Poly(Glu)–DeAC complex from the aqueous bulk phase. This situation was confirmed by the fact that the fluorescence quenching by MV^{2+} occurred when Chl was solubilized in Poly(Glu)–DeAC complexes (Fig. 6.2(b)), whereas no fluorescence quenching by MV^{2+} occurred when similar experiments were carried out in a complex formed between a cationic polypeptide, poly(L-lysine), and an anionic surfactant, sodium dodecyl sulfate, due to the repulsion between the sidechain group (NH^{3+}) of poly(L-lysine) and MV^{2+}. The electrostatic attraction between the side-chain (–COO−) of Poly(Glu) andMV^{2+} is weak, since MV^{2+} alone did not induce a conformation change of Poly(Glu). The above consideration means that Chl and MV^{2+} are close to each other. This juxtaposition makes the electron transfer possible from Chl to MV^{2+}. However, it is not yet clear whether the electron transfer occurs via the singlet or the triplet state. Further experiments are underway to clarify this point. Electron transfer reactions involving the Chl triplet-state and acceptor species in liposomes, lipid vesicles and micelles are known to occur [1,6]. However, in other molecular assemblies such as the Zn(II)porphine derivative–liposome systems, porphyrin–polymer systems, porphyrin–viologen systems and the photosynthetic system in nature, the electron donor and acceptor are close enough to each other so that photoinduced electron transfer can take place via the short-lived singlet excited state [3,11,12,30–33]. In the present system, therefore, we suspect a similar situation in which MV^{2+} is closer to Chl in the polypeptide–surfactant complex, leading to the

electron transfer from Chl to MV^{2+} (via the singlet and/or the triplet state) to form the methylviologen radical (MV^{+}•). In turn a methylviologen cation radical transfers an electron to Pt protected by the Poly(Glu)–DeAC complex and then Pt reduces hydrogen ions to give H_2 gas. The fact that a little amount of hydrogen gas was evolved in the absence of Pt colloid or MV^{2+} suggest that the Poly(Glu)–DeAC complex alone participate in the overall reaction of hydrogen production in this system. The α-helix of Poly(Glu) may serve as an electron relay leading to the formation of hydrogen gas. This agrees with the observation that hydrogen gas was produced only around the concentrations of DeAC at which a conformation change was indicated from the CD spectra (Fig. 6.1(c)–(e) and Fig. 6.4). Although one can also attribute the increase in the rate of hydrogen evolution observed in Fig. 6.4 to the electrostatic repulsion between DeAC and reduced MV^{+}•, this reason seems not to hold in this system because the concentration of DeAC (0–0.6 mM) is much lower than its cmc (67 mM). Hence, the main reason for the increase in the production rate of hydrogen gas above 0.3 mM may be due to the conformation change of the Poly(Glu) induced by DeAC. In the absence of MV^{2+}, it is easy to envision direct electron transfer from Chl to Pt. On the other hand, in the absence of Pt, the folded Poly(Glu) might relay electrons to H^{+} ions in solution, leading to hydrogen production. The increase in the rate of hydrogen evolution at lower concentrations of MV^{2+} (Fig. 6.5(a)) is in correlation with the fact that MV^{2+} is closer to Chl in the polypeptide–surfactant complex leading to the effective electron transfer. However, at higher concentrations of MV^{2+} (Fig. 6.5(a)), the rate of hydrogen evolution decreases. The decrease in the hydrogen gas formation rate at higher MV^{2+} concentrations could be interpreted by the following reasons. A possible side-reaction such as the hydrogenation of MV^{2+} in the presence of Pt colloid may occur. Also the blue color of reduced MV^{+}• can serve as an inner filter and competes with Chl for

absorption of the incident light [11]. Finally the decrease in the rate of hydrogen formation could also be caused by the formation of complex species such as Chl–MV^{2+} in the ground state, which is not photoreactive, since they do not yield photoredox products [19]. Although the first two factors can also account for the decreased rate of hydrogen evolution, we think that the dominant factor is the formation of ground state complex species such as Chl–MV^{2+}. Since MV^{2+} is partially incorporated in the Poly(Glu)–DeAC complex by probably bonding to the side-chain of the Poly(Glu), increasing the concentration of this species might lead to a complication in the electron transfer process. Charge transfer complexes have also been reported to be formed

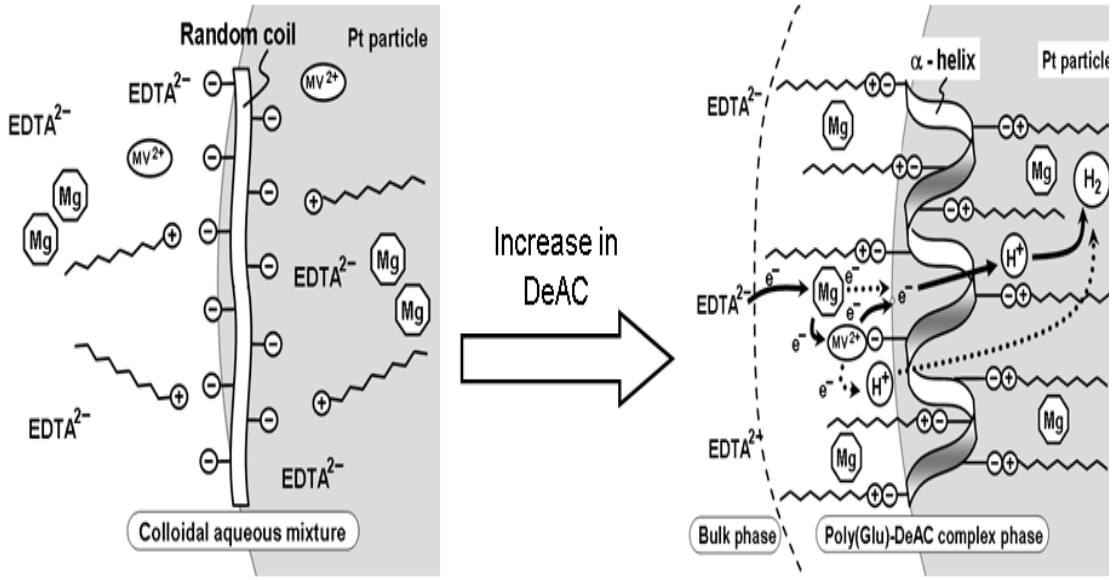

Fig. 6.6. A simplified representation of the mode of solubilization of Chl in the poly(Glu)-DeAC complex and the reaction for hydrogen production in the complex system. We omitted DeAC and MV^{2+} in the bulk phase for clarity.

between electron donors (such as pyrene and porphyrins) and the electron acceptor, MV^{2+} [20,34]. Since $EDTA^{2-}$ is a sacrificial electron donor, it is reasonable that no hydrogen gas is evolved in its absence. Also the fact that hydrogen evolution can be observed only in excess $EDTA^{2-}$ may suggest that $EDTA^{2-}$ is not incorporated into the Poly(Glu)–DeAC complex, but is located at the interphase between the bulk phase and

the complex phase. Based on the present data, we propose a plausible scheme for the solubilization of Chl in the Pt-loaded Poly(Glu)–DeAC complex and the reactions occurring in solution, as shown in Fig. 6.6. At low concentrations of DeAC, we have a colloidal mixture containing random-coil type Pt–Poly(Glu) and aggregated Chl in an aqueous solution containing MV^{2+} and excess $EDTA^{2-}$. Increasing the concentration of DeAC leads to the formation of Poly(Glu)–DeAC complexes and the resultant solubilization of Chl molecules. Another weak electrostatic attraction between MV^{2+} and the side-chain (–COO− group) of Poly(Glu) may lead to partial incorporation of MV^{2+} into the Pt–Poly(Glu)–DeAC complex. The excited Chl transfer an electron to MV^{2+} resulting to the formation of the MV^{+}• radical. This radical transfers the electron to Pt colloid which in turn is used to produce hydrogen gas. In the absence of Pt colloid or MV^{2+}, the α-helix Poly(Glu) may also transfer the electron directly to the nearby protons which are reduced to form hydrogen gas. However, the amount of hydrogen gas formed via this route is very small. The conformation change of Poly(Glu) might also enhance the separation of charged species formed leading to the hydrogen production. Excess $EDTA^{2-}$ found at the interphase between the bulk phase and the polypeptide–surfactant complex donates electrons to the oxidized Chl and thus Chl is regenerated.

Moreover, we replaced Chl with cobalt(II)tetraphenylporphyrin (CoTPP) to improve the stability. The results for hydrogen production under visible and UV irradiation are shown in Fig. 6.7. Photoinduced hydrogen evolution using CoTTP was also performed using a reaction mixture consisting of CoTPP (1×10^{-5} M), Pt-loaded Poly(Glu), MV^{2+} and EDTA (10 mM). This figure shows the time course for hydrogen evolution when the sample was irradiated with (a) visible and (b) UV/visible-light, respectively. The amount of hydrogen gas evolved initially increases with time and then becomes nearly constant. Hydrogen gas was not evolved in the absence of either of CoTPP, MV^{2+} or

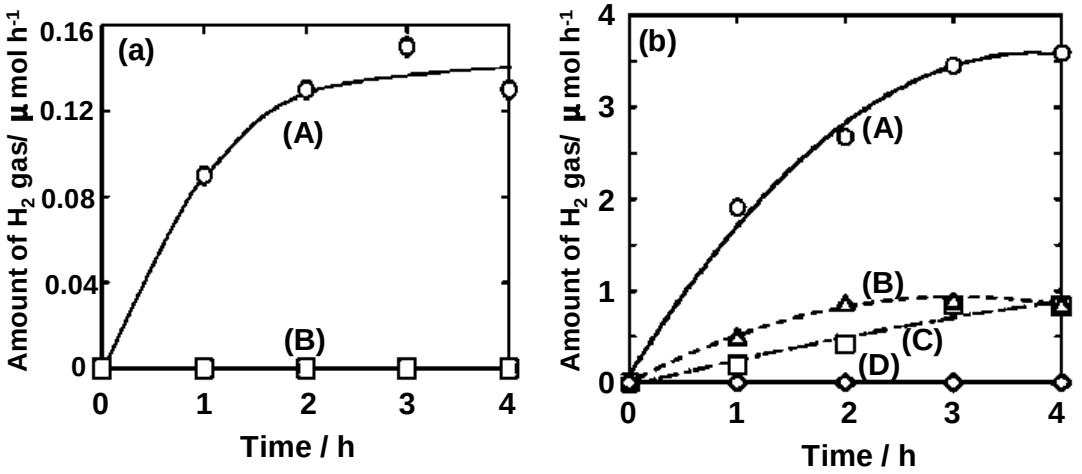

Fig. 6.7. Time course for hydrogen production under (a) visible and (b) UV/visible-light irradiation. CoTTP(1×10^{-5} M), Pt(2.5×10^{-5} M), MV^{2+}(2.5 mM), $EDTA^{-2}$(10 mM), DeAC(0.4 mM) and Poly(Glu)(0.1 mM). (a) (A) All components and (B) absence of any of the components. (b) (A) All components, (B) without Pt-colloid, (C) without Poly(Glu) and (D) without $EDTA^{2-}$, CaTPP or MV^{2+}.

$EDTA^{2-}$ upon irradiation under visible light as well as UV/visible-light, suggesting that these three components are essential for the production of hydrogen in this system and the possible route for electron transfer is via oxidative quenching by MV^{2+}. About 0.15 and 3.5 μmol of hydrogen gas was obtained after irradiation for 3 h using visible as well as combined UV/visible-light. The amount of hydrogen gas produced is larger when the sample was irradiated with UV/visible than when irradiated with visible-light (λ > ca. 400 nm) only. Under visible-light irradiation, hydrogen gas was produced only when all the components were present (Fig. 6.7(a)), whereas under UV/visible-light irradiation, a little amount of hydrogen gas was produced even in the absence of Pt-colloid alone or in the absence of Poly(Glu) alone (Fig. 6.7(b)).

CoTPP or Chl is solubilized in the hydrophobic clusters induced in the Poly(Glu)–DeAC complexes. The solubilized dyes can serve as a photosensitizer for the production of hydrogen. The presence of polypeptide–surfactant complexes enhances the rate of hydrogen production by solubilizing the photosensitizer and possibly

enhancing the separation of charged species. The rate of hydrogen evolution is markedly dependent on the conformational change of Poly(Glu). It is important to use low [MV^{2+}] to avoid the formation of ground-state complexes that have a serious implication for the full understanding of typical water photoreduction systems.

6.4. References

[1] R. B. Park, in The Chlorophylls: Physical, Chemical, and Biological properties, ed. L. P. Vernon and G. R. Seely, Academic press, New York, (1966) 283–309.

[2] H. Scheer, in Chlorophylls, ed. H. Scheer, CRC press, London, (1991) 211–640.

[3] H. Zuber, in Antennas and Reaction Centers of Photosynthetic Bacteria, ed. M. E. Michel-Beyerle, Springer, New York, 42 (1985) 1.

[4] L. Stryer, in Biochemistry, ed.W. H. Freeman, San Francisco, 2nd edn, (1981) 431–445.

[5] H. Dijkmans, Aggregation of chlorophylls in vitro. Absorption spectroscopy of chlorophyll a inwater–methanol solutions, Eur. J. Biochem., 32 (1973) 233.

[6] A. Chibisov, T. D. Slavnova and H. G¨ Orner, J. Photochem. Photobiol., B, 72 (2003) 11.

[7] J. K. Hurley and G. Tollin, Solar Energy, 28 (1982) 187.

[8] A. Harriman, in Energy Resources through Photochemistry and Catalysis, ed. M. Gr¨atzel, Academic Press, New York, (1983) 163–210.

[9] J. Kiwi and M. Gr¨atzel, J. Phys. Chem., 84 (1980) 1503.

[10] N. Sugiyama, M. Toyoda and Y. Amao, Colloids Surf., A, 284-285 (2006) 384.

[11] J. R. Darwent and M.-C. Richoux, in Photogeneration of Hydrogen, ed. A. Harriman and M. A. West, Academic Press, London, (1982) 23.

[12] Photocatalysis: Science and Technology, ed. M. Kaneko and I. Okura, Kodansha and Springer, Tokyo, (2002) 294.

[13] Y. Saiki and Y. Amao, Visible light-induced enzymatic hydrogen production from oligosaccharides using Mg chlorophyll-a and platinum colloid conjugate system, Int. J. Hydrogen Energy, 29 (2004) 695.

[14] K. Hayakawa, T. Nagahama and I. Satake, Conformation of poly(Lglutamic acid) in solutions of a cationic surfactant with an x-hydroxyl group, Bull. Chem. Soc. Jpn., 67 (1994) 1232–1237.

[15] I. Satake, T. Gondo and H. Kimizuka, Conformational transition of poly(L-glutamic acid) in aqueous decylammonium chloride solution, Bull. Chem. Soc. Jpn., 52 (1979) 361.

[16] J. Liu, N. Takisawa, H. Kodama and K. Shirahama, Conformation of poly(L-glutamate) in cationic surfactant solutions with reference to binding behaviors, Langmuir, 14 (1998) 4489.

[17] W. Tu andH. Liu, J. Mater. Chem., 10 (2000) 2207.

[18] Y. Kusumoto, J. Watanabe, J. Kurawak and I. Satake, Chem. Express, 5 (1990) 105.

[19] I. Okura, S. Aono, M. Takeuchi and S. Kusunoki, The photoreduction of viologen dyes with palladium meso-tetraphenylporphyrintrissulfonate, Bull. Chem. Soc. Jpn., 55 (1982) 3637.

[20] Y. Kusumoto, S. Ihara, J. Kurawaki and I. Satake, Chem. Lett., (1986) 1647.

[21] Y. Kusumoto and M. Uchikoba, Chem. Lett., (1991) 1985–1988.

[22] K. Nakashima and N. Kido, Photochem. Photobiol., 64 (1996) 296.

[23] M. Hatano, in Induced Circular Dichroism in Biopolymer–Dye Systems, ed. S. Okamura, Springer, Tokyo, (1985) 50.

[24] C. J. Beverung, C. J. Radke and H. W. Blanch, Adsorption dynamics of L-glutamic

acid copolymers at a heptane/water interface, Biophys. Chem., 70 (1998) 121.

[25] Y. Kusumoto and J. Kurawaki, in Research in Photosynthesis, ed. N. Murata, Kluwer Academic Publishers, Netherlands, 2 (1992) 825.

[26] J. Kurawaki and Y. Kusumoto, in Research in Photosynthesis, ed. N. Murata, Kluwer Academic Publishers, Netherlands, 2 (1992) 817.

[27] Y. Moroi, in Micelles: Theoretical and Applied Aspect, Plenum, New York, (1992) 233.

[28] J. Kurawaki, Y. Sameshima and Y. Kusumoto, Chem. Phys. Lett., 226 (1997) 353.

[29] J. Kurawaki, Y. Sameshima and Y. Kusumoto, J. Phys. Chem. B, 101 (1997) 10548.

[30] K. I. Zamaraev and V. N. Parmon, in Energy Resources through Photochemistry and Catalysis, ed. M. Gr¨atzel, Academic Press, New York, (1983) 123.

[31] H. Hosono, Hydrogen evolution photoinduced by using platinum loaded Langmuir–Blodgett films of viologen-linked porphyrin, J. Photochem. Photobiol., A, 126 (1999) 91.

[32] T. Abe, H. Imaya, M. Endo and M. Kaneko, Polym. Adv. Technol., 11 (2000) 167.

[33] Y. Amao and I. Okura, J. Mol. Catal. B: Enzym., 17 (2002) 9.

[34] Y. Amao, Y. Tomonou and I. Okura, Solar EnergyMater. Solar Cells, 79 (2003) 103.

CHAPTER 7

A NOVEL TYPE SOLAR CELLS BASED ON HEMATITE THIN FILMS

7.1. Introduction

Photovoltaic devices are based on the concept of charge separation at an interface of two materials of different conduction mechanism. To date, this field has been dominated by solid-state junction devices, usually made of silicon, profiting from the experience and material availability resulting from semiconductor industry. The dominance of the photovoltaic field by inorganic solid-state junction devices is now being challenged, for example on nanocrystalline and conducting polymer films [1,2]. Recently, nanocrystalline semiconductor oxide-based dye-sensitized solar cells (DSC) has been recognized as reasonable solar energy conversion devices [3-5]. DSC consists of a nanocrystalline semiconductor film adsorbing dyes such as a Ru-bipyridyl complex, a redox couple such as I^-/I^{3-}, and a counter electrode. DSC has received considerable attention during the last decade due to its potential for low cost and high efficiency. However, there are many problems in the development of DSC such as durability, high cost of a suitable dye, sealing and using organic solvent, etc. for practical applications. Hematite (α-Fe_2O_3) is an attractive semiconductor material because of good stability, low cost and its narrow bandgap (2.2 eV) giving an absorption spectrum in the visible light region [6, 7].

In this study, we used the photocatalyst to prepare novel type of solar cells. Moreover, calcination temperature dependence on the Fe_2O_3 photo cell performance

prepared by only the laser ablation method was also studied.

7.2. Experimental

First, a high compact thin film of Fe_2O_3 was deposited on an ITO glass (indium-tin oxide coated glass, 8-12 ohm resistance, Aldrich) by the laser ablation method [9-11] as shown in Fig.1.4. The Fe_2O_3 target was prepared by mixing 5.5 g of Fe_2O_3 (99.9%, Wako) with 0.55 g of paraffin to prevent cracking. The mixed powder was pressed at 20 MPa for 1 h and calcined at 600 ºC for 6 h to form a Fe_2O_3 pellet. The pellet was introduced into the chamber and the experimental conditions were adjusted. The laser power was 2.8 J / pulse cm^2. The wavelength of the laser (Nd-YAG Laser, Spectra-Physics Co., GCR-130-10) was 532 nm. The distance between the substrate and the target was 3 cm. The substrate was set in room temperature and the laser irradiation time was 1 min. Irradiation of the target with a laser beam melted the target to form a plume. The plume was accumulated on the quartz substrate to form the Fe_2O_3 thin film. Secondly, the high compact thin film was coated with porous Fe_2O_3 by the squeegee method (Fig. 7.1). The preparation method of the Fe_2O_3 paste is as follows: Fe_2O_3 (2 mg) was mixed with conc. nitric acid (0.1 ml) and distilled water (2 ml). After well mixing, 2 ml of Triton X-100 (Wako) was mixed to get paste. The paste of the yellowish powder was prepared using the same method as Fe_2O_3 was prepared by the squeegee method. The TiO_2 film was also prepared by the squeegee method using TiO_2 powder (Degussa P25). An N719 dye was adsorbed on the surface of the TiO_2 film by soaking the film into solution of N719 under the conditions of 40 ºC for 2 h. The Pt counter electrode was prepared by a spattering method. The Fe_2O_3 film was used as a working electrode in a solar cell where a Pt film was used as a counter electrode. The two

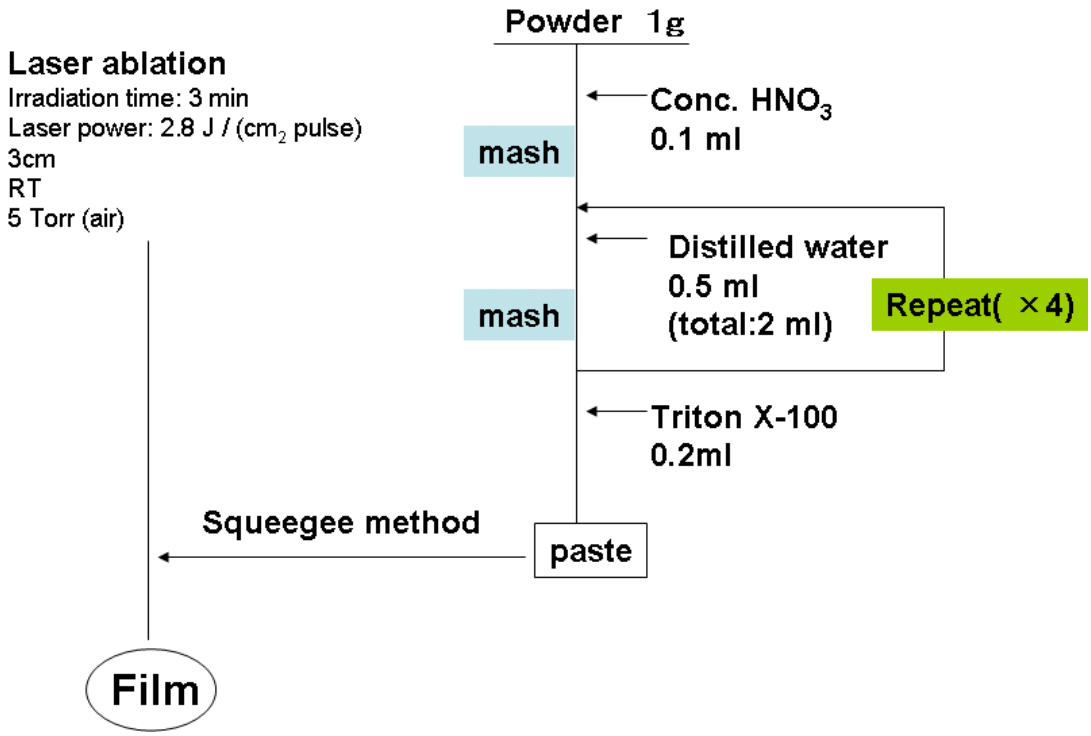

Fig. 7.1. Diagram of the method for preparation of the Fe_2O_3 films.

electrodes were sandwiched, and then the electrolyte solution was filled between the two electrodes. As the electrolyte 0.8 M of KI and 0.2 M of I_2 (Wako) in water or 0.8M of TBAI (tetra butylammonium iodide (Wako) and 0.2 M of I_2 in acetonitrile were employed. Current-voltage characteristics were measured using Peccell I-V curve analyzer and PECK2400-N. The thin films prepared were characterized by X-ray diffraction (XRD) using an X-ray diffractometer (Rigaku) with Cu Kα radiation and absorption spectroscopy (Shimadzu, MPS-2000 spectrophotometer). A xenon lamp (Inotex 300-W LX-300F) with an IR cut-off filter and an L42 cut-off filter (ca. 1/7 sun) was used as a visible light source (λ > ca. 400 nm). The xenon lamp without cut-off filters was used for the durability test.

7.3. Results and discussion

Fig. 7.2 shows the absorption spectrum of the Fe_2O_3 thin film prepared by the laser ablation method. Fe_2O_3 seem to give the absorption edge at around 590 nm.

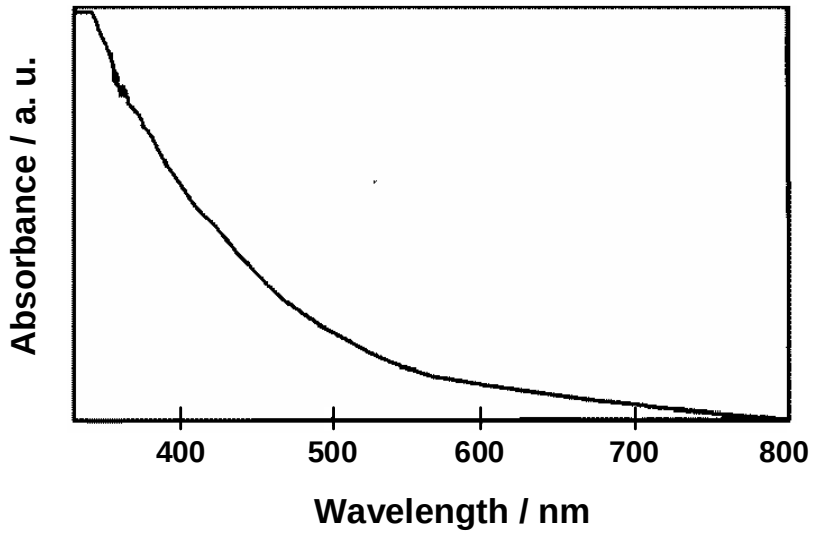

Fig. 7.2. Absorption spectrum of the Fe_2O_3 thin film prepared by the laser ablation method.

The color of the Fe_2O_3 film is orange. XRD patterns of (a) the Fe_2O_3 film prepared by the laser ablation method on an ITO glass, (b) an ITO glass alone and (c) the α-Fe_2O_3 powder are shown in Fig. 7.3. The result shows that the crystal structure of α-Fe_2O_3 was not destroyed by the laser ablation under the conditions used. The effect of the laser ablation for the properties of Fe_2O_3 is under investigation.

Fig. 7.4 shows the SEM image of the Fe_2O_3 thin film prepared by the laser ablation method and squeegee method. From this image, we can see that the surface is rough. A large number of pores were also observed.

Fig. 7.5 shows the current-voltage characteristics obtained with the solar cell based on the Fe_2O_3 film prepared by the laser ablation method under visible light illumination.

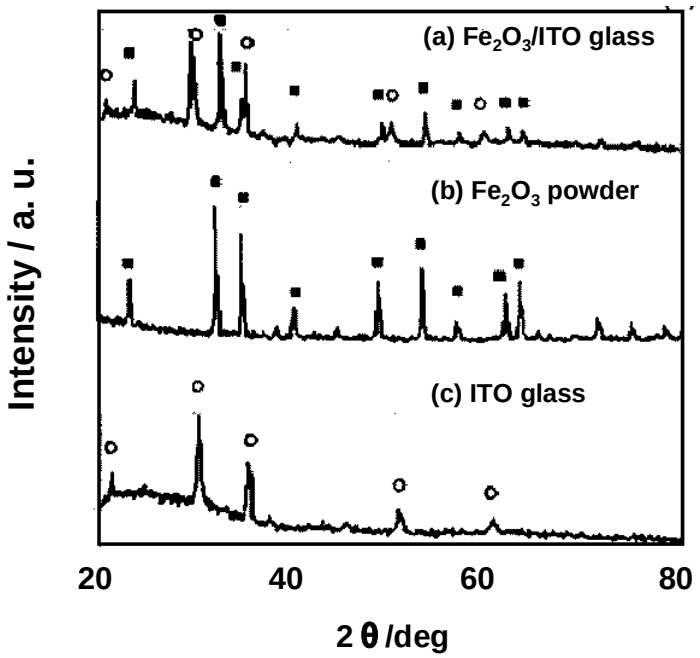

Fig. 7.3. XRD spectra of (a) the Fe_2O_3 film prepared by the ablation method on ITO glass, (b) an ITO glass and (c) Fe_2O_3 powder. The peaks of Fe_2O_3 are marked by the open circle and that of ITO are marked by the close square.

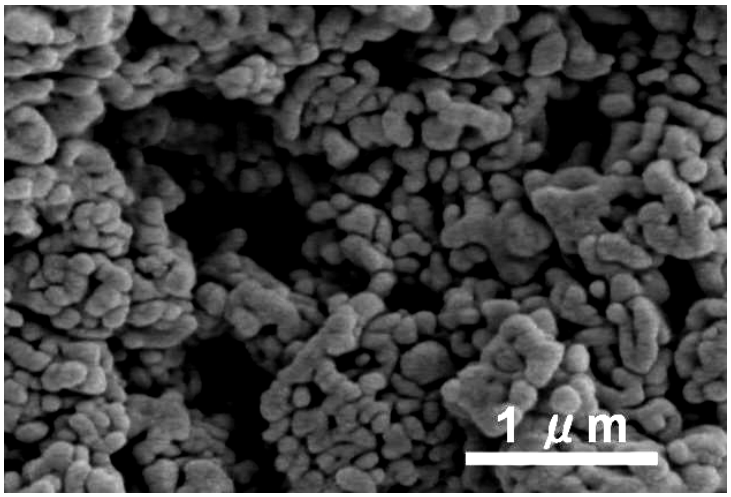

Fig. 7.4. SEM image of the Fe_2O_3 film.

The open circuit voltage, the short circuit current and the fill factor were 0.23 V, 0.28 mA cm^{-2} and 0.35, respectively. In DSC, usually organic solvents are used as an

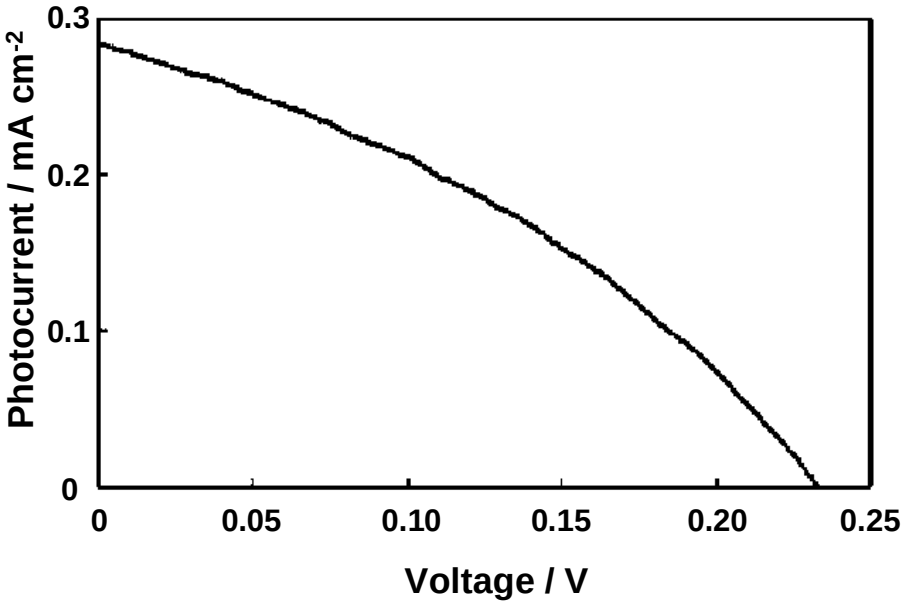

Fig. 7.5. I-V curve of the solar cell based on the Fe_2O_3 film under visible light illumination (ca. 1/7 sun). The electrolyte is 0.8 M of TBAI and 0.2 M of I_2 in acetonitrile.

electrolyte solvent, but in our novel solar cell, water can be used as an electrolyte solvent. For the comparison of the efficiency and the durability of the solar cell based on the Fe_2O_3 film, the dye-fixed TiO_2 film (N719 / TiO_2) was also prepared. Effect of solvents on the performance of the solar cells based on the Fe_2O_3 film (A) and the N719/TiO_2 film (B) are shown in Fig. 7.6. The electrolyte of the solar cells based on the N719/TiO_2 film and the Fe_2O_3 film is (a) 0.8 M of TBAI and 0.2 of I_2 in acetonitrile or (b) 0.8M of KI and 0.2 M of I_2 in water. The suitable dyes for DSC such as N719 are desorbed due to the hydrolysis of the ester bond between –COOH group in the dye and -OH group in the TiO_2 surface by replacing the organic solvent ((a) in Fig. 7.6B) with the water solvent ((b) in Fig. 7.6B) resulting in dropping the efficiency to zero as shown in Fig. 7.6B. In our novel solar cell, the performance was almost the same in water

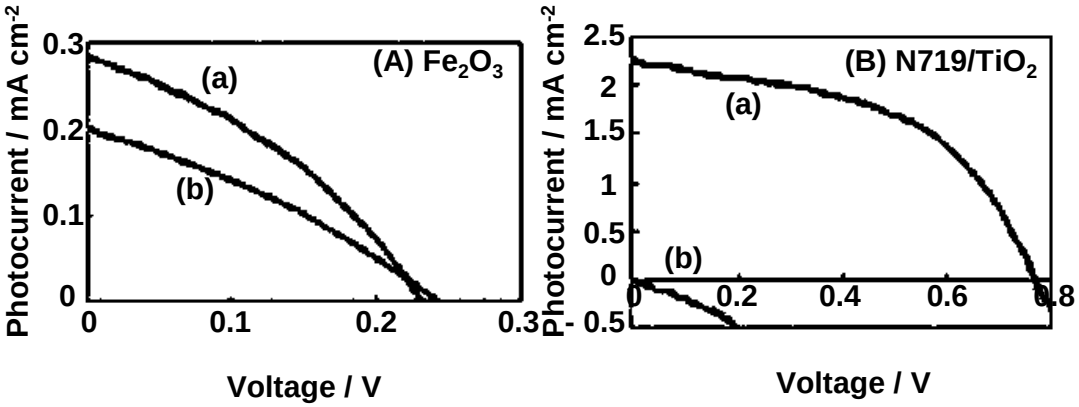

Fig. 7.6. Effect of solvents on the performance of the solar cells: N719/TiO_2 film (bottom) and Fe_2O_3 film (top). The electrolyte is (a) 0.8 M of TBAI and 0.2 of I_2 in acetonitrile, (b) 0.8M of KI and 0.2 M of I_2 in water.

solvent (Fig. 7.6A). It is advantageous for a practical use that water solvent can be used instead of organic solvent because organic solvent is easer to evaporate than water solvent and it is harmful in environment.

Finally the durability tests of the solar cells based on the Fe_2O_3 film and the N719/TiO_2 film were performed with long time continuous irradiation under the severe condition. The light intensity containing both UV and visible light was ca. 5 times as high as 1 sun and the surface temperature was ca. 50-60 ºC. Fig. 7.7 shows the results of the durability test. Even after 5 days irradiation, the stable performance was obtained with our novel solar cell based on the Fe_2O_3 film with water solvent (Fig. 7.7A), whereas the performance of DSC (N719/TiO_2, organic solvent) decreased sharply under the same conditions even after the replacement of a electrolyte and Pt counter electrode (Fig. 7.7B). The solar cell based on the N719/TiO_2 film was outstripped by our solar cell based on the Fe_2O_3 film after 2 days irradiation (Fig. 7.7A).

We estimated the ideal value of the open circuit voltage of the Fe_2O_3 solar cell was 0.35 V (Fig. 7.8). It is decided by the difference of potential level between the

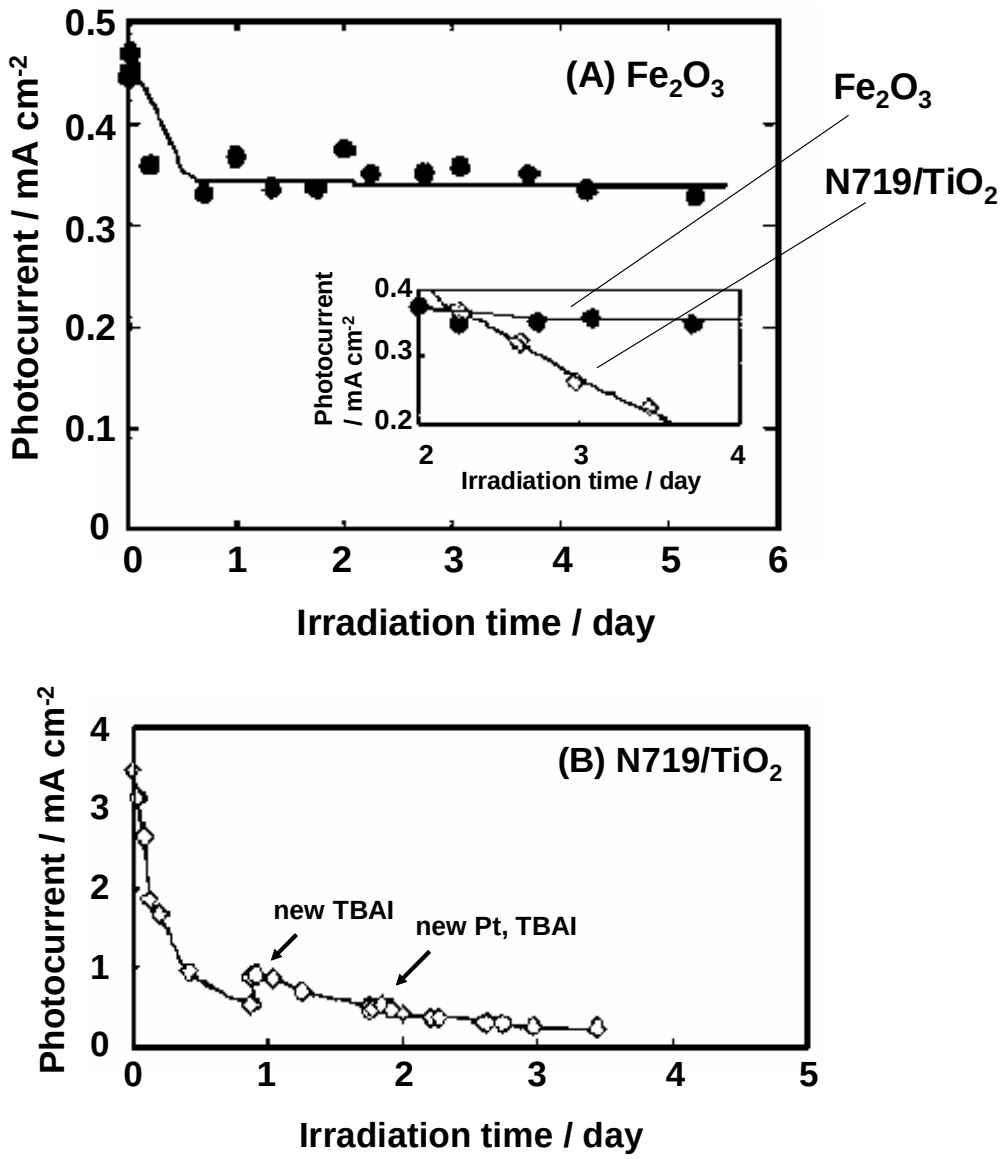

Fig. 7.7. The dependence of the photocurrent on the irradiation time under server conditions (ca. 5 sun containing both UV and visible light, while the surface temperature was 50-60 ºC).

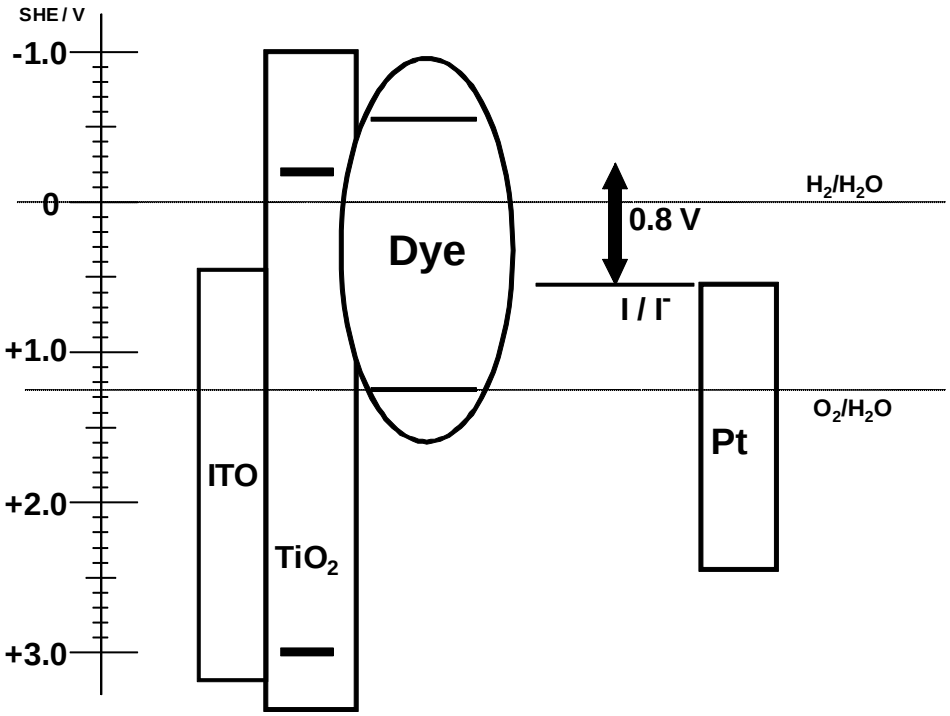

Fig. 7.8. Energy level diagram for Fe_2O_3 in the photo cell system.

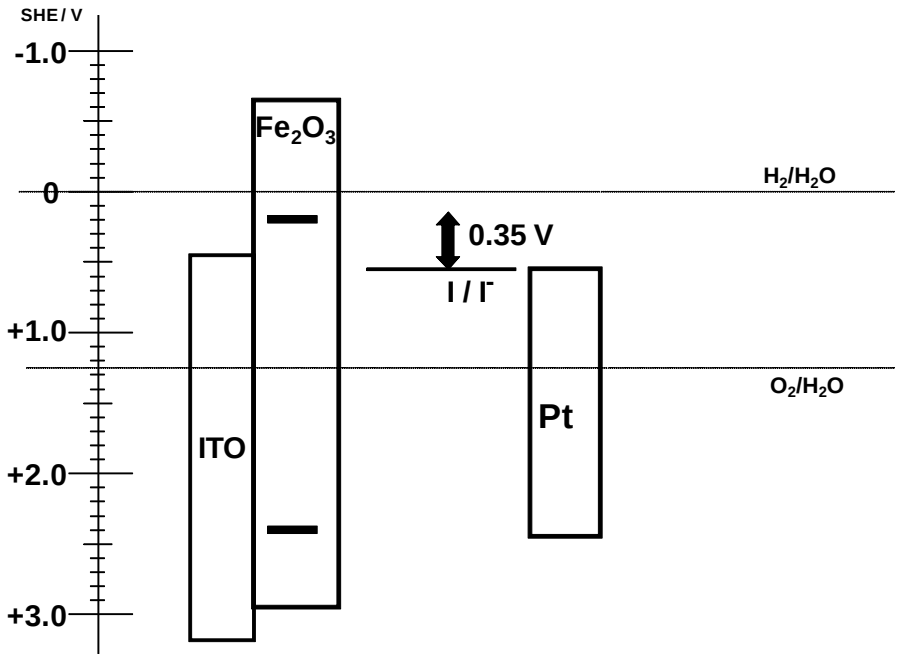

Fig. 7.9. Energy level diagram for N719/TiO_2 in the photo cell system.

conduction band of Fe_2O_3 and the iodine in electrolyte. Whereas N719/TiO_2 system of gave ideal values of the open circuit voltage (Fig. 7.9). The experimental value was not enough when comparing with the ideal value. It is suggested that the Fe_2O_3 film contains some defects in lattice, therefore the voltage decreased due to the electron-hole recombination, the back reaction and the trapping of electrons.

To study why the voltage (V_{oc}) cannot reach the theoretical one, the Fe_2O_3 films after laser ablation were calcined under various temperatures. Fig. 7.10 shows the effect of the calcination on the performance of the Fe_2O_3 solar cells. The performance of the Fe_2O_3 solar cell was increased sharply with the calcination after the laser ablation.

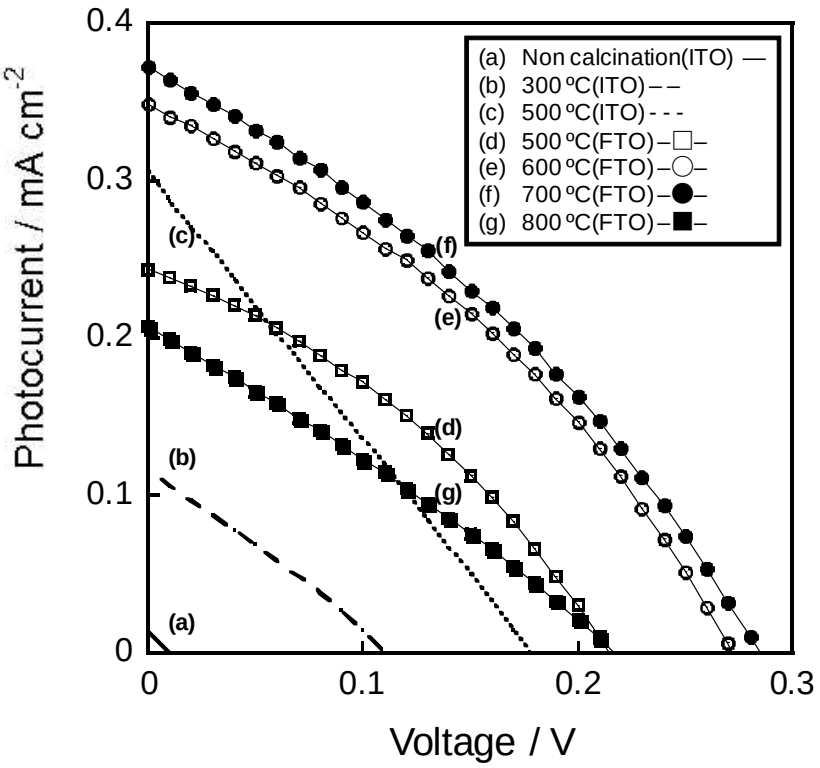

Fig. 7.10. Calcination-temperature dependence on I-V curve of the solar cells under light irradiation (1 sun).

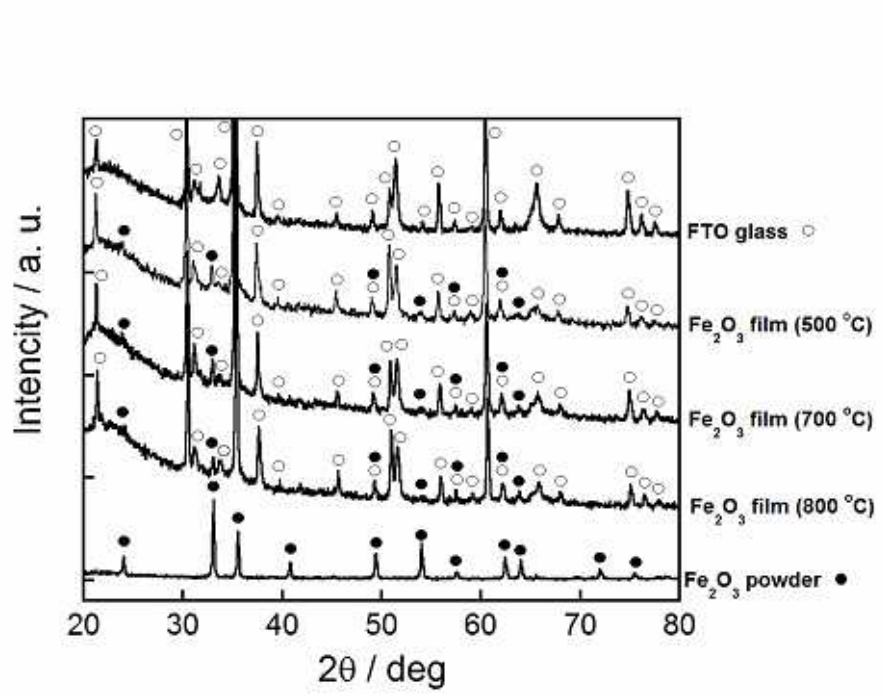

Fig. 7.11. Calcination-temperature dependence on XRD patterns of the solar cells.

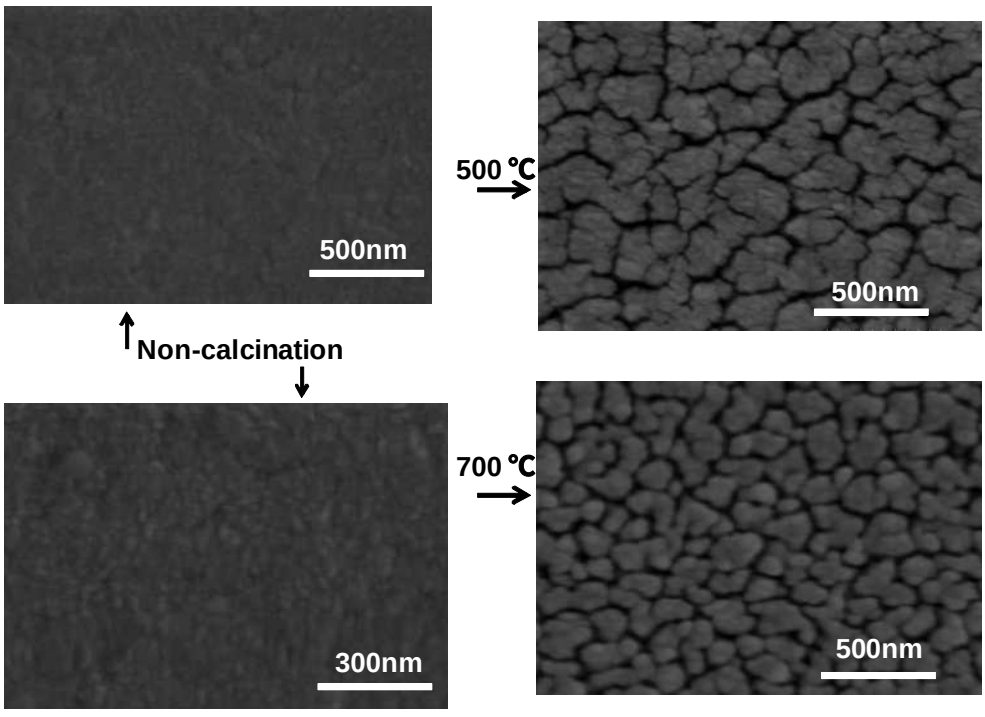

Fig. 7.12. Calcination-temperature dependence on SEM image of the solar cells.

However, it was decreased with the calcination at 800℃.

To ascertain the cause of the improvement of the cell performance by the calcination, the Fe_2O_3 films were analyzed by XRD and SEM as shown in Fig. 7.11 and Fig. 7.12, respectively. The XRD pattern shows the crystalinity of Fe_2O_3 film almost did not change with the calcination temperature .The SEM images show the performance of the Fe_2O_3 solar cells was increased by the calcination in spite of the increase of particle sizes(= the decrease of the surface area). As one of the reasons of the improvement of the cell performance by the calcination, it is suggested that the bonds between Fe_2O_3 and FTO were intensified. The electron conductivity between Fe_2O_3 and FTO was improved due to the strengthened bond. However, the performance of the solar cell decreased at 800℃ because of the damage of FTO.

The IPCE curve showed that the cell was functioned by the light absorption of Fe_2O_3 (Fig. 7.13). This is why the IPCE curve and the absorption spectrum of Fe_2O_3

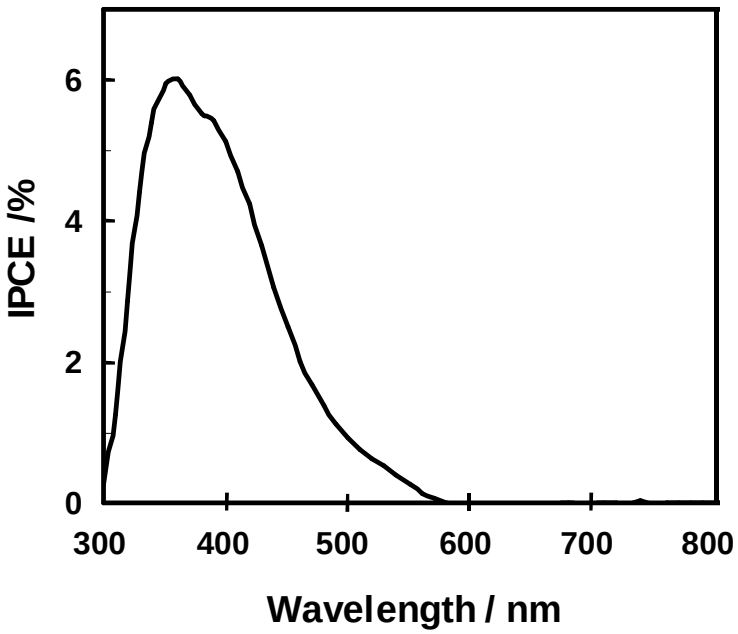

Fig. 7.13. IPCE curve of the Fe_2O_3 solar cell.

overlapped with each other. Our solar cells can utilize ultra violet region efficiently as well as visible region.

7.4. References

[1] H. N. Cong, M. Dieng, C. Sene and P. Chartier, Solar Energy Materials and Solar Cells, 63 (2000) 23.

[2] N. Kudo, Y. Shimazaki, H. Ohkita, M. Ohoka and S. Ito, Solar Energy Materials and Solar Cells, 91 (2007) 1243.

[3] H. Tsubomura, M. Matsmura, Y. Nomura, T. Amamiya, Nature, 261 (1976) 402.

[4] B. O'Regan, and M. Grätzel, Nature, 353 (1991) 737.

[5] M. Grätzel, Nature, 414 (2001) 338.

[6] S.U.M. Khan, J. Akikusa, J. Phys. Chem. B, 103 (1999) 7184.

[7] U. Bjorksten, J. Moster, and M. Gratzel, Chem. Mater., 6 (1994) 858.

[8] Z. Zoua, J. Ye, K. Sayama, H. Arakawa, J. Photochem. Photobiol., A, 148 (2002) 65.

[9] X. Zou, N. Maesako, T. Nomiyama, Y. Horie, T. Miyazaki, Sol. Energy Mater. Sol. Cells, 62 (2000) 133.

[10] H. Usui, O. Miyamoto, T. Nomiyama, Y. Horie, T. Miyazaki , Sol. Energy Mater. Sol. Cells 86 (2005) 123.

[11] S. Somekawa, Y. Kusumoto, M. Ikeda, B. Ahmmad, Y. Horie, Catal. Commun., 9 (2008) 437-440.

CHAPTER 8

PREPARATION OF TaON AND Ta_3N_5 BY LASER ABLATION METHOD

8.1. Introduction

Hydrogen production using visible light-driven photocatalysts has received considerable attention because hydrogen is renewable clean energy and visible light occupies the main part of solar light. Titanium dioxide (TiO_2) is well known as an efficient photocatalyst [1,2]. However, it is only activated by UV light because of its wide band gap. The development of the future generation of visible responsive photocatalytic materials is important for the efficient use of solar light.

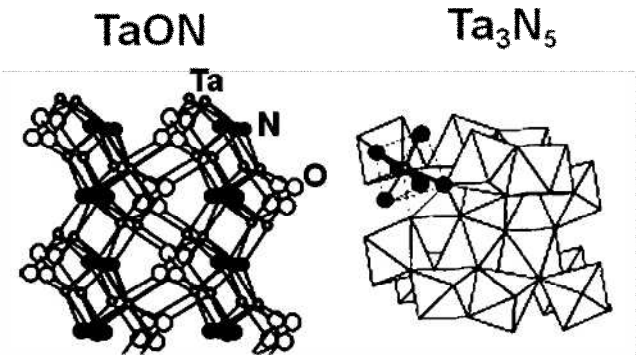

Fig. 8.1. The structures of TaON and Ta_3N_5.

Domen.et al. reported that TaON and Ta_3N_5 have activity for water splitting under visible light irradiation [3-11]. Fig. 8.1 shows the structures of TaON and Ta_3N_5. TaON or Ta_3N_5 was prepared by the treatment of Ta_2O_5 powder under HN_3 gas at high temperatures. Several methods also have been reported for the preparation of tantalum nitride and oxynitride films, such as reactive sputtering [12-14], magnetron sputtering

[15-20], chemical vapor deposition [21-25], atomic layer deposition [26] and electron beam evaporation [27]. In recent years there has been increased research in transition metal oxynitrides.

In this study, we attempted to prepare TaON films by the gas phase laser ablation methods using Ta foil, and also attempted to prepare Ta_3N_5 nanoparticles by the liquid phase laser ablation methods using Ta_2O_5 powder.

8.2. Experimental

A Ta foil and a quartz substrate were used as a target and a substrate, respectively. A schematic configuration of the laser ablation system is shown in Fig. 1.4. The second harmonics of a Nd:YAG pulse laser (Spectra-Physics Co., GCR-130-10) was use with the pulse width of 7 ns and the repetition rate of 10 Hz. The laser beam of cross section 0.8 cm^2 was focused into an area of about 0.03 cm^2 using a quartz lens with focal distance of 30 cm. To avoid the damage of the target by a continuous irradiation of the laser beam, the target was rotated at 14 rpm during the deposition. The foil was introduced into the chamber and the experimental conditions were adjusted. Irradiation of the target with a laser beam melted the target to form a plume ablated TiO_2 particles. The plume was accumulated on the quartz substrate. The fluence of 3.2 J / pulse cm^2 and the laser irradiation time of 12 min were used throughout the experiment. The wavelength of the laser was 532 nm. The distance between the substrate and the target was fixed at 2 cm. The experiments were carried out under the substrate temperatures and nitrogen gas pressures were 300 ℃ - 600 ℃ and 133 Pa, respectively. Ta_2O_5 thin film as a reference was also prepared by the laser ablation method under O_2 atmosphere of 133 Pa and the substrate temperature of 600℃ using a Ta_2O_5 target.

The prepared thin films were characterized by absorption spectroscopy (Shimadzu, MPS-2000), XRD (X-ray diffraction, Rigaku Rint-2000) and FT-IR (Fourier Transform Infra-Red Spectroscopy, PerkinElmer, Spectrum One A).

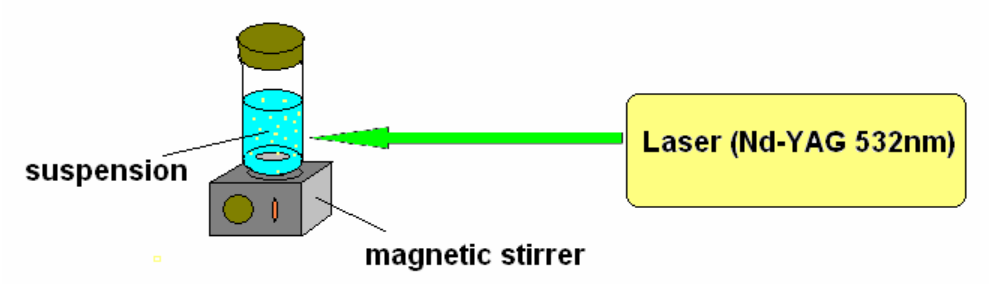

Fig. 8.2. A schematic figure of the liquid phase laser ablation system.

Next we attempted to prepare TaON or Ta_3N_5 nanoparticles by the liquid phase laser ablation method as shown in Fig. 8.2. 25 mg of Ta_2O_5 powders (wako) were dispersed in 5 ml of 4 mol/ml ammonium water. This solution was white. The laser used was a 532 nm Nd-YAG laser. The pulse width was nominally 7 ns and the repetition rate was fixed at 10 Hz. For laser irradiation, 9 ml sample tube was used. The sample was irradiated under agitation using a magnetic stirrer. The size of the irradiated spot was cm^2. The irradiation time is 1h. The absorption spectra of the samples were measured by absorption spectroscopy (Shimadzu, MPS-2000). The size and shape of particles were also observed using FE-SEM (Field emission scanning electron microscopy, Hitachi, S-4100).

8.3. Results and discussion

A purplish thin film was prepared by the laser ablation of a Ta foil under N_2 133 Pa atmosphere. A yellowish thin film was gotten by keeping of the purplish thin film in the atmospheric condition for 6 months. Fig. 8.3 shows the absorption spectra of (b) the thin films deposited at 400 °C by the laser ablation method under N_2 pressure of 133 Pa

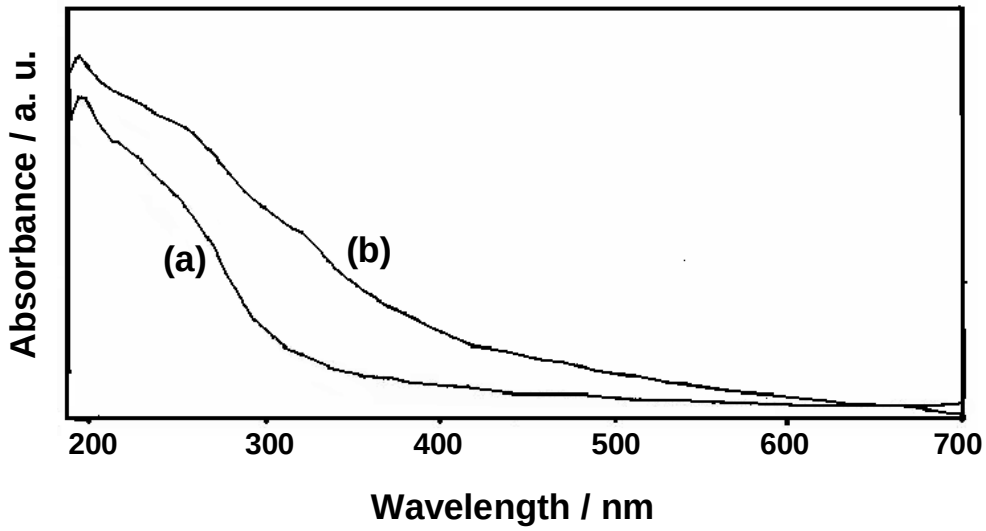

Fig. 8.3. Absorption spectra of thin films deposited at (b)400 °C by the laser ablation method under N_2 pressure (133Pa) (After 6 months) and Ta_2O_5 film (a) prepared at 600 °C under O_2 133 Pa.

(after 6 months) and (a) the Ta_2O_5 film. The absorbance edge is ca. 500 nm. Fig. 8.4 shows XRD patterns of the yellowish thin films deposited at (a) 300, (b) 400, (c) 500 °C by the laser ablation method under N_2 pressure of 133 Pa (after 6 month). Blackish parts in the thin films increased as increasing the substrate temperature. No clear peaks of TaON are found because it suggested that the thickness of the TaON film is very small. Ta_3N_5 peaks are found when the temperatures are over 400 °C clearly. To prove the existence of TaON, FT-IR of the thin films were measured as shown in Fig. 8.5. The TaON peaks increases up to 400 °C and decreases through the maximum.

We suggest the mechanism as follows (see Fig. 8.6). First an unstable film composed by Ta and N spaces was formed by the ablation of Ta target under N_2 atmosphere. Next the surface of the compound composed with Ta and N was oxidized by oxygen in air while stacking for six months in air. Finally, very thin TaON film was prepared.

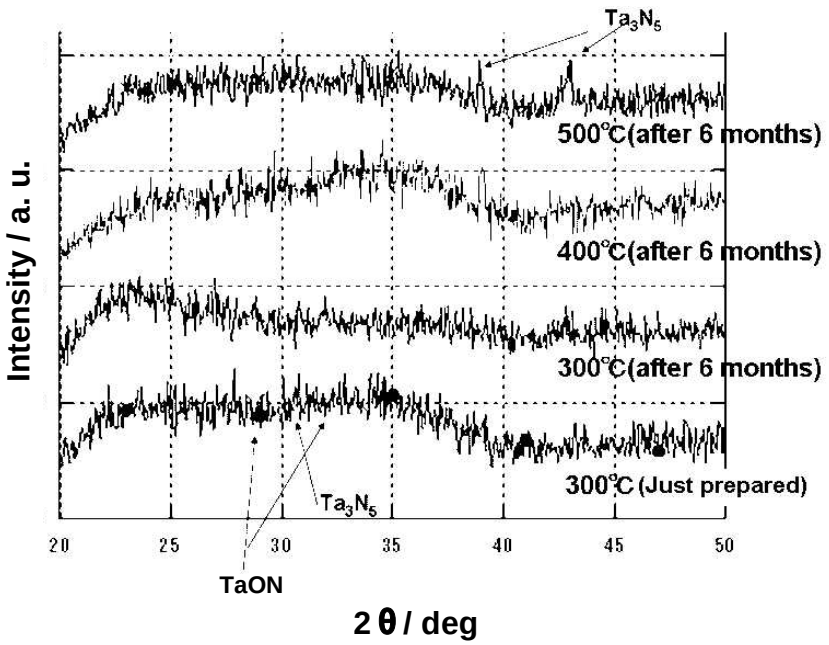

Fig. 8.4. XRD patterns of thin films deposited at (a)300, (b)400, (c)500 °C by the laser ablation method under N_2 pressure (133 Pa), substrate-target distance (3cm), laser power (3.2 J/cm^2 Pulse) and deposition time (12min) (After 6 month).

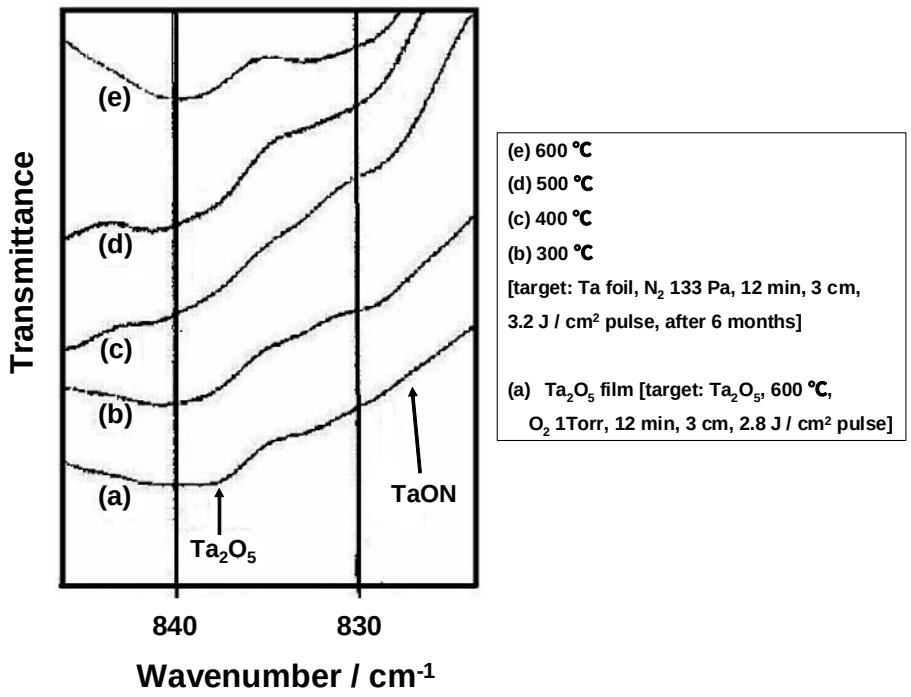

Fig. 8.5 FT- IR spectra of the yellowish thin films prepared by the laser ablation method under nitrogen atmosphere.

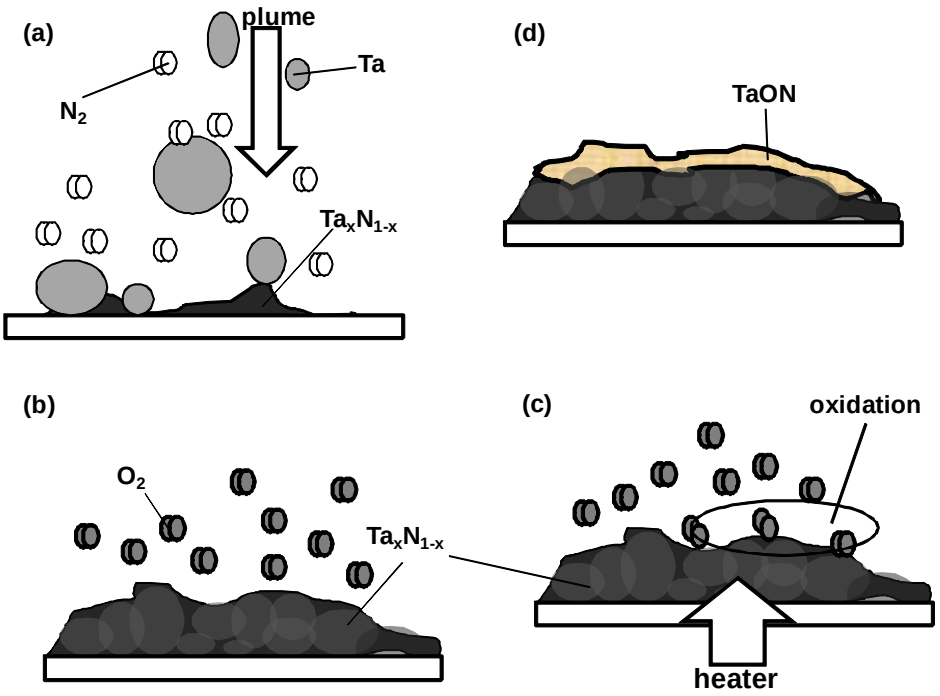

Fig. 8.6. Schematic figure of the process of preparation TaON thin film.

We also tried to prepare TaON and Ta_3N_5 from Ta_2O_5 powder by the liquid laser ablation method. Ta_2O_5 suspension was lased in aqueous NH_3, resulting in getting the reddish suspension. The suitable concentration of NH_3 for getting the reddish

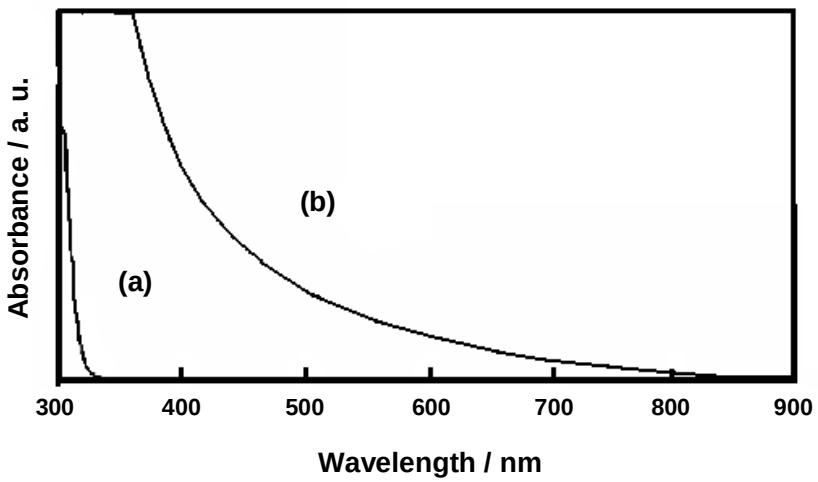

Fig. 8.7. Absorption spectra of (b) the supernatant of the suspension prepared by the laser ablation and (a) Ta_2O_5 suspension.

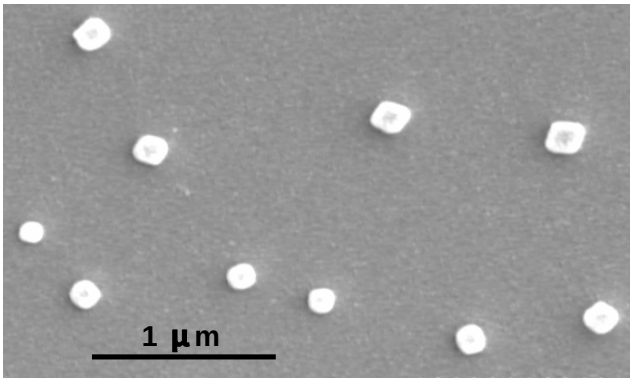

Fig. 8.8. SEM image of the particles prepared by the liquid laser ablation.

suspension was 4 mol/dm^{-3}. When the concentration was higher than 4 mol/dm^3, the color of the suspension was changed to black. When it was lower than 4 mol/dm^3, the color of the suspension was changed to white. Fig. 8.7 shows the absorption spectra of the supernatant of the reddish suspension. The absorption edge shifted longer wavelength. We suggest that Ta_3N_5 was prepared by the liquid laser ablation of Ta_2O_5 powder in aqueous NH_3. The SEM images are also shown in Fig. 8.8.

8.4. References

[1] A. Fujishima, K. Honda, Nature 37 (1972) 238.

[2] A. Heller, Acc. Chem. Res. 28 (1995) 141.

[3] M. Hara, T. Takata, J.N. Kondo, K. Domen, Catal. Today 90 (2004) 313.

[4] D. Yamasita, T. Takata, M. Hara, J.N. Kondo, K. Domena, Solid State Ionics 172 (2004) 591.

[5] K. Nakajima, D. Lu, M. Hara, K. Domen, J.N. Kondo, Stud. Surf. Sci. Catal. 158 (2005) 1477.

[6] D. Yamasita, T. Takata, M. Hara, J.N. Kondo, K. Domen, Solid State Ionics 172 (2004) 591.

[7] M. Hara, T. Takata, J.N. Kondo, K. Domen, Catal. Today 90 (2004) 313.

[8] J.N. Kondo, T. Katou, D. Lu, M. Hara, K. Domen, Stud. Surf. Sci. Catal. 154 (2004) 951.

[9] M. Hara, G. Hitoki, T. Takata, J.N. Kondo, H. Kobayashi, K. Domen, Catal. Today 78 (2003) 555.

[10] Y. Takahara, J.N. Kondo, D. Lu, K. Domen, Solid State Ionics 151 (2002) 305.

[11] K. Maeda, K. Domen, J. Phys. Chem. C (Feature Article) 111 (2007) 7851.

[12] C. Jong, T. Chin, W. Fang, Thin Solid Films 401 (2001) 291.

[13] C. Jong, T. Chin, Mater. Chem. Phys. 74 (2002) 201.

[14] G. Brauer, J.R. Weidlein, Angew. Chem. Int. Ed. 4 (1965).

[15] I. Ayerdi, Sens. Actuators A 46–47 (1995) 218.

[16] G.S. Chen, S.T. Chen, S.C. Huang, Y. Lee, Appl. Surf. Sci. 169–170 (2001) 353.

[17] G.S. Chen, P.Y. Lee, S.T. Chen, Thin Solid Films 353 (1999) 264.

[18] Y.M. Lu, R.J. Weng, W.S. Hwang, Y.S. Yang, Mater. Chem. Phys. 72 (2001) 278.

[19] K. Radhakrishnan, Mater. Sci. Eng. B 57 (1999) 224.

[20] M. Stravrev, D. Fischer, C. Wenzel, K. Drescher, N. Mattern, Thin Solid Films 307 (1997) 79.

[21] H. Jung, K. Im, H. Hwang, Appl. Phys. Lett. 76 (2000) 3630.

[22] H. Jung, K. Im, D. Yang, H. Hwang, IEEE Electron Device Lett. 21 (2000) 563.

[23] M. Kerlau et al., Solid State Sciences 6 (2004) 101.

[24] G.B. Alers, R.M. Fleming, Y.H. Wong, B. Dennis, A. Pinczuk, G.. Redinbo, R. Urdahl, E. Ong, Z. Harsan, Appl. Phys. Lett. 72 (1998) 1308.

[25] D.M. Hoffman, Polyhedron 13 (1994) 1169.

[26] M. Ritala, P. Kalsi, D. Riihelä, K. Kukli, M. Leskelä, J. Jokinen, Chem. Mater. 11 (1999) 1712.

[27] K. Baba, R. Hatada, Surf. Coat. Technol. 84 (1996) 429.

CHAPTER 9

GENERALIZATION

9.1. Summary

This thesis mainly comprises the experimental results and discussion on studies of visible light-responsive photocatalysis systems. N-doped TiO_2 films were prepared by the laser ablation and evaluated. The doping process was clarified on the basis of the data. The basic research for the enhancement of the hydrogen production, the decomposition of organic compounds using the photocatalyst films, the artificial photosynthetic system and a novel type solar cell using Fe_2O_3 were carried out under light irradiation.

Chapter 1 gives a general introduction of the study. First, the backgrounds of the study are shown. Next, the reviews of the photocatalysis and the laser ablation method are explained. Finally, we stated the aim and the objects.

In Chapter 2, N-doped TiO_2 thin films were prepared by the laser ablation method under an N_2 gas atmosphere. The properties of the films such as color, the relative amount of N doped and the crystal structure strongly depended on substrate temperature and N_2 gas pressure. XPS data indicated that the amount of doped N unexpectedly increases with decreasing N_2 gas pressure in the range of ca. 40 – 270 Pa. We proposed that the N-doping occurred when N species and TiO_2 particles collide on the substrate. The decomposition of methylene blue using the N-doped TiO_2 thin film was also performed under visible light irradiation. Moreover we succeeded in enhancing the photocatalytic activity of the thin films under visible light by changing the distance

between the target and the substrate.

Chapter 3 discusses the effect of graphite silica (GS) on TiO_2 photocatalysis in hydrogen production from water-methanol mixtures. Hydrogen production was drastically enhanced by GS in water-methanol mixtures. A synergy effect between TiO_2 and the clay portion of GS was proposed. The clay in GS has an ion-exchange property which leads to an increase in protons in the water-alcohol mixture leading to the increase in hydrogen production.

Chapter 4 describes the photocatalytic activity of a two-layer thin film (GS/TiO_2) composed of GS and TiO_2, prepared by the laser ablation method. The photocatalytic activities of the GS/TiO_2 film were evaluated by measuring the rate constant for the decomposition of methylene blue in water and the photocatalytic hydrogen evolution in water-ethanol solutions. The clay portion of GS was found to enhance the photocatalytic activity by increasing the surface charge of TiO_2 and the number of protons around TiO_2 due to the ion exchange property of GS. This leads to the decomposition of methylene blue and also photoinduced hydrogen production.

Chapter 5 presents the effect of nanomaterials on the photocatalytic activity of TiO_2 on the hydrogen production from water-alchol mixtures. The drastic synergy effect was found with an increase in the amount of H_2 gas by a factor of ca. 400 for single-walled carbon nanotubes (SWNT). It is suggested that the electron transfer takes place more easily due to the aggregation of TiO_2 and SWNT, resulting in the enhancement of the hydrogen production.

Chapter 6 discusses the photoinduced hydrogen production with the photosensitization of chlorophyll (or Co(II)tetraphenylporphyrin) in Poly(L-glutamate) (Poly(Glu)) - decylammonium chloride (DeAC) complex system with α-helix structure.

The hydrogen production was carried out in the presence of methylviologen (MV^{2+}) as an electron acceptor and ethylenediaminetetraacetic acid disodium salt as a sacrificial electron donor. The exited electron can transfer to MV^{2+} from the photosensitizer, and then the electron transfers to Pt colloid in Poly(Glu)-DeAC complex. The conformation of the polypeptide, hydrogen-evolution dependence on DeAC or MV^{2+} concentration and surface conditions were also investigated.

In Chapter 7, we present a novel attempt to replace a dye/TiO_2 composite film in dye-sensitized solar cells (DSC) by a visible light-responsive photocatalyst film. The durability test was performed by long time continuous irradiation (ca. 5 sun containing both UV and visible light, while the surface temperature was 50-60 ºC). Even after 5 days irradiation, a stable photocurrent (I) – voltage (V) curve was found with our novel cell (Fe_2O_3, water solvent), whereas performance of DSC (N719/TiO_2, organic solvent) decreased sharply under the same conditions.

In Chapter 8, TaON which is expected to split water under visible light was prepared by the gas or liquid phase laser ablation method. The preparation of TaON was confirmed by the detailed analysis such as FT-IR. The process of the preparation of the TaON thin film was also suggested.

The elucidation of the mechanism of the forming process of visible light-responsible photocatalysts and the fabrication of co-catalysts will contribute to the development of more useful visible light-responsive photocatalysis systems. The photocatalysis systems are very important for the preservation of our earth. The goal is almost within our reach. We hope that photocatalytic technologies will be adopted extensively in order to achieve and maintain a high level of harmony of human and nature.

9.2. List of publications

(1) Miyuki IKEDA, Yoshihumi KUSUMOTO, Shouichi SOMEKAWA, Pascaline NGWENIFORM, Bashir AHMMAD, "Effect of Graphite Silica on TiO_2 Photocatalysis in Hydrogen Production from Water–Methanol Solution", Journal of Photochemistry and Photobiology A: Chemistry, 184 (2006) 306.

(2) Pascaline NGWENIFORM, Yoshihumi KUSUMOTO, Miyuki IKEDA, Shouichi SOMEKAWA, Bashir AHMMAD, "Conformation-dependent Hydrogen Evolution with Co(II)tetraphenylporphyrin Solubilized into Poly(L-glutamate)-decylammonium Ion Complex" Chemical Physics Letters, 428 (2006) 436.

(3) Miyuki IKEDA, Yoshihumi KUSUMOTO, Yohei YAKUSHIJIN, Pascaline NGWENIFORM, Shouichi SOMEKAWA, "Highly Enhanced Photocatalytic Hydrogen Production by the Addition of Graphite Silica and Noble Metals to TiO_2 Suspension", Proceedings of the Renewable Energy 2006, Chiba, Japan (2006) 1341.

(4) Shouichi SOMEKAWA, Yoshihumi KUSUMOTO, Miyuki IKEDA, Masato TAKENOUCHI, Pascaline NGWENIFORM, Yuji HORIE, "Fabrication of Two-layers Thin Film by Laser Ablation Method and Application to Hydrogen Production System", Proceedings of the Renewable Energy 2006, Chiba, Japan, (2006) 1368.

(5) Pascaline NGWENIFORM, Yoshihumi KUSUMOTO, Takeo TESHIMA, Miyuki IKEDA, Shouichi SOMEKAWA, Bashir AHMMAD, "Visible-light Induced Hydrogen Production Using a Polypeptide-Chlorophyll Complex with α-helix Conformation", Photochemical and Photobiological Sciences, 6 (2007) 165.

(6) Pascaline NGWENIFORM, Yoshihumi KUSUMOTO, Miyuki IKEDA, Shouichi SOMEKAWA, Bashir AHMMAD, "Conformation-dependent Photoinduced Hydrogen Evolution with Co(II)tetraphenylporphyrin-Poly(L-glutamate) Complex", Journal of Photochemistry and Photobiology A: Chemistry, 189 (2007)198.

(7) Pascaline NGWENIFORM, Yoshihumi KUSUMOTO, Miyuki IKEDA, Shouichi SOMEKAWA, Bashir AHMMAD, Junichi KURAWAKI, Katumitu HAYAKAWA, "Photophysical and Photochemical Studies of Chlorophyll a and Cobalt(II)tetraphenylporphyrin in

Poly(L-glutamate)-Decylammonium Ion Complex" Journal of Photochemistry and Photobiology B: Biology, 87 (2007)154.

(8) Bashir AHMMAD, Yoshihumi KUSUMOTO, Miyuki IKEDA, Shouichi SOMEKAWA, Yuji HORIE, "Photocatalytic Hydrogen Production from Diacids and Their Decomposition over Mixtures of TiO_2 and Single Walled Carbon Nanotubes", Journal of Advance Oxidation Technology, 10 (2007) 415.

(9) Miyuki IKEDA, Yoshihumi KUSUMOTO, Yohei YAKUSHIJIN, Shouichi SOMEKAWA, Pascaline NGWENIFORM, Bashir AHMMAD, "Hybridized Synergy Effect Among TiO_2, Pt and Graphite Silica on Photocatalytic Hydrogen Production from Water-Methanol Solution", Catalysis Communications, 8 (2007) 1943.

(10) Shouichi SOMEKAWA, Yoshihumi KUSUMOTO, Katsuichi MIYAMAE, Takaomi KAMIWAKI, Yuji HORIE, "A Novel Type of Solar Cell Based on Visible-light Responsive Photocatalyst Films", Proceedings of ISES Solar World Congress 2007, Beijing, China 5 (2007) 1329.

(11) Hailong YANG, Yoshihumi KUSUMOTO, Miyuki IKEDA, Hayato UENJYO, Md. Abdulla-Al-Mamun, Shouichi SOMEKAWA, Bashir AHMMAD, "Enhancement Effect of Laser Ablation in Liquid on Hydrogen Production Using Titanium(IV) Oxide and Graphite Silica", Proceedings of ISES Solar World Congress 2007, Beijing, China 5 (2007) 2790.

(12) Shouichi SOMEKAWA, Yoshihumi KUSUMOTO, Miyuki IKEDA, Bashir AHMMAD, Yuji HORIE, "Fabrication of N-doped TiO_2 thin films by laser ablation method: mechanism of N-doping and evaluation of the thin films", Catalysis Communications, 9 (2008) 437.

(13) Miyuki IKEDA, Yoshihumi KUSUMOTO, Hailong YANG, Shouichi SOMEKAWA, Hayato UENJYO, Md. Abdulla-AL-MAMUN, Yuji HORIE, "Photocatalytic Hydrogen Production Enhanced by Laser Ablation in Water-Methanol Mixture Containing Titanium(IV) Oxide and Graphite Silica", Catalysis Communications, in press.

(14) Bashir AHMMAD, Yoshihumi KUSUMOTO, Shouichi SOMEKAWA, Miyuki IKEDA, "Carbon Nanotubes Synergistically Enhance Photocatalytic Activity of TiO_2", Catalysis Communications, in press.

9.3. Acknowledgements

I am delighted to finish writing this thesis. I am particularly grateful to my supervisor Professor Yoshihumi Kusumoto for his friendliness and encouragement while supervising this research work and also for his original ideas. Special thanks go to the entire staff of the department of Science, especially to Dr. Junichi Kurawaki and Dr. Tanaka whom I received practical advises in this study and also for the useful discussions. I want to say special thanks to Dr. Yuji Horie of the faculty of Engineering for all the useful advice, discussions and giving opportunity to use the laser ablation apparatus. I also thank sincerely to a member of Horie-Nomiyama lab for giving much help. In analysis of the photocatalysts, I thanks to Mr. Ozono and Mr. Kakoi of Frontier Science Research Centre for measurement of XPS and FE-SEM etc., and I thanks to Professor Hiroi for measurement of XRD. I want to say thanks to Professor Domen and Domen-lab member of Tokyo University for offering the samples and fatherly advices for the joint research. To my Family, your support has been immersed. I want to say thank you for taking care of me. Finally, I thanks gratefully to all Kusumoto-Kurawaki lab member for the kind helps and encouragements every day, I say thank you the useful discussions and friendliness, especially to Dr. Bashir Ahmmad, Dr. Miyuki Ikeda, Dr. M. Muruganandham Dr. Ngeniform Pascaline, Mr. Hairong Yang and Mr. Md. Abdulla-Al-Mamun as co-workers, I say thank you the useful discussions and friendliness. I also thank my friends in and out of the Kagoshima university vicinity. I have no words to express my gratitude.